②

**US Army Corps
of Engineers**

AD-A191 480
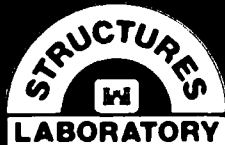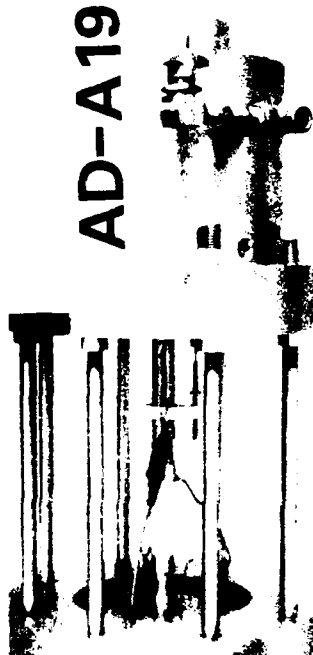
FAST TRIAXIAL SHEAR DEVICE EVALUATION

by

William F. Carroll

Department of Civil Engineering
and Environmental Sciences
University of Central Florida
Orlando, Florida 32816

DTIC
SELECTE
FEB 2 9 1988
D

January 1988
Final Report

88 2 29 054

Unclassified
SECURITY CLASSIFICATION OF THIS PAGE

A191 480

REPORT DOCUMENTATION PAGE			Form Approved OMB No 0704-0188 Exp Date Jun 30, 1986
1a. REPORT SECURITY CLASSIFICATION Unclassified		1b RESTRICTIVE MARKINGS	
2a. SECURITY CLASSIFICATION AUTHORITY		3 DISTRIBUTION/AVAILABILITY OF REPORT Approved for public release; distribution unlimited.	
2b. DECLASSIFICATION/DOWNGRADING SCHEDULE			
4. PERFORMING ORGANIZATION REPORT NUMBER(S)		5 MONITORING ORGANIZATION REPORT NUMBER(S) Technical Report SL-88-2	

6a. NAME OF PERFORMING ORGANIZATION University of Central Florida	6b OFFICE SYMBOL (If applicable)	7a NAME OF MONITORING ORGANIZATION USAEWES Structures Laboratory
6c. ADDRESS (City, State, and ZIP Code) Orlando, FL 32816		7b ADDRESS (City, State, and ZIP Code) PO Box 631 Vicksburg, MS 39180-0631

8a. NAME OF FUNDING/SPONSORING ORGANIZATION US Army Corps of Engineers	8b OFFICE SYMBOL (If applicable)	9 PROCUREMENT INSTRUMENT IDENTIFICATION NUMBER		

8c. ADDRESS (City, State, and ZIP Code) 20 Massachusetts Ave., N.W. Washington, DC 20314-1000	10. SOURCE OF FUNDING NUMBERS			
	PROGRAM ELEMENT NO	PROJECT NO 4A161102AT22	TASK NO BO	WORK UNIT ACCESSION NO 005

11 TITLE (Include Security Classification)
Fast Triaxial Shear Device Evaluation

12. PERSONAL AUTHOR(S)
Carroll, William F.

13a TYPE OF REPORT Final report	13b TIME COVERED FROM _____ TO _____	14 DATE OF REPORT (Year, Month, Day) January 1988	15 PAGE COUNT 99

16. SUPPLEMENTARY NOTATION
Available from National Technical Information Service, 5285 Port Royal Road,
Springfield, VA 22161.

17.	COSATI CODES		18. SUBJECT TERMS (Continue on reverse if necessary and identify by block number)
FIELD	GROUP	SUB-GROUP	Dynamic soil properties Shear strength
			Loading rate effects Stress-strain
			One-dimensional wave analyses Triaxial shear tests

19. ABSTRACT (Continue on reverse if necessary and identify by block number)

This report documents the most current evaluation of the US Army Engineer Waterways Experiment Station fast triaxial shear device (FTRXD). It describes the FTRXD, pertinent properties of the soil tested in the FTRXD, preliminary results from the testing, and a one-dimensional (1-D) nonlinear wave analysis of the FTRXD specimen.

The FTRXD is a triaxial cell which loads its 0.75-inch-diameter by 1.5-inch-long cylindrical specimen by displacing the top of the specimen downward at a rapid rate. The specimen may be subjected to confining pressures up to 1,000 psi. Displacement, load at the top of the specimen, and load at the bottom are measured as continuous functions of time. To date, specimens have been brought to failure in as little as 2 milliseconds. Loading is accomplished with a piston and cylinder assembly powered by compressed nitrogen.

Soil from the CARES-Dry test site on Luke Gunnery range in Arizona was used in the
(Continued)

20 DISTRIBUTION/AVAILABILITY OF ABSTRACT ☐ UNCLASSIFIED/UNLIMITED ☒ SAME AS RPT ☐ DTIC USERS	21 ABSTRACT SECURITY CLASSIFICATION Unclassified	
22a NAME OF RESPONSIBLE INDIVIDUAL	22b TELEPHONE (Include Area Code)	22c OFFICE SYMBOL

DD FORM 1473, 84 MAR
83 APR edition may be used until exhausted
All other editions are obsolete

SECURITY CLASSIFICATION OF THIS PAGE
Unclassified

19. ABSTRACT (Continued).

evaluation. It classifies as a clayey sand (SC) in the Unified Soil Classification System. It exhibits a principal stress difference (PSD)-axial strain curve which may be represented by a function which is initially linear, then hyperbolic.

The preliminary load-time data from the FTRXD revealed larger loads recorded at the top than at the bottom of the specimen. The differences were less than 1 percent for tests with durations of 2 to 120 seconds, but increased to 40 percent for tests with a duration of 2 milliseconds. Part of the difference is attributed to wave effects in the specimen, but a major part is due to the dynamics of the FTRXD. Additional significant effects from the dynamics of the FTRXD were recorded by the moving load cell at the top of the specimen.

The 1-D wave analysis of the specimen, first employing an initially linear, then hyperbolic stress-strain curve for the specimen, and having the top of the specimen displace downward in the manner measured during testing, provided axial stress at the top and bottom of the specimen. These were plotted against gross strain, the displacement of the top divided by the specimen length. The specimen's true stress-strain curve may be determined from these plots, although the details of the determination depend on the details of the displacement-time data of the top of the specimen. For specimens brought to failure in 20 milliseconds or more, the top and bottom stress intersect repeatedly when plotted against gross strain. The intersections trace the specimen's true stress-strain curve accurately. For faster tests, the top and bottom stress intersect infrequently, if at all. However, they are an upper and lower limit of the actual stress, which might be located as a function of these bounds.

PREFACE

The Geomechanics Division of the Structures Laboratory (SL) at the US Army Engineer Waterways Experiment Station (WES) designed and constructed a fast triaxial shear device (FTRXD) and is currently evaluating it under the sponsorship of the Office, Chief of Engineers, US Army, as a part of Project 4A161102AT22, Task BO, Work Unit 005, "Constitutive Properties for Natural Earth and Manmade Materials."

The investigation was conducted under the general supervision of Mr. Bryant Mather, Chief, SL. Mr. John Q. Ehrgott, Geomechanics Division (GD), SL, was responsible for development and evaluation of the FTRXD under the general direction of Dr. J. G. Jackson, Jr., Chief, GD, SL. Performance tests were conducted by Mr. Toney K. Cummins, GD, SL. Numerical evaluation of the FTRXD was undertaken by Dr. William F. Carroll, Professor of Engineering at the University of Central Florida (UCF) in Orlando, FL, under an Intergovernmental Personnel Act agreement with WES. This report, prepared by Dr. Carroll, documents the first phase of the evaluation of the FTRXD.

Dr. David R. Jenkins is Chairman, Department of Civil Engineering and Environmental Sciences at UCF, and Dr. Robert D. Kersten is Dean of the College of Engineering.

COL Dwayne G. Lee, CE, is Commander and Director of WES, and Dr. Robert W. Whalin is Technical Director.

Accesion For

NTIS CRA&I	☑
DTIC TAB	☐
Unannounced	☐
Justification	

By

Distribution /

Availability Codes

| Dist | Avail and / or Special |
| A-1 | |

i

CONTENTS

CONVERSION FACTORS, NON-SI TO SI (METRIC)
UNITS OF MEASUREMENT

Non-SI units of measurement used in this report can be converted to SI
(metric) units as follows:

Multiply	By	To Obtain
feet	0.3048	metres
inches	25.4	millimetres
inches per second	0.0254	metres per second
mils	0.0254	millimetres
pounds (force)	4.448222	newtons
pounds (force) per square inch	0.006894757	megapascals
pounds (mass)	0.4535924	kilograms
pounds (mass) per cubic foot	16.01846	kilograms per cubic metre

FAST TRIAXIAL SHEAR DEVICE EVALUATION

CHAPTER 1

INTRODUCTION

1.1 BACKGROUND

In 1981 the US Army Engineer Waterways Experiment. Station (WES) undertook the design and construction of a test apparatus to provide a capability for conducting laboratory testing of soils in times to failure of less than one millisecond. A test apparatus patterned after the traditional triaxial shear device was developed. The apparatus applies axial loads to a cylindrical soil specimen 0.75 inches in diameter and 1.5-inches high. Load is measured at the top and bottom of the specimen as a function of time and the displacement of the top of the specimen is also measured. The constant confining pressure on the specimen during testing is controlled and recorded. The apparatus is the Fast Triaxial Shear Device (FTRXD). The device and some soil specimens tested to failure in it are shown on Figures 1.1 and 1.2.

The rapid loading of soils in a triaxial testing device was done by WES earlier in the 1960's in conjuction with research on the dynamic bearing capacity of soils. A dynamic triaxial test apparatus was designed and constructed. The results from testing with the apparatus on highly plastic clay specimens, 1.4 inches in diameter by 3.0-inches long, were used to interpret dynamic bearing tests of small plates resting on the clay. The apparatus, the results obtained from it, and their uses are described in Reference 1.

1.2 PURPOSE AND SCOPE

The purpose of this report is to define the nature of the problem posed in interpreting the results of testing soils with the Fast Triaxial Device (FTRXD), to present the steps taken to date in the evaluation of the device, and to outline those planned for the future. To the extent necessary to understand its operation and therefore the difficulties in understanding the meaning of test results, pertinent characteristics of the FTRXD are presented in Chapter 2. Moreover, a description of selected properties of the soil used in the FTRXD that bear on its evaluation are presented in Chapter 3. A complete description of the FTRXD is contained in Reference 2. The extensive earlier testing by WES of the soil used is reported in Reference 3.

1.3 EVALUATION OF THE FAST TRIAXIAL SHEAR DEVICE

The steps taken so far in the evaluation of the FTRXD include a modest amount of testing of remolded soils taken from

1

the CARES-Dry test site located at Luke Bombing and Gunnery Range in Arizona and examination of the results of this testing. These results are described in Chapter 4.

An analytical study of a model of the soil specimen as an initial value-boundary value problem was undertaken to assess the extent of inertial effects on stress at the top and bottom of the model specimen. A purpose of this study was also to evaluate "gross stress", the stress that is realized when the displacement of the top of the specimen divided by the specimen length is entered as strain into the soil's constitutive relationship. The premise of this analysis is that the behavior of the specimen during rapid testing could be described satisfactorily as one-dimensional wave phenomena in a continuous medium exhibiting realistic, nonlinear, uniaxial stress-strain characteristics. The initial values and boundary conditions employed were analytical representations of the measured conditions during testing. This analysis is presented in Chapter 5.

Where inertial effects within the soil specimen are not overriding, the FTRXD with a soil specimen in it has been modeled as a two degree of freedom lumped mass system. A nonlinear spring element and damper represent the soil specimen; linear springs, dampers, and lumped masses represent the remainder of the device. This modeling work is incomplete and will not be presented in this report; it will be the subject of a later report.

Future plans call for modifications to the FTRXD for improved control of the boundary conditions for the system and improved measurement of them. Further testing on the CARES-Dry remolded soil and other different soil types will be necessary to refine and validate conclusions drawn from the analytical studies of the FTRXD. Moreover, to more clearly define the very rapid end of the testing spectrum, further analysis of the soil specimen as an initial value-boundary value problem employing two-dimensional axisymmetric wave phenomena with non-linear constitutive behavior will be necessary.

Fig 1.1, The Fast Triaxial Device (FTRXD)
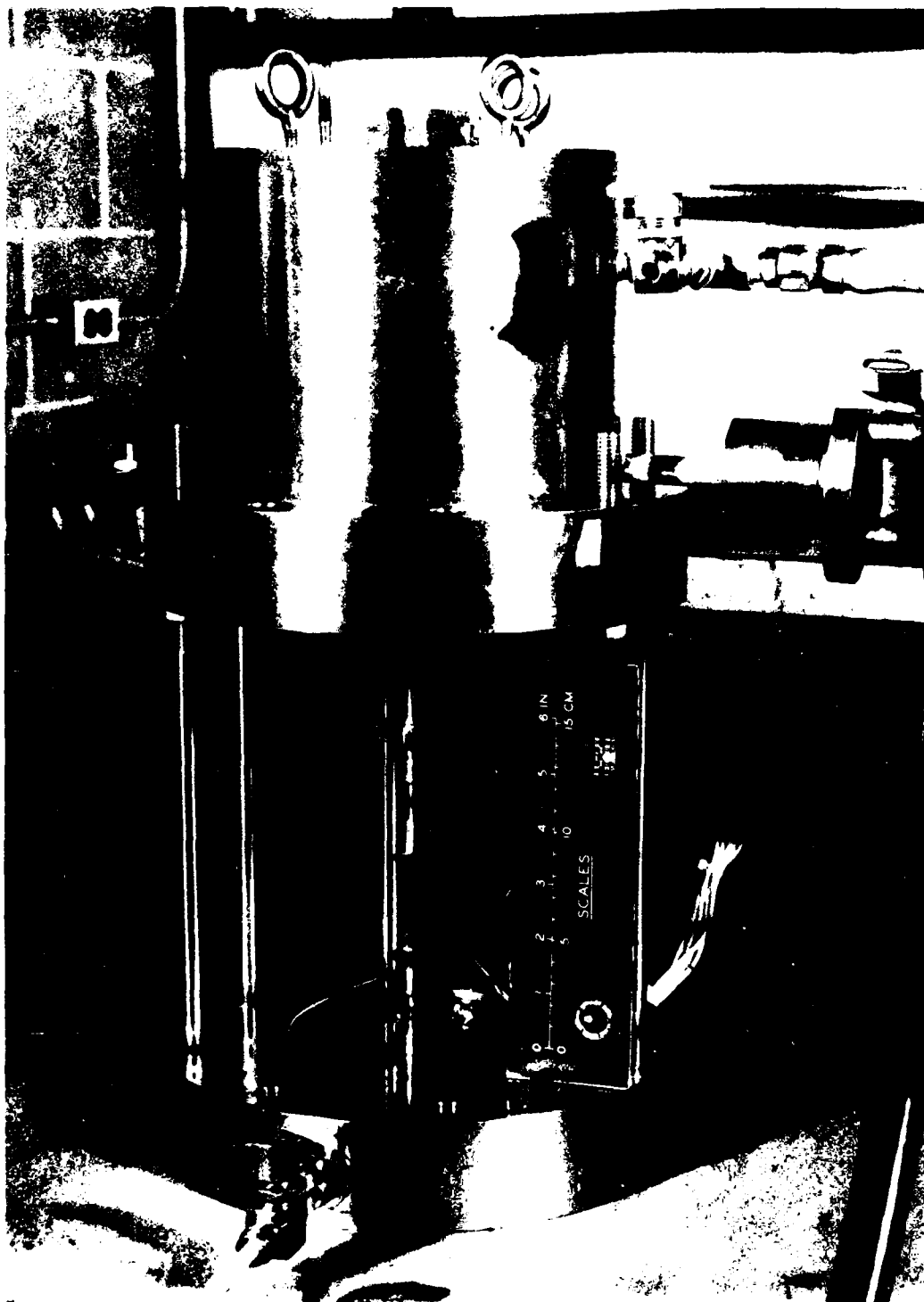
Fig 1.2, Failed FTRXD CARES-Dry Specimens

CHAPTER 2

THE FAST TRIAXIAL SHEAR DEVICE (FTRXD)

2.1 THE APPARATUS

The FTRXD is a triaxial soil testing device. It consists of a loading assembly, a base, a specimen chamber, a pressurization system, upper and lower load cells, a Kaman gage, and a data recording system. Schematics of it are on Figures 2.1 and 2.2, photographs are on Figures 1.1 and 2.3, and Reference 2 provides more complete details.

2.2 THE LOADING ASSEMBLY

The loading assembly is a piston-cylinder arrangement. The piston consists of a 4.0-inch-diameter steel piston to which is rigidly attached a 0.75-inch-diameter by 7.125-inch-long steel ram. The piston-ram has a mass of 1100 grams; the mass of the ram alone is about 405 grams. Initially the piston is positioned with its ram in contact with the upper load cell which in turn is in contact with the top of the soil specimen. The chamber in the cylinder above the piston is pressurized to a pre-determined level using compressed nitrogen. For the slower tests — those in which failure occurs in 20 milliseconds or more — the chamber in the cylinder below the piston is filled with oil and sealed until the test is initiated. For faster tests, this chamber contains air and is open to the atmosphere, and the piston and ram are held in position by a tubular shear pin.

The loading assembly is activated for the slower tests by the rapid opening of a solenoid valve in the lower chamber of the cylinder which allows the oil to escape. The ability to control the magnitude of the pressure in the upper chamber and the rapid opening of the valve releasing the oil from the lower chamber, provides a measure of control of the rate and magnitude of the load pulse impressed on the soil specimen. The presence of the oil in the lower chamber flowing from the chamber as the specimen is loaded causes a characteristic shape in the load pulse and damps undesirable vibrations in the system during testing.

The oil in the lower chamber does not permit the system in its present configuration to bring a specimen to failure in less than 20 milliseconds. For faster tests, therefore, there is no oil in the lower chamber. The loading assembly is activated by applying sufficient pressure in the upper chamber to shear the tubular shear pin holding the piston and ram in place. The result is a rapid application of load to the soil specimen. A variety of tubular shear pins are available in both aluminum and plastic and with several different wall thicknesses. The rate of loading is increased by applying higher pressure in the upper chamber above the piston and this is made possible by employing stronger tubular shear pins.

2.3 THE BASE

The base is a steel disk which serves to support the chamber, the lower load cell, and eight studs which in turn support the loading assembly.

2.4 THE SPECIMEN CHAMBER

The specimen chamber surrounds the soil specimen and contains fluid subjected to the pressure which equals the confining pressure for the test. There is a steel or plexiglas chamber for tests with high or low confining pressures. When testing with the plexiglas chamber, a wire mesh cylinder is placed around the plexiglas to serve as a safety shield. The chamber is sealed to the base and the loading assembly by O-rings and held in place by the eight studs which also support the weight of the loading assembly.

2.5 THE PRESSURIZATION SYSTEM

Compressed nitrogen is the source of pressure used to drive the piston and ram downward which loads the soil specimen during testing. It is also used to apply the constant confining pressure to the soil specimen. Two different arrangements are employed: one for the slower tests (times to failure greater than 20 milliseconds) when oil is in the lower chamber of the cylinder below the piston, and one for the faster tests with no oil in this lower chamber. A schematic of the pressurization system is shown in Figure 2.2.

In both arrangements, the confining pressure is applied to the specimen chamber as pressurized nitrogen over oil and the chamber is sealed until the test is completed. After the test, this pressure and the system applying it are used to drain the specimen chamber of the oil.

In the slow test arrangement, pressurized nitrogen is applied to the oil in the accumulator forcing it into the lower chamber of the loading assembly cylinder. This provides an ability to carefully control the positioning of the piston and ram and to set it for testing by sealing the lower chamber of the cylinder. Once this lower chamber is sealed, the pressure on the oil in the accumulator is relieved. Pressure is then introduced into the upper chamber of the loading assembly above the piston. The test is initiated by the rapid opening of the solenoid valve to the lower chamber so the oil can return to the accumulator.

In the fast test arrangement, the lower chamber of the cylinder is left open to the atmosphere. The piston and ram are adjusted manually and set for testing by emplacing the tubular shear pin. Pressure is introduced into the upper chamber above the piston and the test is initiated when the tubular pin shears.

2.6 THE LOAD CELLS

The load cells used in the FTRXD were designed and built at WES. There are four matched pairs of load cells. Each pair consists of two essentially identical load cells - one which is placed above the soil specimen during testing (the upper load cell: ULC) and the other below the soil specimen (the lower load cell: LLC). The differences between the ULC and LLC are only in the manner in which they attach to the loading assembly and base. There are four pairs to permit testing with load ranges of 500, 1000, 2500, and 10000 pounds. A photograph of a specimen installed between an upper and a lower load cell is shown on Figure 2.3.

The load cells are stainless-steel cylinders loaded along their axes. The central part of the load cells are hollow cylinders about 0.6-inches long with 0.6 inches for their outer diameters (the 500-pound set has an outer diameter of 0.575 inches). The inner diameters of each set differ to permit increasing wall thicknesses for the increasing load ranges. The 500- and 1000-pound sets have inner diameters of 9/16 inches, the 2500-pound set's is 1/2 inches, and the 10,000-pound set's is 1/4 inches. Two pairs of strain gages are mounted on the outside surface of each hollow cylindrical part. Each strain gage of the pair is located at the midpoint of the cylindrical axis and diametrically opposite of its mate. One pair is oriented along the axis of the cylinder and the other at right angles to it. The four strain gages are equally spaced around the circumference of the load cell.

A solid cylindrical piece of stainless steel is an integral part of each load cell and is located between the hollow cylindrical part and the soil specimen. It is 0.75 inches in diameter and about 0.5-inches long - a 35 to 40 gram mass. This solid piece serves as a pedestal directly in contact with the soil specimen. At the other end of the hollow part are stainless-steel pieces which permit the load cells to be engaged by the loading assembly (ULC) or attached to the base (LLC).

The 500 and 1000-pound load cells have natural periods of about 0.11 and 0.07 milliseconds respectively.

2.7 THE KAMAN GAGE

The displacement of the moving piston and ram with respect to the fixed part of the loading assembly is measured with the Kaman gage and its cantilever target. The Kaman gage is the KD2300 series displacement measuring system manufactured by Kaman Measuring Systems. It is a variable impedance transducer and is attached to the stationary underside of the loading assembly. Its target is an aluminum bar 0.385-inches thick by 1.0-inches wide rigidly attached to the moving ram as a cantilever. The · cantilever extends 1.625 inches from the edge of the ram to a

7

region directly under the Kaman gage. The target for the gage, therefore, is an aluminum surface about 1.625 inches by 1.0 inches in plan and 0.385-inches thick. Eddy currents induced in the moving target result in variations in the impedance in the Kaman gage. Since the strength of the impedance variations depends on the distance between Kaman gage and the target, the displacement of the target, and therefore of the ram, is sensed and measured. The linear range of the Kaman gage is 300 mils and its static frequency response is 50KHz at -3dB. The manufacturer also suggests its transient response is 0.01 milliseconds with no overshoot.

The Kaman gage is designed to perform under static pressures to 20,000 psi. Confining pressures in the FTRXD are not intended to exceed 1000 psi. The gage's ability to perform under high pressures and to sense accurately displacements up to 0.1 inches occurring well within the sub-millisecond range was reported in Reference 4. Preliminary analysis of displacement data recorded during testing with the FTRXD indicates that the Kaman gage can measure displacement variations at least this fast, meaning its response time is considerably less than 0.1 milliseconds. The natural period in the fundamental mode of the cantilever target, however, is from 0.20 to 0.30 milliseconds, depending on how the rigidity of its attachment to the ram is viewed.

2.8 THE DATA RECORDING SYSTEM

An AD509J amplifier was used to generate an excitation circuit through the Kaman gage and the strain gages of the load cells. The signals produced by these gages during testing were thus amplified and could be recorded. The AD509J is a high-speed amplifier exhibiting response times of less than 0.001 milliseconds.

A Rascal Stole 7DS tape recorder made a continuous record of load and displacement data during testing. Magnetic tape recording was employed to obtain high resolution load and displacement data during the very rapid testing. At its top recording speed of 60 inches/second, the recorder has a time base error of less than 0.0015 milliseconds and an interchannel time displacement error of less than 0.0007 milliseconds.

Fig 2.1, FTRXD Schematic

Fig 2.2, FTRXD Pressurization Schematic


```
(G)      (G)           V
 |        |    (X)    (X)
       (X)
        R

            (G)    (G)
             |      |   (X)
                   (X)
                    R

                              RV
                             (X)

 (X) RV   (X) RV   (X) RV   (X) RV

                          Accum-
                          ulator

  N         N
  I         I
  T         T
  R         R
  O         O
  G         G
  E         E
  N         N
```

Load
Cylinder

Upper
Chamber
- - - -
Lower
Chamber

SV
(X)

Fast
Triaxial
Cell

V
(X)

Oil
Can-
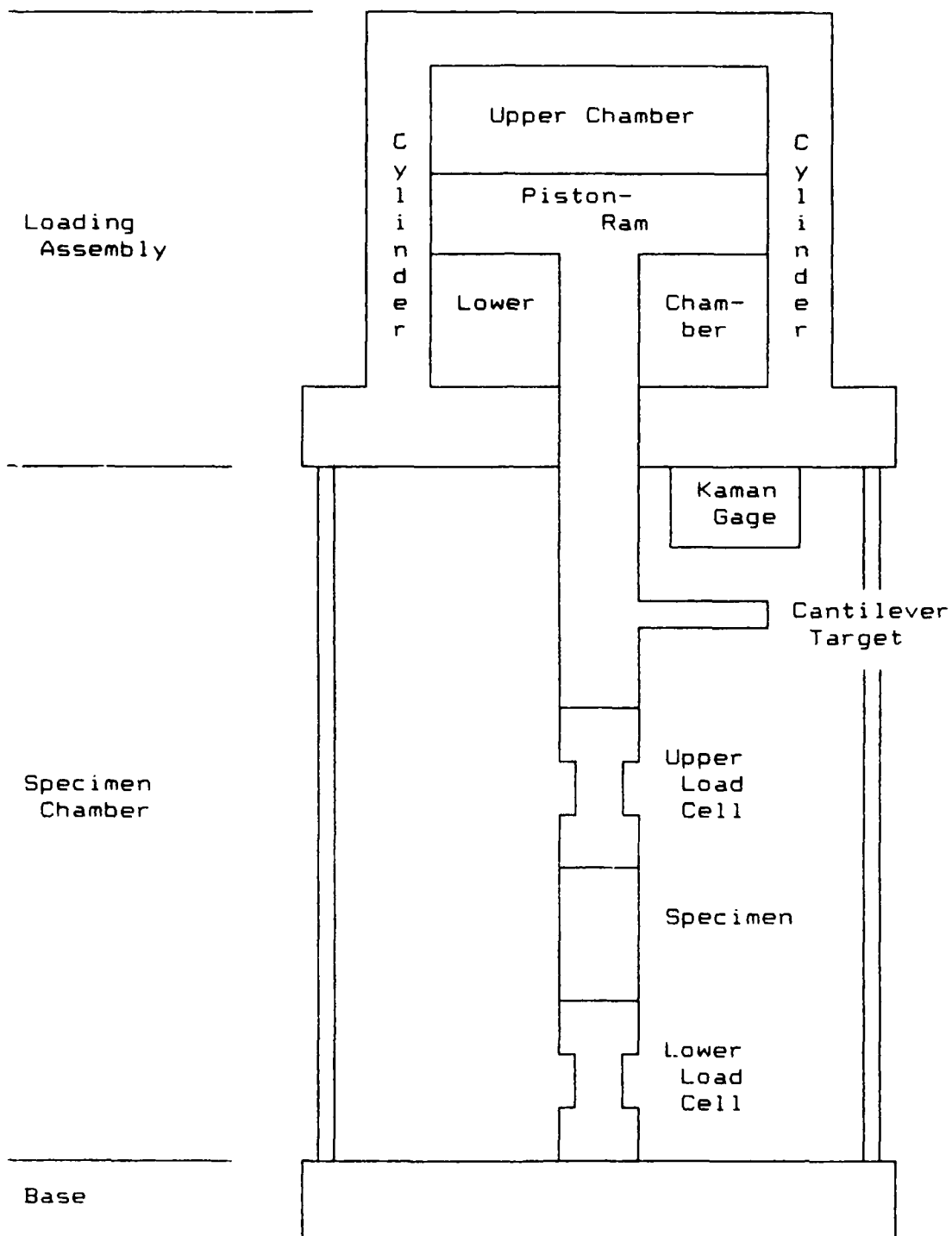ister
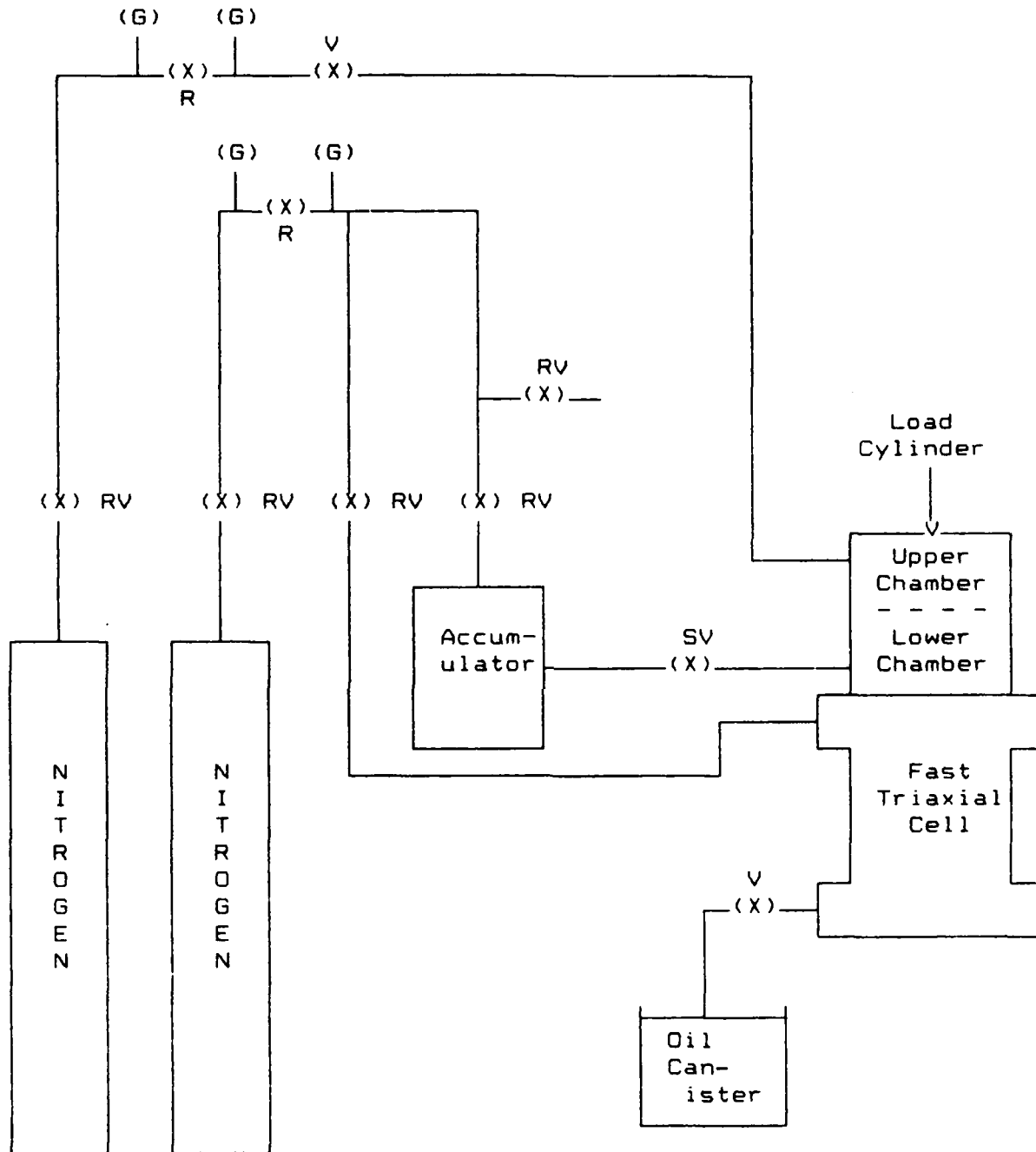
V - Ball Valve
R - Pressure Regulator
RV - Regulating Valve
SV - Solenoid Valve
P - Pressure Gage

Fig 2.3, Mounted FTRXD Specimen
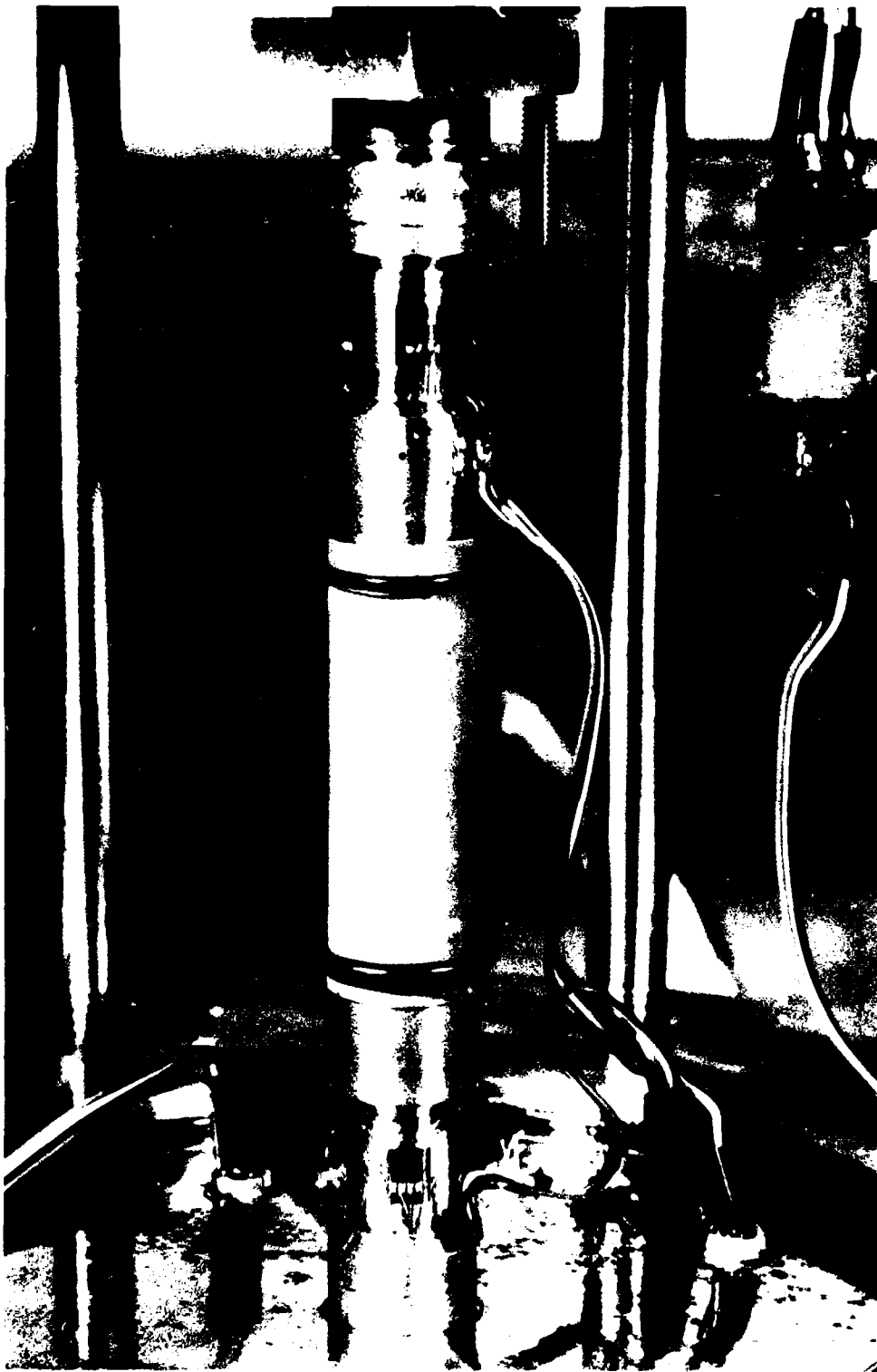
CHAPTER 3

SELECTED PROPERTIES OF THE CARES-DRY SOIL

3.1 DESCRIPTION

The soil used was from the CARES-Dry test site located at
Luke Bombing and Gunnery Range in Arizona. Soil was obtained from
near the surface of the ground and passed through a number 4
sieve (4.76-mm opening); only the portion finer than the number 4
sieve was used. It classifies as SC (clayey sand) in the Unified
Soil Classification System with 33 percent fines, a Liquid Limit
of 36 percent, and a Plasticity Index of 19 percent. An average
gradation curve is shown on Figure 3.1. Standard Proctor
compaction testing revealed a maximum dry density of 122 pounds
per cubic foot at an optimum water content of 11.6 percent.
Modified Proctor testing showed a maximum dry density of 132
pounds per cubic foot at an optimum water content of 7.9 percent.
This testing and the standard triaxial shear testing described
below are reported comprehensively in Reference 3.

3.2 STANDARD TRIAXIAL SHEAR (STRX) TESTING

Remolded specimens tested in STRX were prepared at water
contents of about 5 percent and compacted to wet densities of
118-120 pounds per cubic foot. This was done for eleven specimens
by rodding the soil in three lifts into a mold 2.0 inches in
diameter by 5.0-inches high; there were also three specimens
prepared in this mold using five lifts. In addition, four
specimens were prepared in three lifts in a 3.0-inch-diameter by
6.0-inch-high mold and one in a 3.0-inch-diameter by 5.0-inch-
high mold.

STRX testing was performed on specimens which had been first
subjected to isotropic compression under an equal all-around
confining pressure. With the confining pressure held constant on
the specimen, axial load was applied to the specimen and the
consequent changes in the specimen's height and diameter were
measured. Pore pressures were not measured since the soil was
only 26-29 percent saturated. Stresses computed are total
stresses. The duration of these tests was five to ten minutes.

The reported STRX test results most comparable to the
initial FTRXD test results are those that relate principal stress
difference to axial strain in remolded specimens of the soil at
comparable confining pressures. There are five such STRX test
results: one at a confining pressure of 0.4 MPa (50 psi), three
at 0.7 MPa (100 psi), and one at 1.4 MPa (200 psi). Linearized
plots of principal stress difference versus axial strain for
these five specimens are shown on Figure 3.2. Pertinent test
parameters for the five soil specimens are listed in Table 3.1.

3.3 FAST TRIAXIAL SHEAR DEVICE (FTRXD) SLOW TESTING

The soil used initially in the FTRXD was remolded CARES-Dry soil prepared as 0.75-inch-diameter by 1.5-inch-high specimens, rodded into a suitably sized mold in three to five lifts. Specimen wet densities were 112-119 pounds per cubic foot and their water contents were 0.0-4.3 percent. Because these specimens were smaller than the specimens used in the STRX testing, only soil passing the number 8 sieve (2.38-mm opening) was used.

Slow testing in the FTRXD was done in much the same manner as for STRX testing. A constant confining pressure was applied, the specimen was loaded axially, and measurement was made of axial load and change in the height of the specimen (see Chap 2). The confining pressures employed were 50, 100, and 200 pounds per square inch and pore pressures were not measured. In the results reported here for six specimens, test durations were 120 seconds and 1.2 seconds. Plots of principal stress difference versus axial strain for these six tests are shown on Figures 3.3 and 3.4. Pertinent test parameters for the six specimens are listed in Table 3.2.

The stress-strain curve for the specimen tested at a confining pressure of 200 pounds per square inch with a test duration of 1.2 seconds showed values of principal stress difference of about one-half of what was expected. The shape of the curve, however, was as expected. This curve is plotted with its principal stress difference values doubled. All of the plots on Figure 3.3 are pairs of principal stress difference curves reflecting the readings from both the upper and lower load cells in the FTRXD. The upper load cell readings consistently plot above the lower load cell readings in each pair. Though the difference is small (less than 1.0 percent), it appears to be larger in the tests completed in 1.2 seconds than those completed in 120 seconds.

3.4 THE LINEAR-HYPERBOLIC STRESS-STRAIN CURVE

Examination of the "static" plots of principal stress difference (PSD) versus axial strain for the CARES-Dry soil (Figures 3.2 to 3.4) reveals a characteristic shape of the curves. They are relatively linear for stress levels up to 20-60% of the maximum principal stress difference (peak PSD). Thereafter they exhibit a smooth, non-linear trace with decreasing slope. Some of the curves achieve a peak PSD where their slopes are zero, prior to reaching 15% axial strain. Some do not, however, especially those at the higher confining pressures. Increasing confining pressure appears to increase the values of PSD at corresponding axial strains and to increase the slope of the curves. It also seems to cause the peak PSD to occur at larger axial strains, or not at all prior to reaching 15% axial strain. These characteristics are not atypical for many soils which

14

exhibit changes in stress-strain behavior due to changes in confining pressure.

The stress-strain curves for the soil were not examined at axial strains exceeding 15%. Axial strain is calculated as the difference in axial displacement between the top and bottom of the soil specimen divided by the specimen length. The calculation assumes a uniform strain throughout the specimen. At small strains specimen deformation is quite uniform, especially in the central portion of the specimen. The calculated uniform strain in this circumstance gives an acceptable indication of the actual strain distribution. As strains increase, however, specimen deformation becomes increasingly nonuniform and the calculated uniform strain becomes less representative of the actual strain distribution. At some point, there is little relationship between the calculated uniform strain and the actual strain distribution. This point is considered to occur at least by the time 15% axial strain is reached.

To accomplish dynamic analyses of the soil specimen as it is tested in the FTRXD, it is necessary to employ a stress-strain relationship. Although the magnitudes of PSD, slopes of the curves, and other properties must necessarily be the result of testing, the manner of variation of stress with strain is required to employ a form of the wave equation to gain insights into the inertial effects in the specimen during testing. To this end, a mathematical model of the specimen's stress-strain curve, a constitutive relationship, must be specified.

Clearly any stress-strain relationship used should conform to as many of the known facts about the soil as is possible. However, the complexity of the relationship must be minimized or the ensuing wave equation will at best be extremely difficult to deal with, and may be unsolvable. At worst, it may not be possible to even develop a wave equation. If the significant behavior of the specimen is assumed to occur only in the axial direction, then a one-dimensional (axial) stress-strain relationship might suffice and a one-dimensional wave equation can be developed and solved. Since each test is performed at a constant confining pressure, the effects of the confining pressure might be accounted for in part by assuming a unique variation of principal stress difference (PSD) with axial strain for each test - different for each test but related to the test's constant confining pressure. Other effects of confining pressure will be reflected in the measured values of PSD and slopes of the PSD-axial strain curve for the tests. One-dimensional wave propagation through a cylindrical specimen twice as high as it is wide is doubtless a reasonable characterization of specimen behavior for some portion of its dynamic spectrum. It was employed in the initial analyses of the FTRXD and is reported in detail in Chapter 5.

The nature of the experimental PSD-axial strain curves for the CARES-Dry soil suggests that to describe them in one-dimensional (axial) loading, several parameters are required . The initial linearity of the curves requires two. The subsequent smooth nonlinear yielding of the curves with decreasing slopes requires at least two more parameters. Accounting for the peak PSD when it occurs would require still another. Of the many mathematical functions possible, what was selected and used was a simple straight line for the initial part of the curve from the origin to a stress level designated the maximum linear stress (MLS). The remainder of the curve was portrayed as a two parameter hyperbola which smoothly connected to the initial straight line portion with the initial slope of the hyperbola equal to the slope of the straight line portion. The hyperbola continues to rise with decreasing slopes approaching an upper limiting stress as strain increases indefinitely. For identification, the function is called linear-hyperbolic.

Only three parameters are required to define this functional representation of stress versus strain. Since the slopes of the linear part and the initial slope of the hyperbolic part are the same one parameter is eliminated, and since a peak PSD is not directly accounted for another is eliminated also. Of the several sets of three parameters which could be used, the set chosen was:

- the maximum linear stress (MLS),
- the corresponding maximum linear strain (EL), and
- the upper limiting stress (MS).

These three parameters are relatively easy to determine directly from an experimental plot of PSD versus axial strain and provide a good measure of flexibility in fitting a broad range of experimental curves. Moreover, the initial linear part lends itself to an easy beginning for a wave propagation analysis. Figures 3.5 and 3.6 illustrate the linear-hyperbolic stress-strain function. Shown are two sets of four different curves. The first set (Figure 3.5) reflects a modest range of stress levels (MS=400-800 psi; MLS=25, 50, 75, and 100% of MS). The maximum linear strain was arbitrarily set at 2%. The four resulting curves exhibit a broad range of curve shapes from the smoothly yielding lower curve (MLS=100 psi, EL=2%, MS=400 psi) to the elasto-plastic upper curve (MLS=800 psi, EL=2%, MS=800 psi). The second set (Figure 3.6) illustrates the magnitude of change of curve shapes that can be effected by varying the parameter EL alone. Comparing the two sets of curves to one another (Figures 3.5 and 3.6), the corresponding stresses in each set of curves are the same while the maximum linear strains differ.

On Figure 3.7 is reproduced the experimental principal stress difference versus axial strain curve obtained using the upper load cell during FTRXD test RDCFS14 (see Figure 3.3 also). Fitting of the linear-hyperbolic function to this experimental curve is illustrated on Figure 3.8. The fitting was accomplished

by selecting values of the three parameters (MLS, EL, and MS) from a visual examination of the experimental curve. These values were then used to calculate linear-hyperbolic stress-strain values and plot the results. Visual examination of Figure 3.8 suggests that the linear-hyperbolic stress-strain plot is an acceptable representation of the experimental curve. The center linear-hyperbolic plot seems to be the best fit of the three shown.

A more refined curve fitting process is certainly possible. However, first the on-going wave analyses of the test specimen or the analyses of the test apparatus system should validate the usefulness of the linear-hyperbolic function as representative of soil stress-strain behavior. One approach to the curve fitting process is to define criteria for fitting the mathematical functions to the experimental curves, and then automate the process using system identification techniques.

17

TABLE 3.1

Test Parameters for STRX Testing of Five CARES-Dry Specimens

Test Number	Confining Pressure	Wet Density	Water Content	Number of Lifts	Mold Size	Test Duration
RDX-TXC-10	50 psi	119 pcf	5.0%	3	2 × 5	5-10
RDX-TXC-11	100 psi	119 pcf	4.9%	5	2 × 5	min
RDX-TXC-12	100 psi	119 pcf	5.0%	5	2 × 5	do
RDX-TXC-13	100 psi	119 pcf	4.9%	5	2 × 5	do
RDX-TXC-01	200 psi	119 pcf	5.1%	3	3 × 6	do

TABLE 3.2

Test Parameters for FTRXD Slow Testing of Six CARES-Dry Specimens

Test Number	Confining Pressure	Wet Density	Water Content	Number of Lifts	Mold Size	Test Duration
RDCFS10	50 psi	113 pcf	4.0%	3-5	0.75 × 1.5	120 sec
RDCFS14	100 psi	113 pcf	3.8%	3-5	0.75 × 1.5	120 sec
RDCFS18	200 psi	113 pcf	4.4%	3-5	0.75 × 1.5	120 sec
RDCFS36	50 psi	119 pcf	*4.0%	3-5	0.75 × 1.5	1.2 sec
RDCFS40	100 psi	118 pcf	*4.0%	3-5	0.75 × 1.5	1.2 sec
RDCFS43	200 psi	119 pcf	*4.0%	3-5	0.75 × 1.5	1.2 sec

* batch value: specimens contaminated by posttest leakage

Fig 3.1, CARES-Dry Average Grain Size Distriburion

Sample No.	Elev or Depth	Classification	Nat w %	LL	PL	PI
		Clayey Sand (SC), Brown		36	17	19
		Gs = 2.68				
		(Average of 3 Data Sets)				

Project REMOLDED CARES-DRY SAND

Area

Boring No.

GRADATION CURVES

Date
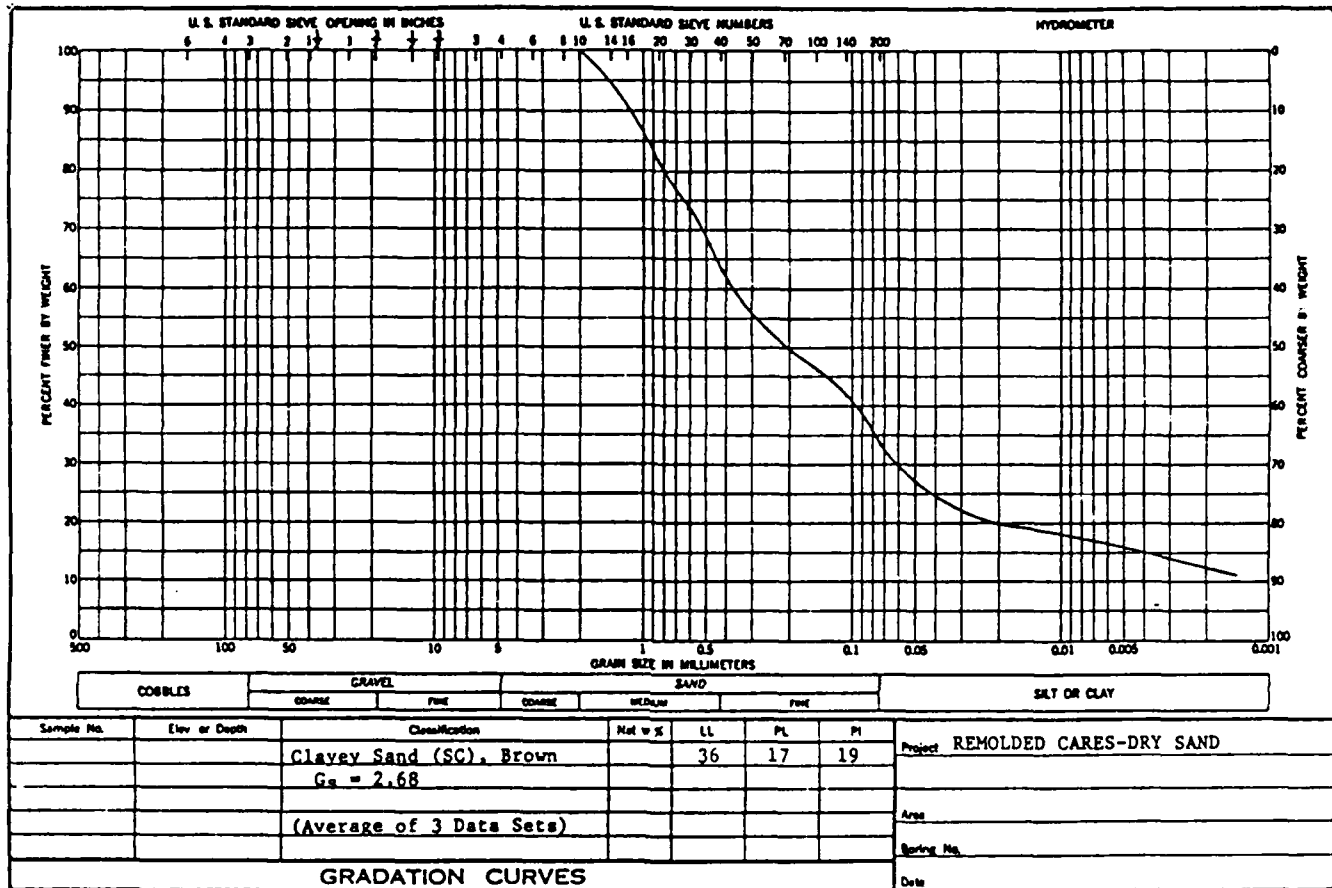
Fig 3.2, STRESS−STRAIN TEST DATA

DURATION = 5 MIN : RDX−TXC10,11,12,13,1
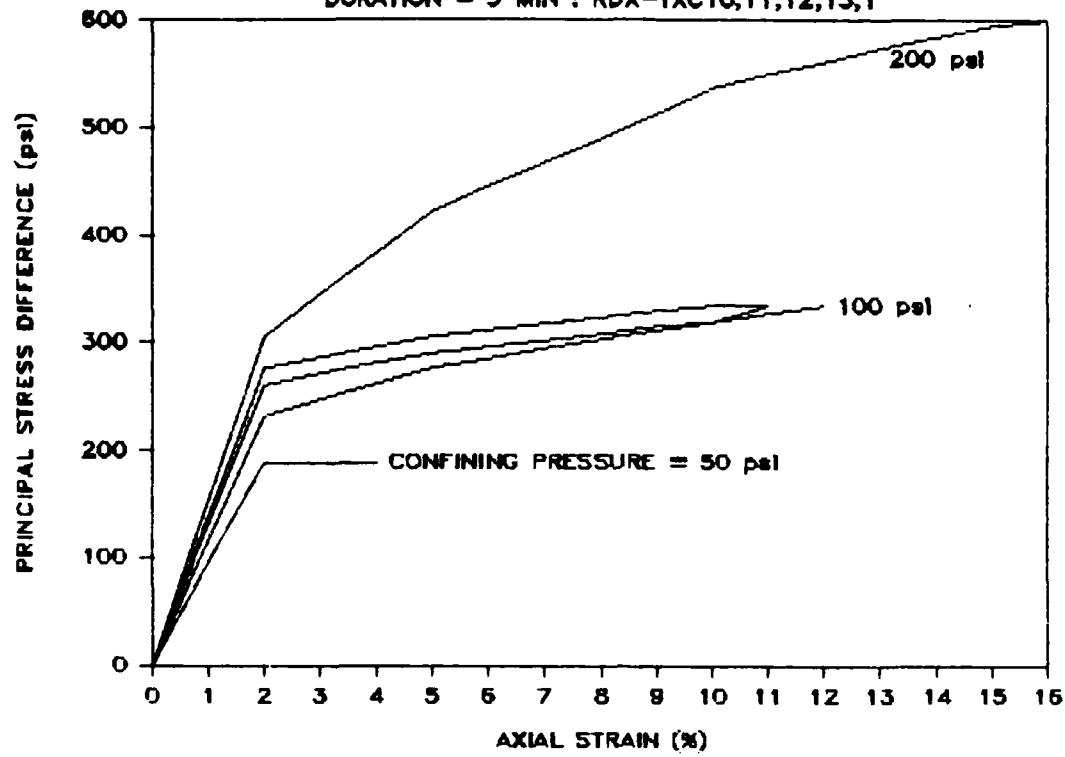
Fig 3.3, STRESS-STRAIN TEST DATA

DURATION = 120 SEC : RDFCS 10, 14, 18
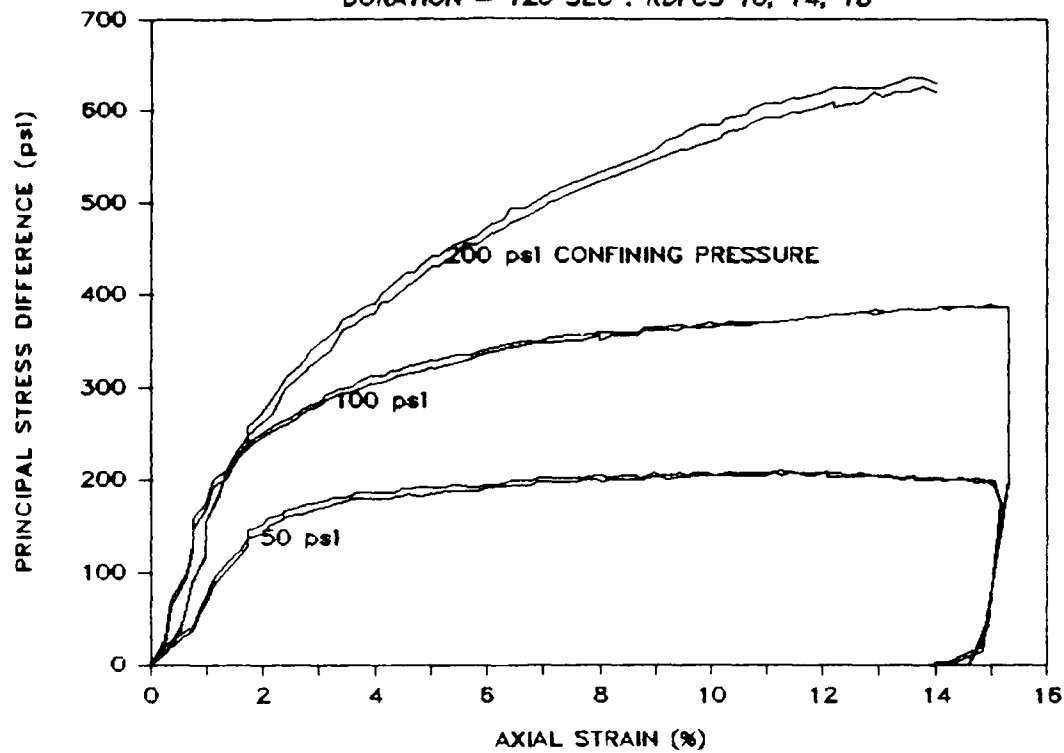
Fig 3.4, STRESS-STRAIN TEST DATA

DURATION = 1.2 SEC : RDCFS 38, 40, 43

21

Fig 3.5, LINEAR−HYPERBOLIC FUNCTION

STRESS−STRAIN RELATIONSHIPS

MLS=800 psi, EL=2.0 %, MS=800 psi

MLS=450 psi, EL=2.0 %, MS=600 psi

MLS=250 psi, EL=2.0 %, MS=500 psi

MLS=100 psi, EL=2.0 %, MS=400 psi
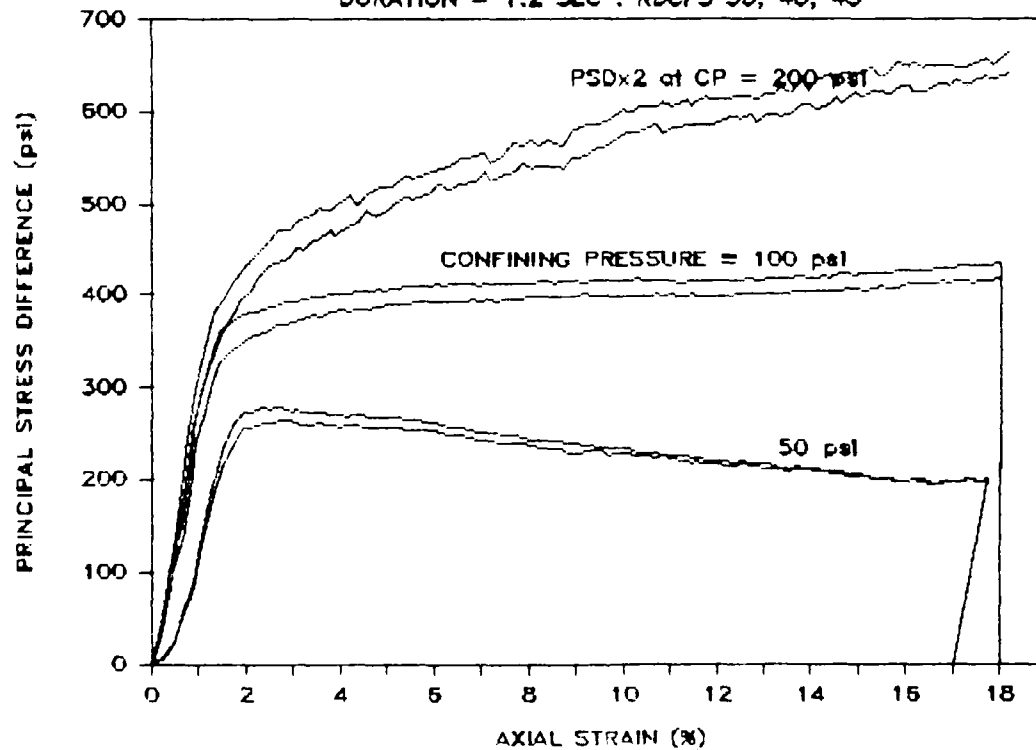
STRAIN (%)

Fig 3.6, LINEAR−HYPERBOLIC FUNCTION

STRESS−STRAIN RELATIONSHIPS

MLS=800 psi, EL=12.5 %, MS=800 psi
MLS=450 psi, EL= 5.0 %, MS=600 psi
MLS=250 psi, EL= 1.0 %, MS=500 psi
MLS=100 psi, EL= 0.2 %, MS=400 psi

STRAIN (%)

22
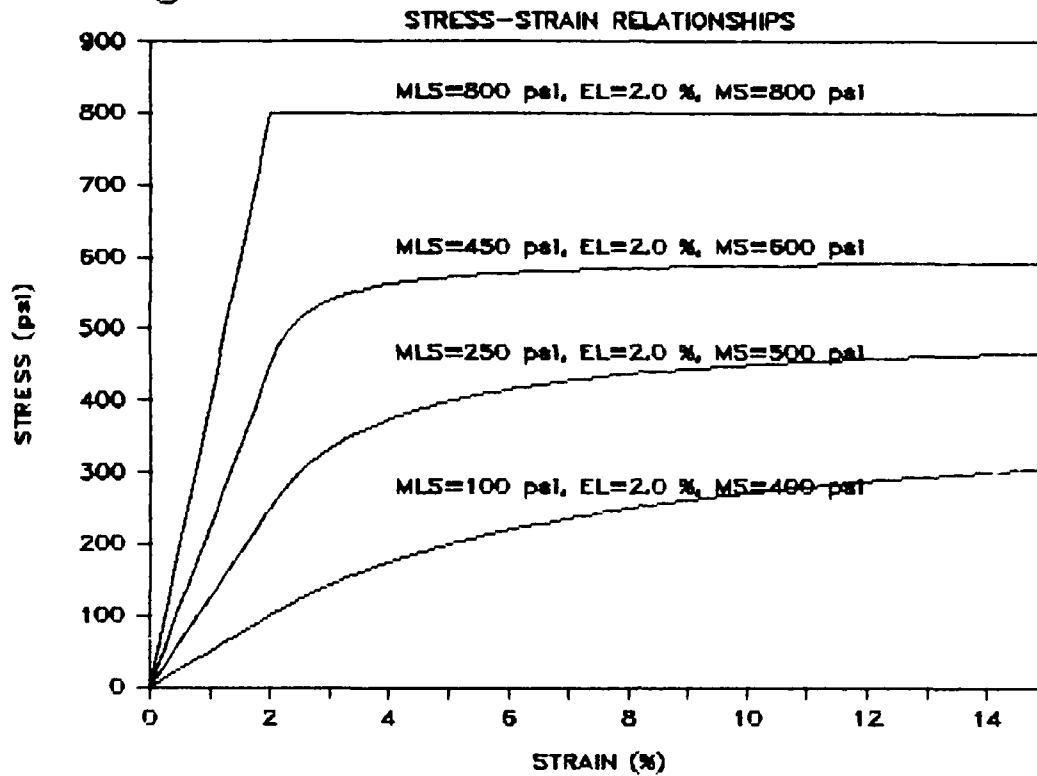
Fig 3.7, STRESS–STRAIN TEST DATA

UPPER LOAD CELL, TEST RDCFS14
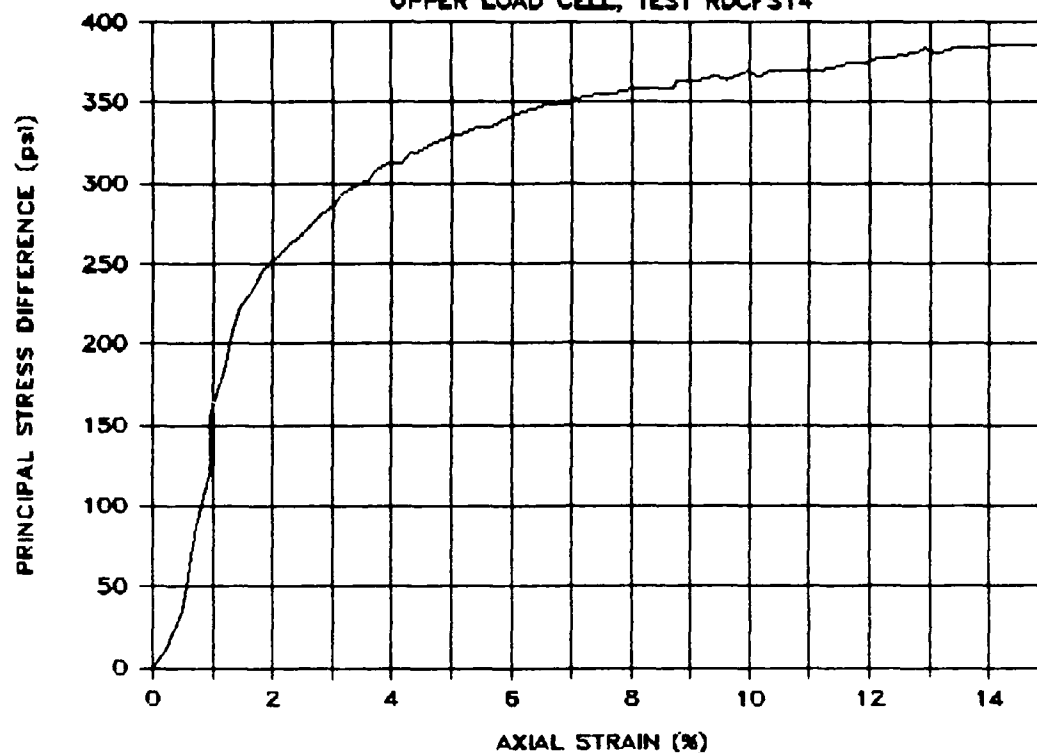
Fig 3.8, TEST & LIN–HYP STRESS–STRAIN

UPPER LOAD CELL, TEST RDCFS14

EXPERIMENTAL
MLS=200 psi, EL=1.4 %, MS=400 psi
MLS=150 psi, EL=1.0 %, MS=425 psi
MLS=100 psi, EL=0.8 %, MS=450 psi

23
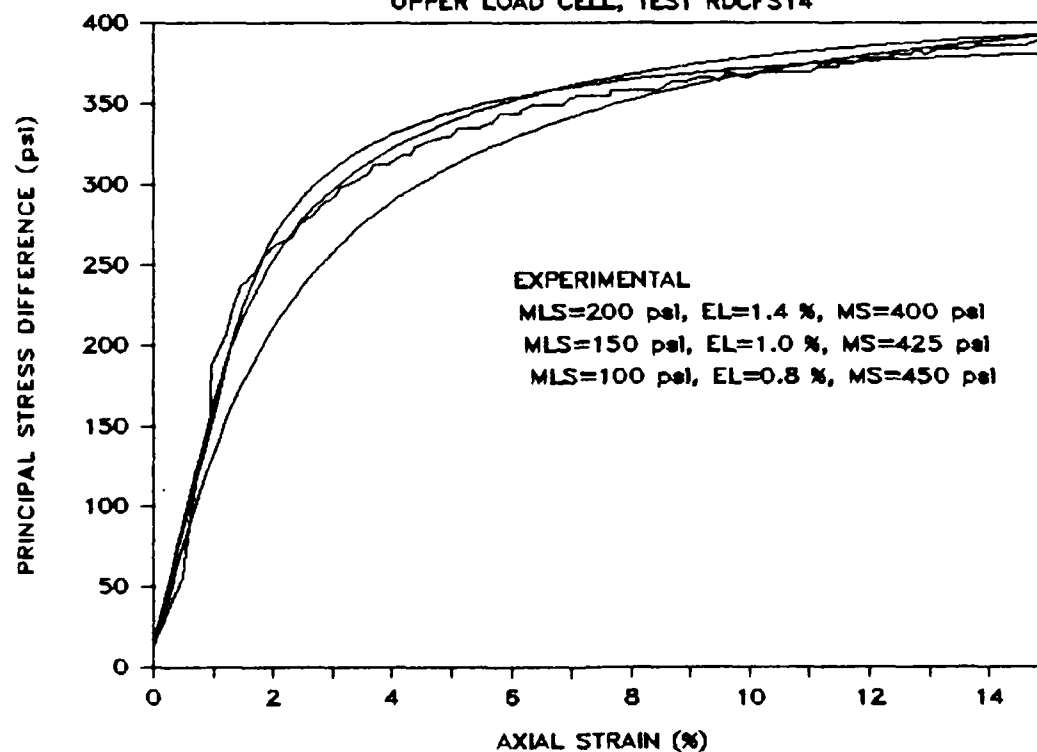
CHAPTER 4

PRELIMINARY DYNAMIC TEST RESULTS FROM THE FTRXD

4.1 INTRODUCTION

Dynamic tests are those run rapidly enough to begin to cause inertial effects to occur in the specimen, and consequently to make wave analyses of the specimen of interest. For these purposes, the dynamic tests were identified as those in which the test duration was 30 milliseconds or less. The test duration was considered over when an axial strain of 15% was reached in the specimen. Seven such tests are described here to illustrate the nature of the dynamic test results. Four of the tests were completed in 28 milliseconds and three in 2 milliseconds. Confining pressures of 50, 100, and 200 psi were imposed in both the 28-millisecond and 2-millisecond duration tests.

4.2 LOAD-TIME DATA

Figures 4.1 through 4.4 show measured load versus time for the four 28-millisecond duration tests with results from both the upper and lower load cells. The confining pressure used is indicated and is the only experimental quantity that differs among the four tests; it is 50 psi for test RDCFS49 (Figure 4.1), 100 psi for test RDCFS52 (Figure 4.2), and 200 psi for both tests RDCFS56 and 57 (Figures 4.3 and 4.4). For some reason, the magnitudes of upper and lower load readings in these latter two tests was recorded as about one-half of what was expected, just as occurred in the slow test on the FTRXD at a confining pressure of 200 psi (see Figure 3.4). Other testing of the CARES-Dry soil at confining pressures of 50, 100, and 200 psi are the basis for expecting the load values in these three tests at a confining pressure of 200 psi to be much higher. The load recorded in all four tests by the upper load cell was about 12 to 15 percent higher than for the lower load cell. Recall that this phenomenon was also evident, but less pronounced, in the slow tests with durations of 120 and 1.2 seconds.

Figures 4.5 through 4.7 show measured load versus time for the three 2-millisecond duration tests. Confining pressures of 50, 100, and 200 psi were employed on these tests, RDCFS69, 72, and 74 respectively (Figures 4.5, 4.6, and 4.7). The conduct of these very rapid tests precluded the use of oil in the lower chamber of the l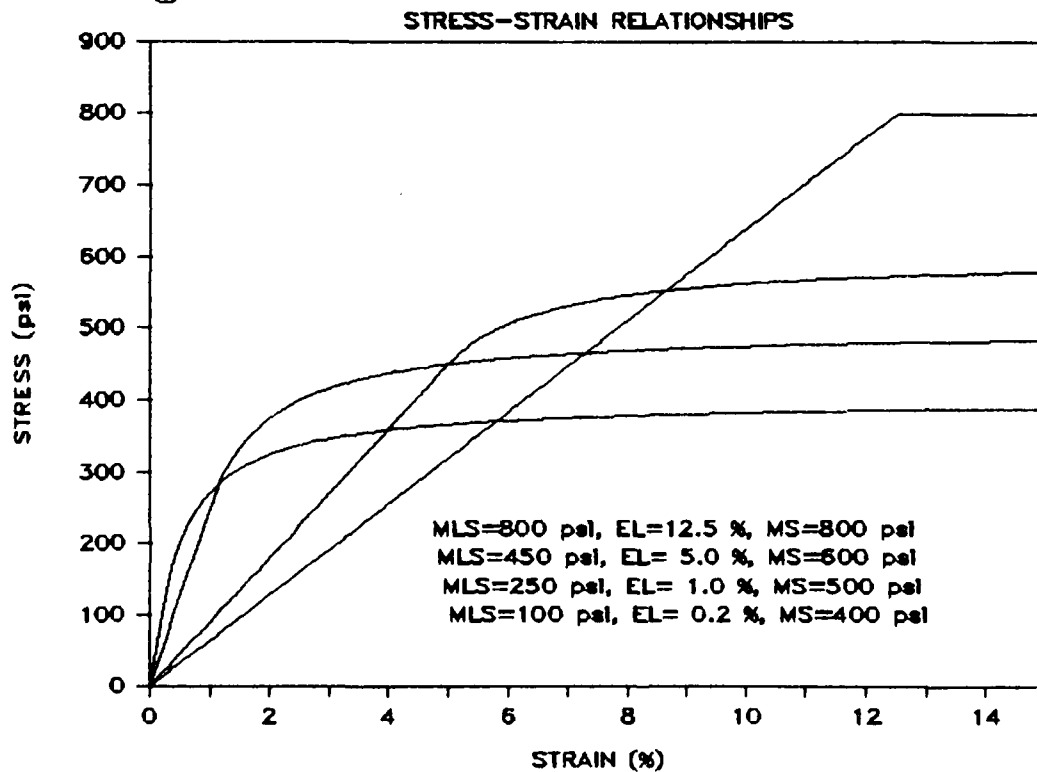oad cylinder to control and damp the motion of the piston-ram assembly. In test RDCFS69 (Figure 4.5) where the confining pressure was 50 psi, the resistance which the specimen could offer to oppose the loosely controlled motion of the ram seems to have been obscured by the motion of the ram. The readings from the upper load cell (which moves with the ram) reflect this strongly. The readings from the stationary lower load cell are more predictable. The situation is similar, but

less pronounced in test RDCFS72 (Figure 4.6) where the confining pressure was 100 psi and the specimen stronger. In test RDCFS74 (Figure 4.7) where the confining pressure was 200 psi, the readings from the upper load cell show a variation one might anticipate in a very rapid test, while the stationary lower load cell shows a smooth variation, similar to what was exhibited in the slower tests. Note the magnitudes of the load cell readings in this test are about what one might expect rather than half that much. Also note the upper load cell readings, at least in test RDCFS74 (Figure 4.7), are on the order of 40 percent higher than those for the lower load cell. The discrepancy between the upper and lower load cell readings was consistent from the very slow to the very rapid tests. The upper load cell always read higher values. The discrepancy also increased significantly from about 1 percent for the slow tests to 40 percent for the very rapid tests.

4.3 DISPLACEMENT-TIME DATA

The measured variation with time of the displacement of the top of the specimen during the seven dynamic tests is shown on Figures 4.1 through 4.7 along with the load-time variation discussed above. The displacement variation is not linear; it curves upward with increasing slope – more severely the more rapid the test. Displacement-time variation of the top of the specimen is essential to the wave analysis of the specimen. It is taken as the boundary condition at the top of the specimen so that displacements, strain, stress, and load can be calculated throughout the specimen. Moreover, the displacement versus time data must permit the calculation of velocities and accelerations with reasonable accuracy since acceleration and perhaps velocity will appear in any form of the wave equation employed. One way to achieve this calculation ability is to fit a mathematical function to the displacement data, and then differentiate the function to obtain velocities and acceleration. Measured velocity and acceleration data along with measured displacement data would be the best approach, but this was not possible at the time these tests were run.

In tests RDCFS49, 52, 56, and 57 (Figures 4.1 through 4.4), the variation of displacement with time is smooth with an increasing slope throughout the duration of the test. The curves approach a straight line during the latter part of each test. This variation suggests a function whose slope or velocity begins at an initial value of zero and then increases smoothly to a limiting value. One might expect such a variation in the FTRXD since these and all the slower tests were run with oil in the lower chamber of the load cylinder. During the conduct of the tests the piston-ram was initially at rest, the upper chamber of the load cylinder was under pressure, and the oil in the lower chamber was under pressure. The test was initiated by rapidly opening a valve in the lower chamber connecting it to the accumulator at atmospheric pressure, while maintaining the

pressure in the upper chamber. Thus the oil was forced out of the lower chamber through the opened valve. The piston-ram moved under the influence of the constant upper chamber pressure and the lower chamber oil flowing back to the accumulator. The ram therefore started from rest, its velocity increasing but approaching a limit since the rate at which the oil could pass through the opened valve was limited.

A simple mathematical function describing a smoothly increasing velocity which approaches an upper limit is a two-parameter hyperbola. Figure 4.8 shows a plot of the two-parameter hyperbola (velocity), its integral (displacement), and its first derivative (acceleration). The two parameters needed to define the curve are its initial slope and its limiting value. The initial slope (Ao) is the initial acceleration and its limiting value (Vo) is the terminal velocity. Another useful calculated parameter is the characteristic time (To), which is the ratio Vo/Ao. The hyperbola can easily be fitted to the velocity variation with time, if good velocity data is available and varies as described. The fitting procedure is to plot the reciprocal of velocity versus the reciprocal of time. The result is a straight line for the hyperbolic function. The slope of this line is the reciprocal of the initial acceleration (Ao); the intercept of the line on the 1/V axis is the reciprocal of the terminal velocity (Vo). If the experimental velocity data also plots as a straight line on these reciprocal axes, the hyperbolic fit is achieved by reading the slope and intercept of the experimental line.

On Figure 4.9 is reproduced the plot of measured displacement versus time of the top of the specimen in test RDCFS56 (see also Figure 4.3). The data were reported at 0.3-millisecond intervals. The displacement was differentiated numerically with a 3-point central difference expression on a 0.6-millisecond time increment to obtain velocities at intervals of 0.3 milliseconds. The result is also shown on Figure 4.9. The oscillating nature of the calculated velocity is not easy to interpret. It probably reflects the effects of dynamics in the FTRXD system, innaccuracies in recording the displacement data, and the details of the numerical process used in differentiation. Higher order difference expressions and corresponding larger time increments were tried. They smooth the peaks and valleys of the oscillations some, but they also seem to change the overall shape of the velocity-time curve. This overall shape of the velocity curve is apparent on Figure 4.9, and could be represented approximately by the two-parameter hyperbola.

Figure 4.10 repeats the motion data of Figure 4.9 and also shows the comparable motion described by a two-parameter hyperbola. The velocity data derived from the experimental displacement data was not good enough to permit fitting the hyperbola to it using a reciprocal axes plot. Consequently, the limiting velocity, Vo, was estimated by examining the slope of

27

the overall displacement plot in the latter part of the test duration. The characteristic time, To, was obtained by trying several values and selecting the one that produced the best visual fit of both velocity and displacement. The result is shown on Figure 4.10. As with fitting of the linear-hyperbolic function to stress-strain data, a more refined fitting procedure for the upper pedestal motion of the FTRXD could be developed. However it should be justified by the motion data, the wave analyses of the specimen, and the analyses of the FTRXD system. Moreover, the addition of accelerometers or other motion measuring devices to the upper pedestal may be necessary to validate both the mathematical functions used and the procedures followed to fit them to the motion data.

Figure 4.11 repeats the data of Figure 4.10, but adds acceleration data. Differentiating the measured displacement twice to obtain acceleration data required smoothing the velocity data first. The smoothing procedure was to average the eleven velocity values nearest each time value (the velocity value at the time value with the five velocity values immediately before and after). These eleven values included about one period of observed oscillation on each side of the time value. The smoothed velocity-time variation was then differentiated to obtain accelerations in the same manner that the displacement-time variation was differentiated earlier to obtain velocities. The acceleration data is less meaningful than the velocity data and affected by the same unknown factors, even more strongly. The overall variation of acceleration, however, does seem to follow the fitted hyperbolic acceleration which is plotted through it.

Figures 4.5 through 4.7 show the variation of the displacement of the top of the specimen with time during the very rapid tests RDCFS69, 72, AND 74. In these very rapid tests the displacement curves turn up more sharply than in the slower tests, especially during the latter part of each test. Recall that to achieve test durations of two milliseconds, oil could not be used in the lower chamber of the load cylinder. Consequently the motion of the ram in these tests is not restricted by the flow of oil through a valve.

Figures 4.12 and 4.13 show the results of an analysis of the motion of the top of the specimen during the very rapid test RDCFS74. As with the data from the slower test RDCFS56 (Figures 4.9 though 4.11), the displacement data and the results of differentiating it to obtain velocities are shown. Oscillations are again present, but the overall variation of velocity with time is apparent. Clearly in these very rapid tests, a two-parameter hyperbola cannot be used to describe the motion. The velocity was smoothed by averaging the thirteen values of velocity nearest each time value. The data were reported at time intervals of 0.02 milliseconds so that the six velocity values on each side of the time value included approximately one period of the observed oscillations. The smoothed velocity variation was

then differentiated to obtain accelerations in the same manner as was done earlier. Displacement, velocity, and acceleration data are shown on Figure 4.13. It is worth noting that the calculated accelerations are large. The initial spike at 0.05 milliseconds is 2200 g's. The calculated acceleration reaches values of 400 g's several times during the test, and sustains them from about 0.9 to 1.4 milliseconds. At this stage in the project no attempt was made to fit a mathematical function to the motion data of the very rapid tests. The initial wave analyses used to model these tests were based on an assumed constant acceleration of the upper pedestal through out the test, which leads to an upward curving parabolic displacement-time variation.

4.4   DYNAMIC STRESS-STRAIN DATA

The experimentally calculated values of stress versus strain for the dynamic tests are shown on Figures 4.14 and 4.15. Since the stress was calculated from the load cell readings, it necessarily includes the effects of inertial forces in the specimen and the dynamics of the FTRXD, if they are present. When these effects are significant, they will mask the stress-strain properties of the specimen on experimental plots such as these.

For the tests with a duration of 28 milliseconds (Figure 4.14), the relationships are very similar to all of the slower tests. The differences in the upper and lower load cell readings are noticeably larger than they were in the slower tests, and the magnitudes of principal stress difference are larger also. These curves can be represented by the linear-hyperbolic function equally as well as the slower tests can be, though clearly the magnitudes of the parameters MLS, EL, AND MS would differ. It would appear that the 28-millisecond duration and slower tests on 0.75-inch-diameter by 1.5-inch-high specimens of the CARES-Dry soil are not significantly affected by specimen inertia or the dynamics of the FTRXD.

The tests of 2-millisecond duration (Figure 4.15) also show a similar manner of variation of stress with strain - that is one which can be reasonably represented by the linear-hyperbolic function - when the effects of inertia and system dynamics can be screened. Figure 4.15 shows the plots of stress and strain for the very rapid tests using only the stationary lower load cell. For test RDCFS74 at a confining pressure of 200 psi, the curve is remarkably similar to stress-strain curves of slower tests. Recall at this high confining pressure the specimen was strong enough to not be dominated by the loosely controlled motion of the piston and ram. The very rapid tests at lower confining pressures are also shown on Figure 4.15. Stress and strain does not track so well for these tests since the overpowering motion of the piston and ram is evident. Attempting to calculate stress directly from the upper load cell readings is not meaningful. The moving upper load cell clearly registered significant inertial effects of its motion as well as that of the rest of the FTRXD.

29

Fig 4.1, LOAD-DISPLACEMENT TEST DATA

CONFINING PRESSURE = 50 psi, (RDCFS49)
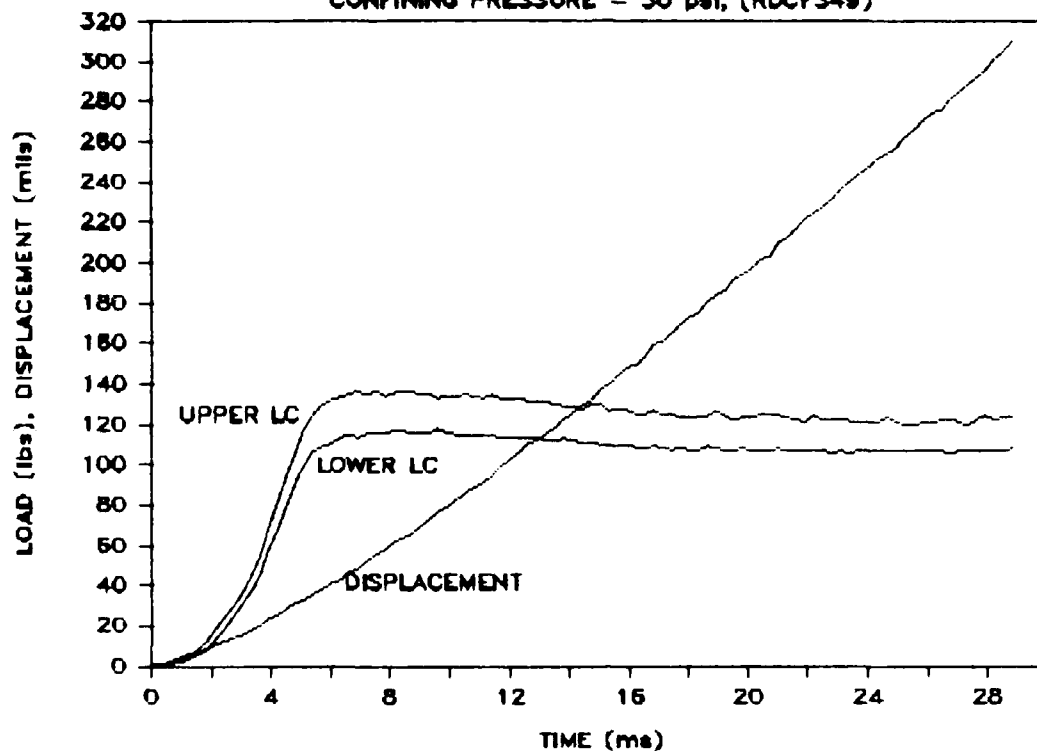
Fig 4.2, LOAD-DISPLACEMENT TEST DATA

CONFINING PRESSURE = 100 psi, (RDCFS52)

30
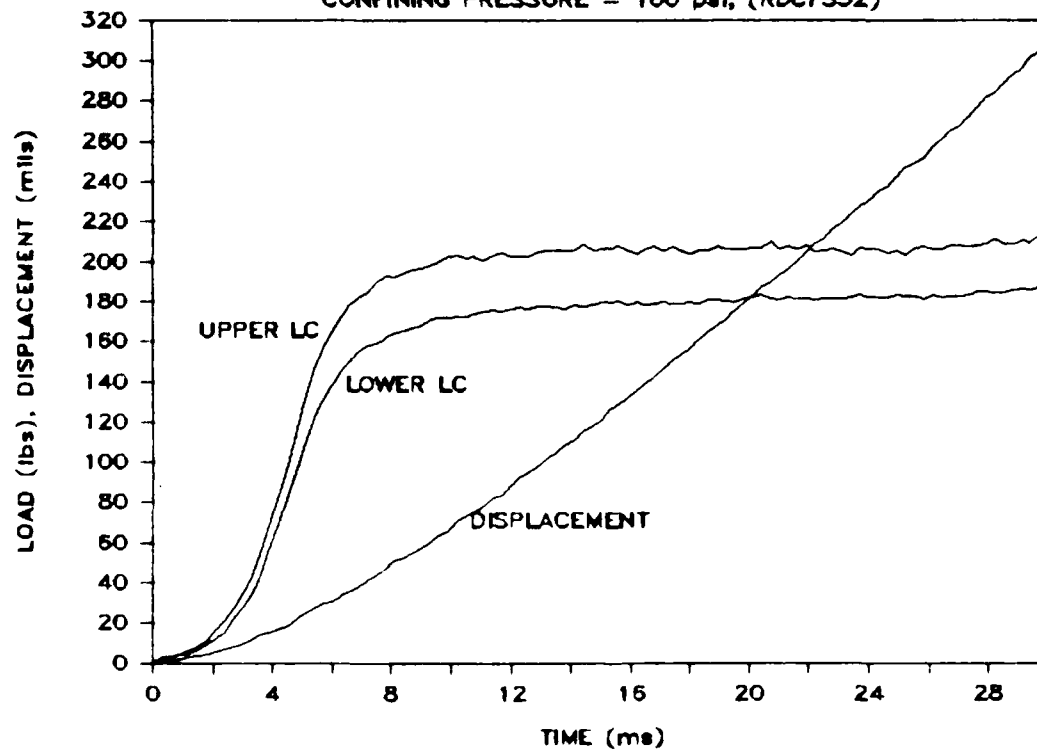
Fig 4.3, LOAD-DISPLACEMENT TEST DATA

CONFINING PRESSURE = 200 psi, (RDCFS56)
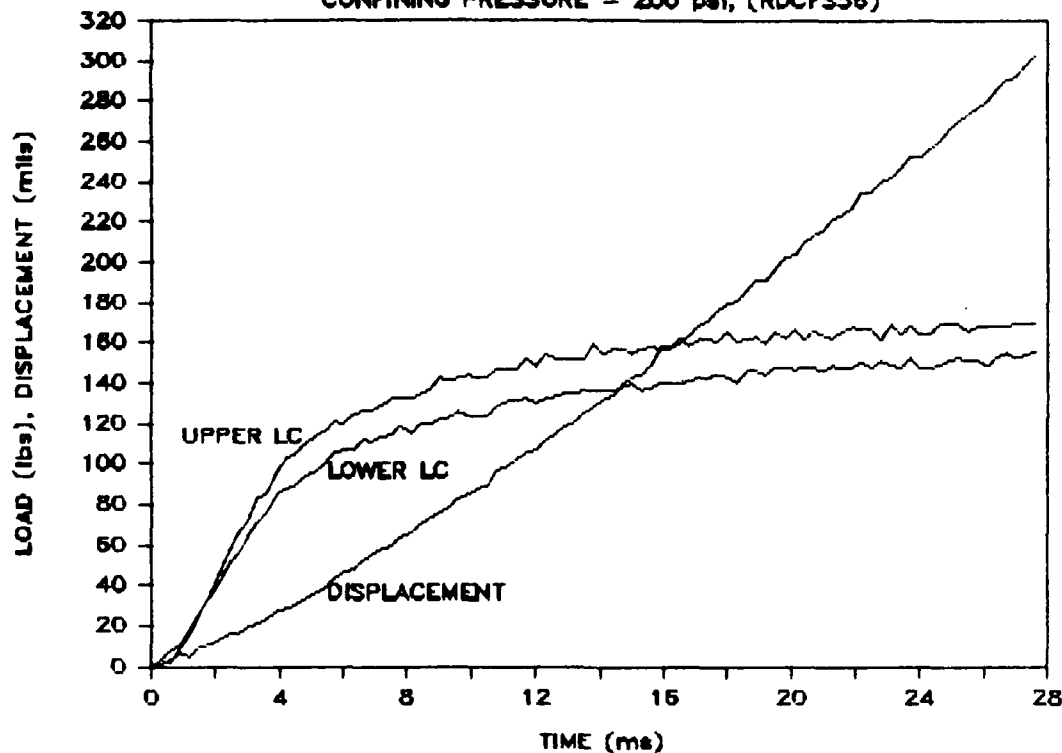
Fig 4.4, LOAD-DISPLACEMENT TEST DATA

CONFINING PRESSURE = 200 psi, (RDCFS57)

31
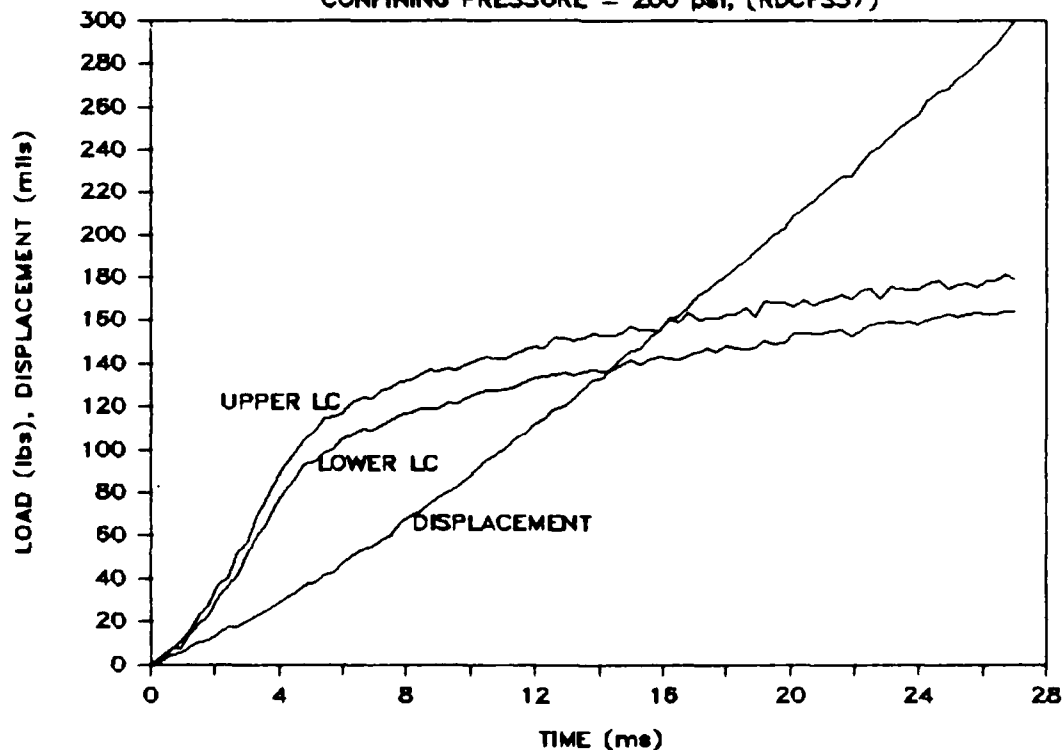
Fig 4.5, LOAD–DISPLACEMENT TEST DATA

CONFINING PRESSURE = 50 psi, (RDCFS59)
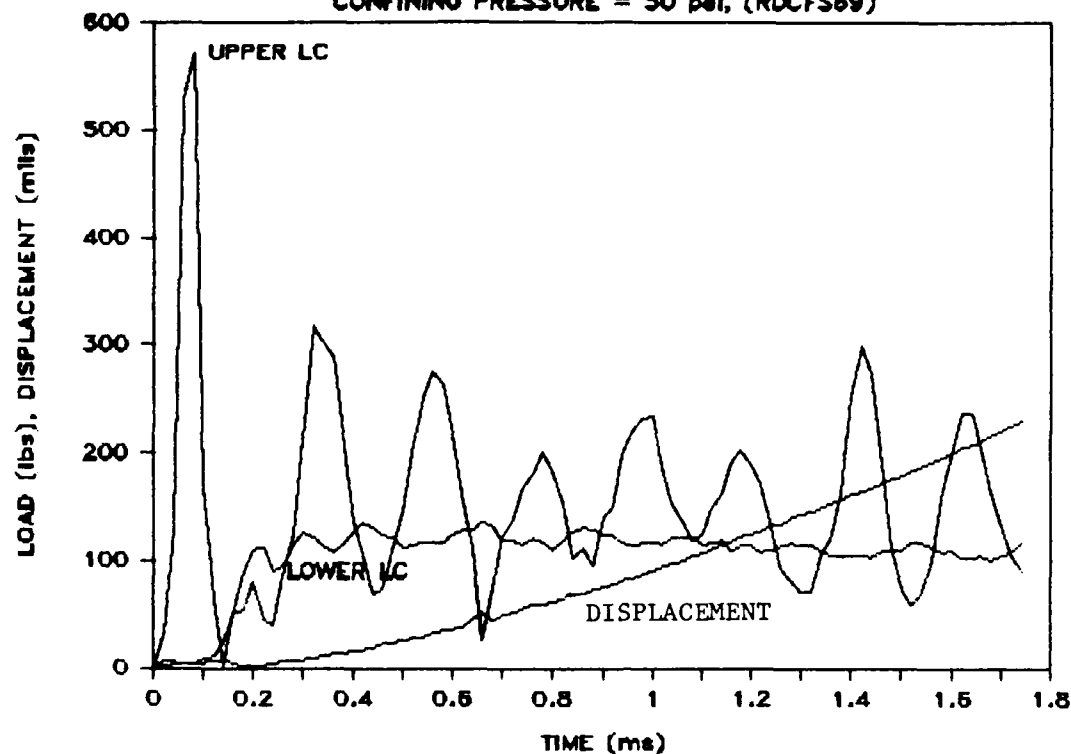
Fig 4.6, LOAD–DISPLACEMENT TEST DATA

CONFINING PRESSURE = 100 psi, (RDCFS72)
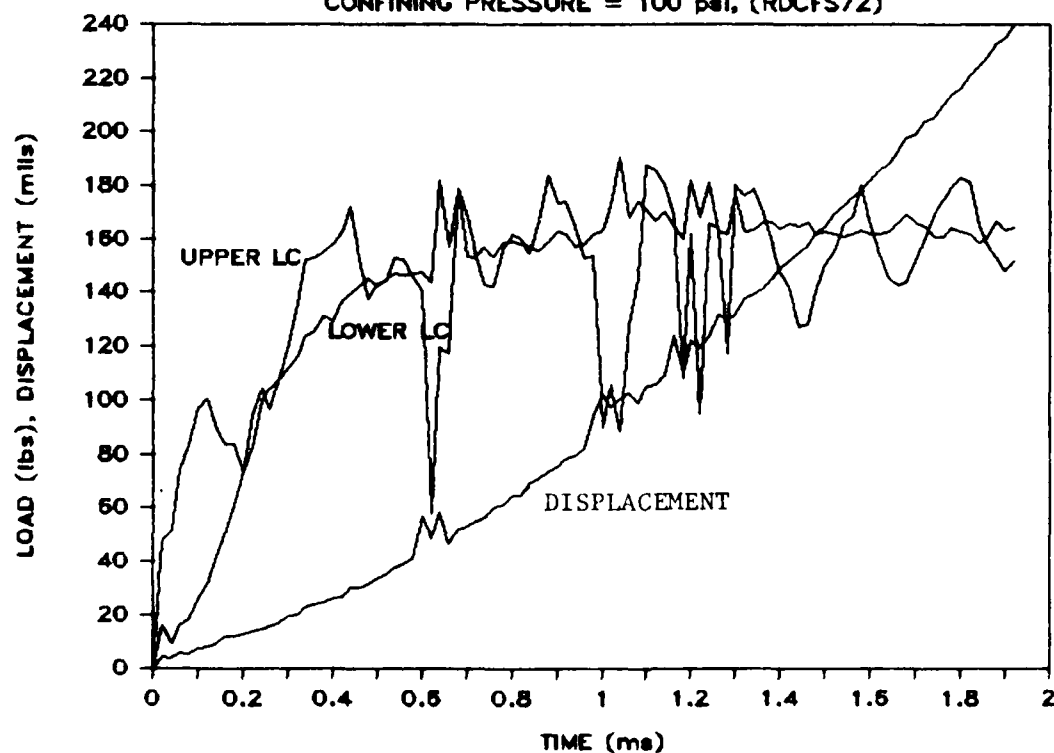
Fig 4.7, LOAD−DISPLACEMENT TEST DATA

CONFINING PRESSURE = 200 psi, (RDCFS74)

33
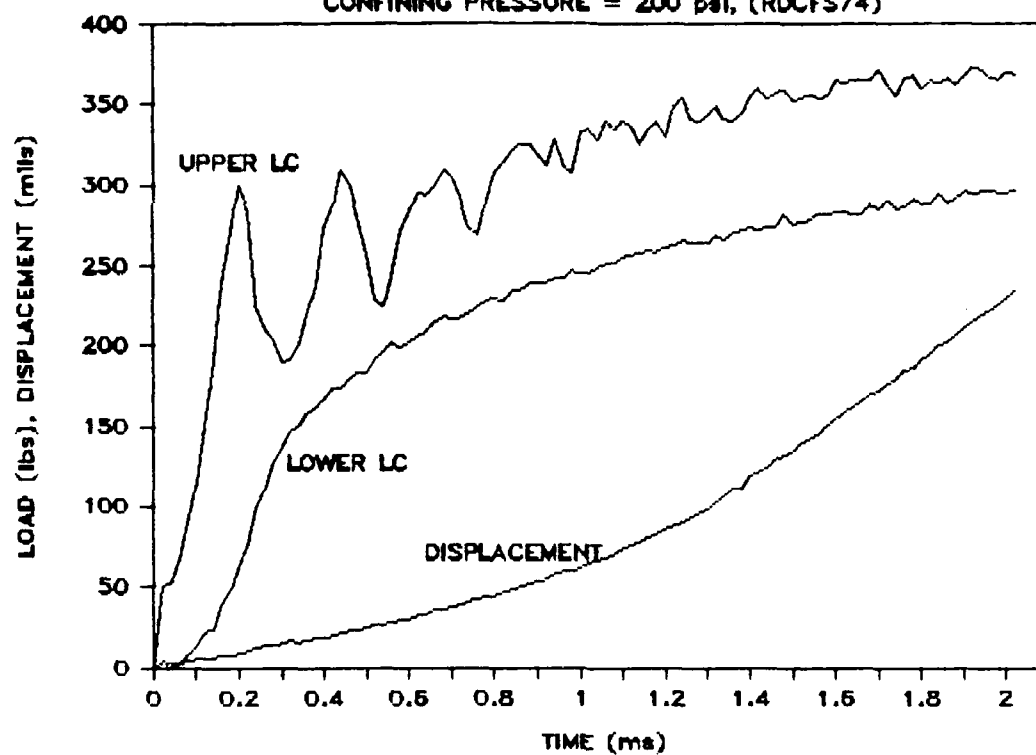
Fig 4.8, HYPERBOLIC UPPER PED. MOTION

Vo = 10.0 ips; To = 2.0 ms

V=VoT/(To+T)

D=VoT−VoToLN(1+T/To)

A=VoTo/(To+T)**2

VELOCITY

DISPLACEMENT

ACCELERATION

ACC (g), VEL (ips), DISP (mils/10)

TIME (ms)

Fig 4.9, UPPER PEDESTAL VELOCITY

TEST RDCFS56

CONFINING PRESSURE = 200 psi

DISPLACEMENT/10

VELOCITY

DISPL (mils), VEL (ips)

TIME (ms)

34
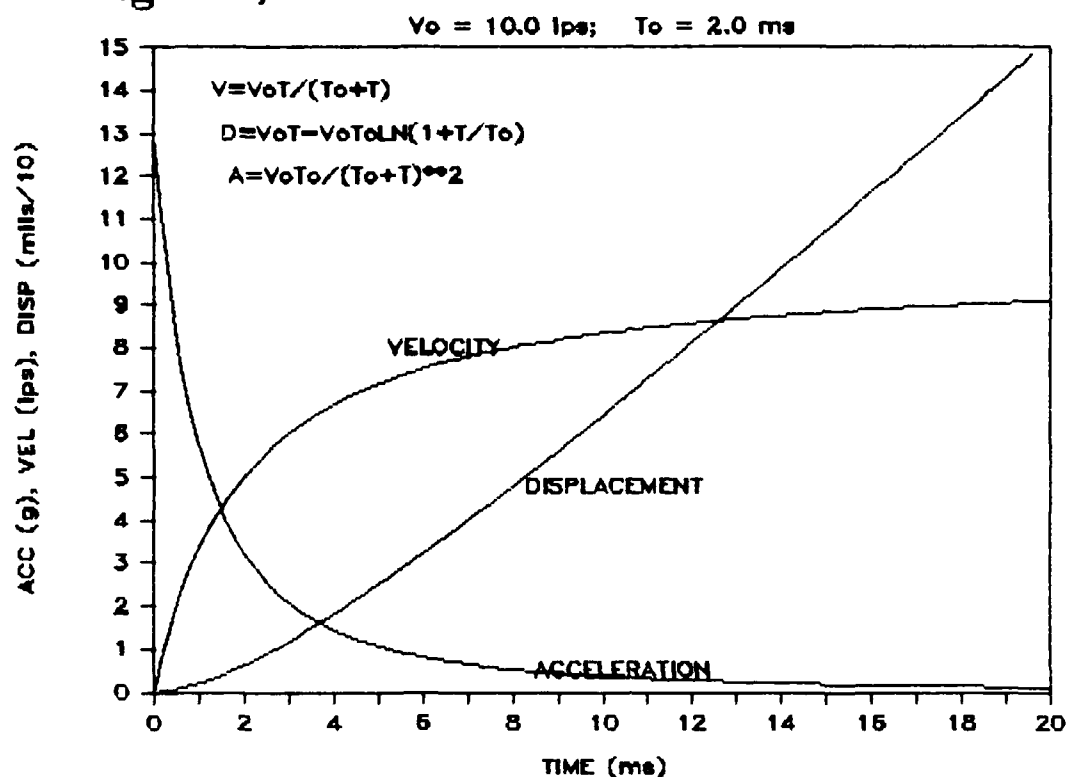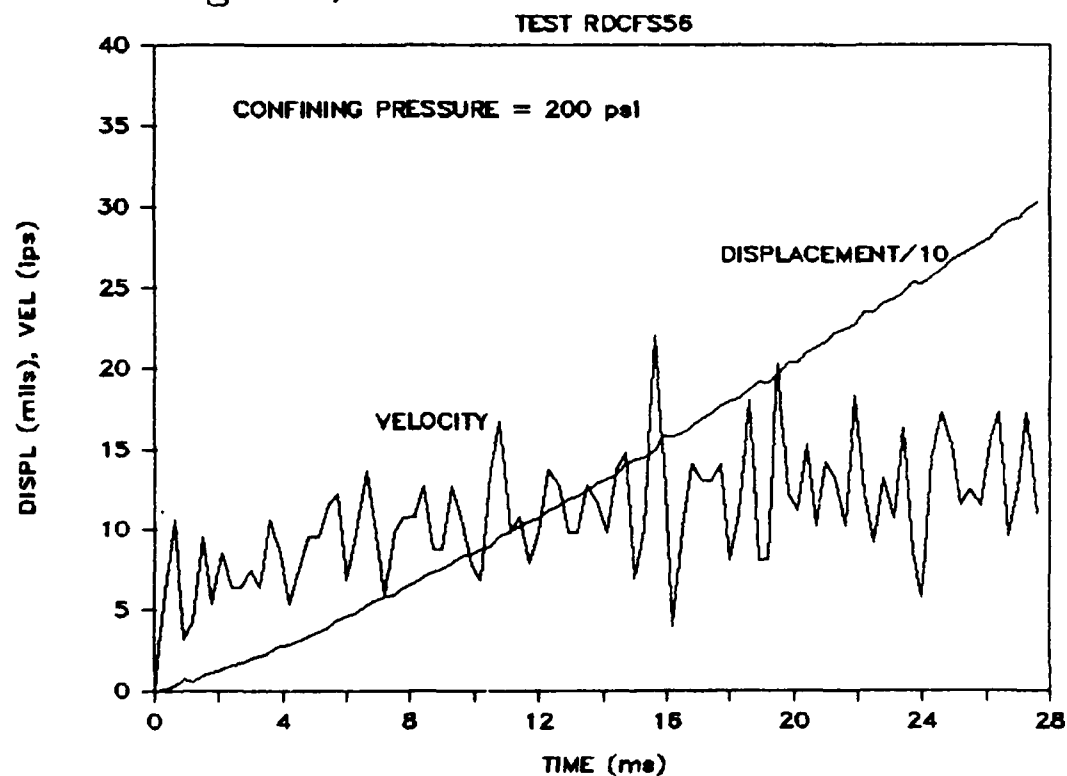
Fig 4.10, UPPER PEDESTAL VELOCITY
MEAS & HYP, TEST RDCFS56
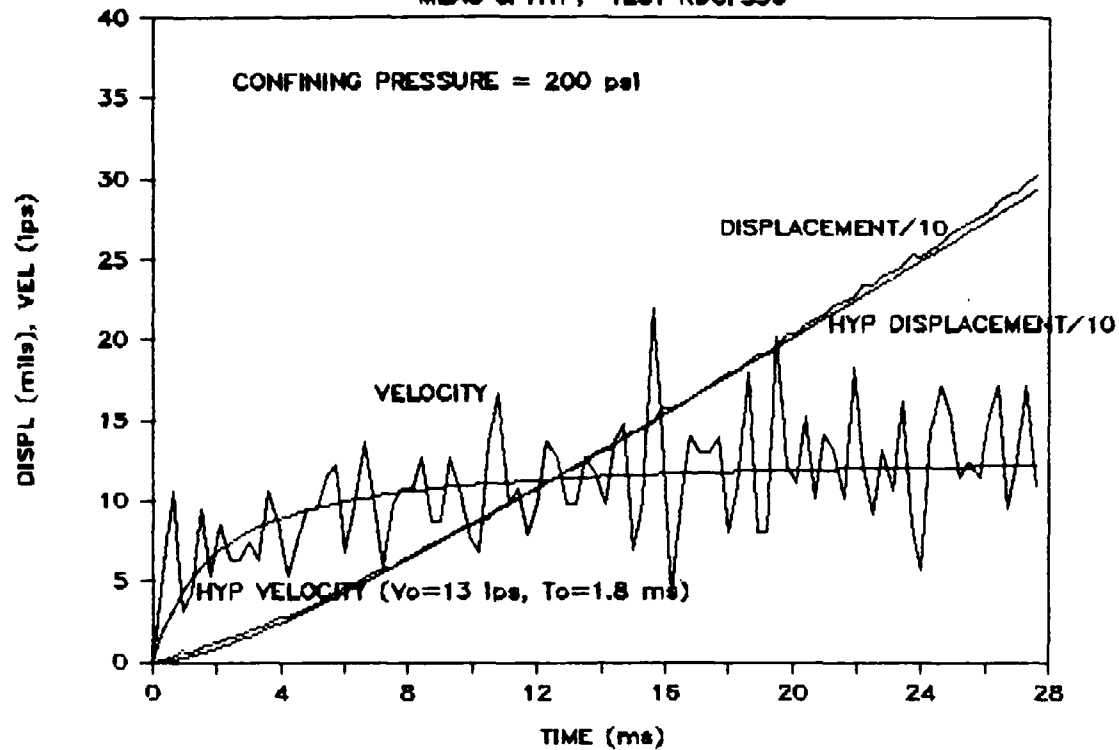
Fig 4.11, UPPER PEDESTAL MOTION
MEAS & HYP, TEST RDCFS56

35
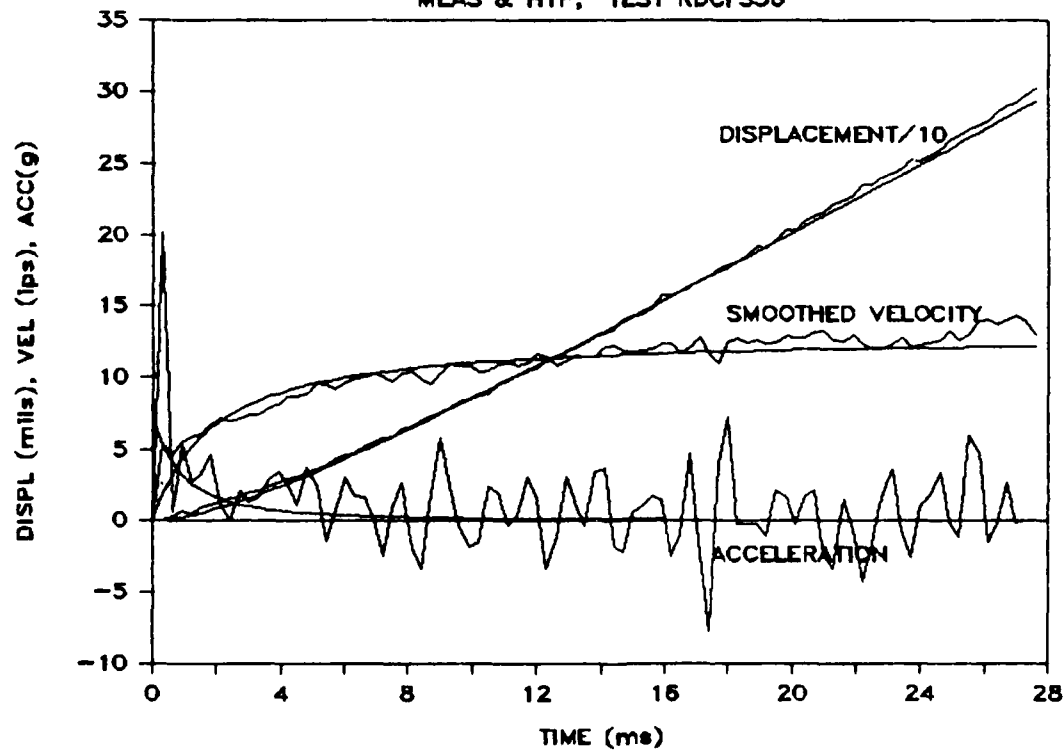
Fig 4.12, UPPER PEDESTAL VELOCITY

TEST RDCFS74

Velocity and displacement plot. Y-axis: DISPL (mils), VEL (ips), ranging from -20 to 260. X-axis: TIME (ms), 0 to 2. CONFINING PRESSURE = 200 psi. Curves labeled VELOCITY and DISPLACEMENT.
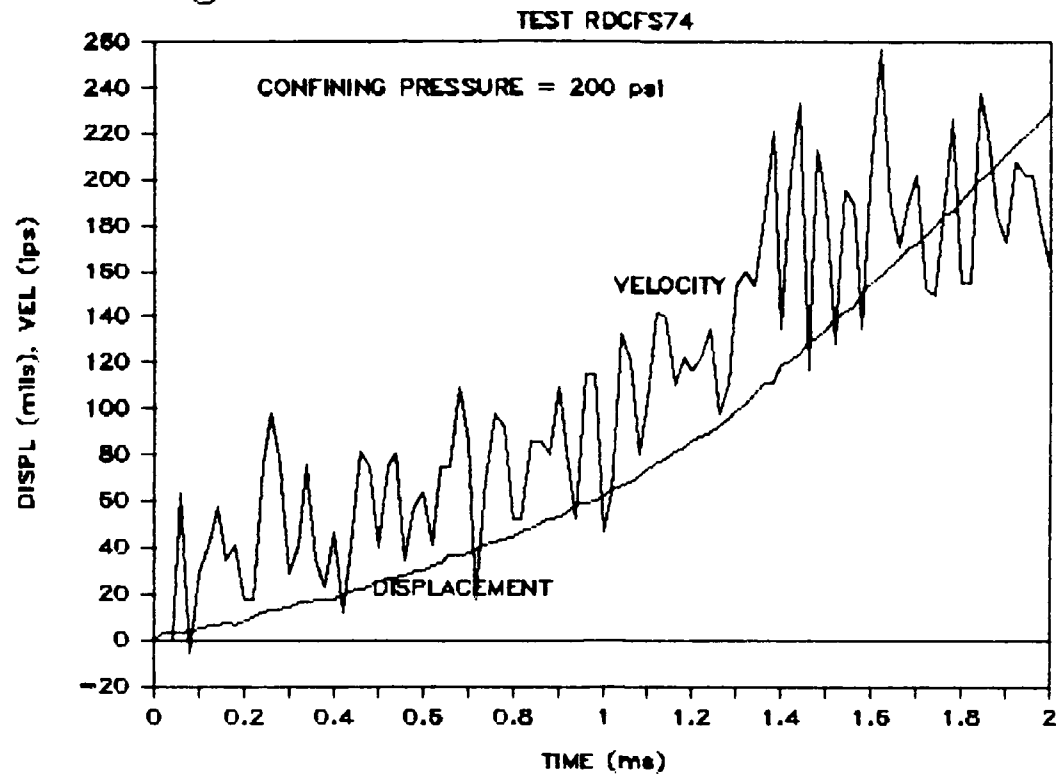
Fig 4.13, UPPER PEDESTAL MOTION

TEST RDCFS74

Motion plot. Y-axis: DISPL (mils), VEL (ips), ACCEL(G/10), ranging from -20 to 260. X-axis: TIME (ms), 0 to 2. CONFINING PRESSURE = 200 psi. Curves labeled SMOOTHED VELOCITY, DISPLACEMENT, and ACCELERATION.

36
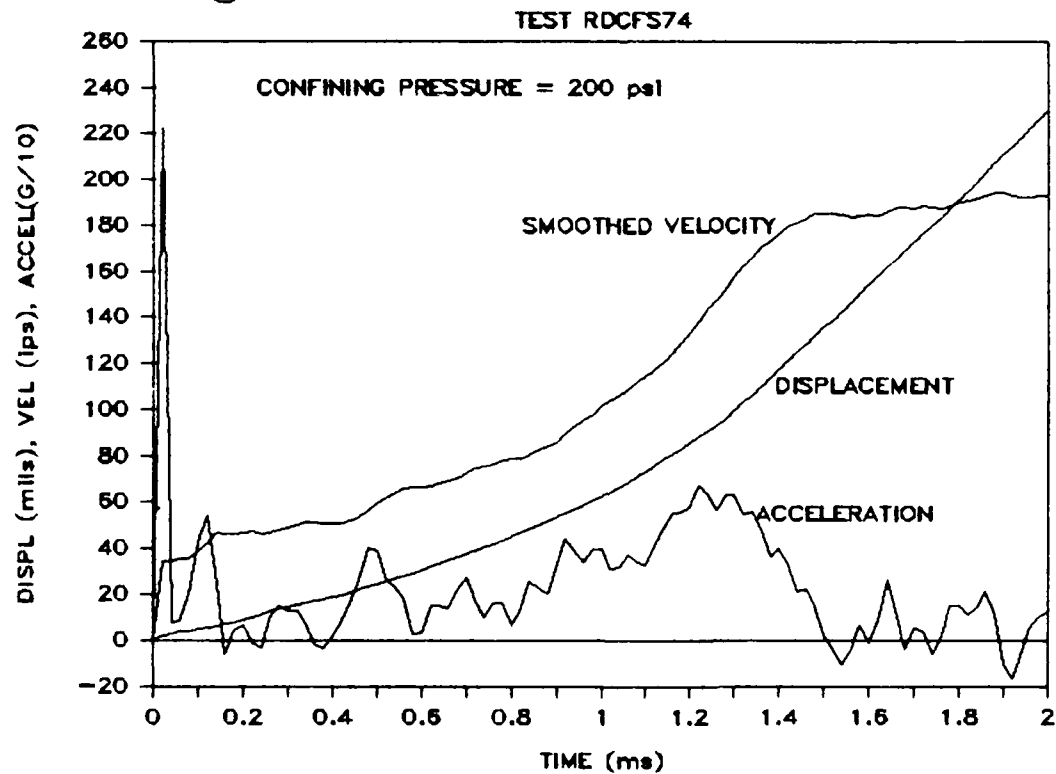
Fig 4.14, STRESS-STRAIN TEST DATA

DURATION = 28 ms : RDCFS 49, 52, 58

PSDx2 at CP = 200 psi

CONFINING PRESSURE = 100 psi

50 psi

PRINCIPAL STRESS DIFFERENCE (psi)

AXIAL STRAIN (%)
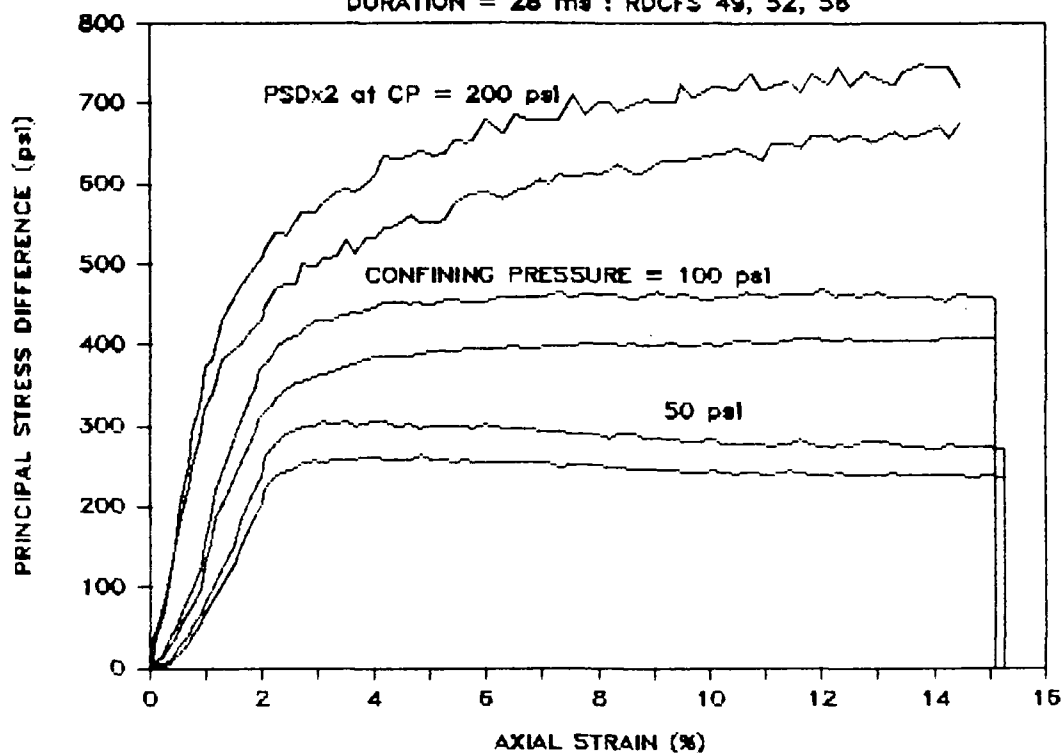
Fig 4.15, STRESS-STRAIN TEST DATA

DURATION = 2 ms : RDCFS 69, 72, 74

LOWER LOAD CELL ONLY

CONFINING PRESSURE = 200 psi

100 psi

50 psi

PRINCIPAL STRESS DIFFERENCE (psi)

AXIAL STRAIN (%)

37
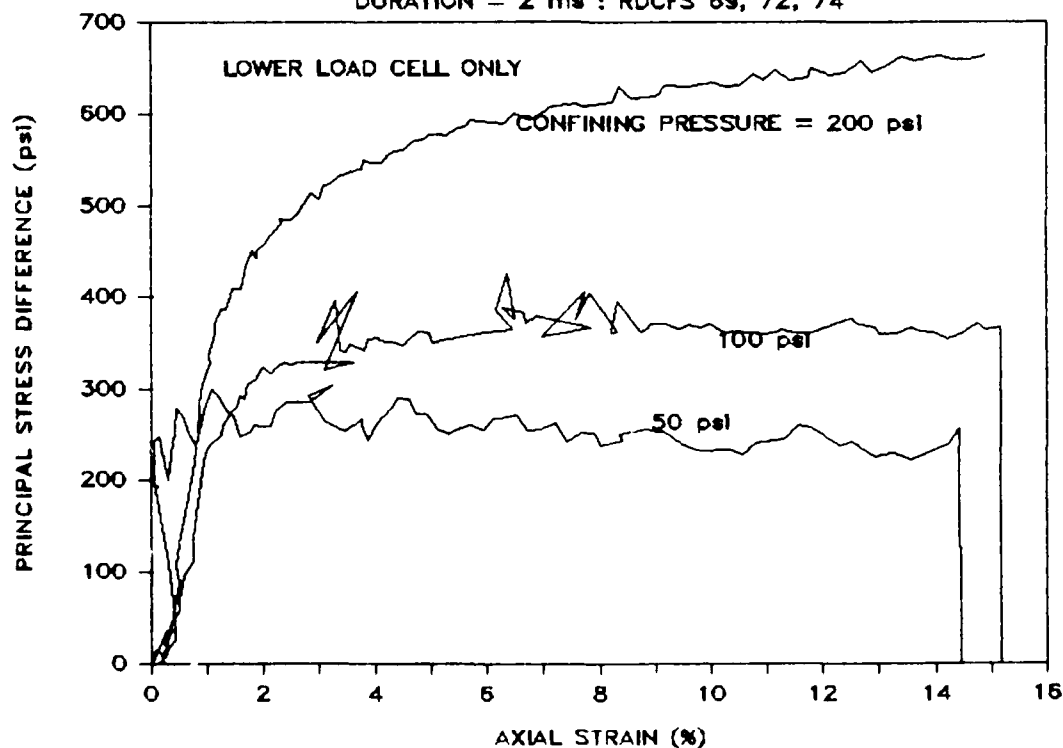
CHAPTER 5

THE ONE-DIMENSIONAL FTRXD SPECIMEN MODEL

5.1 BACKGROUND

The FTRXD soil specimen is a right circular cylinder whose height is twice its diameter. For static or slow testing, it is assumed to be a differential element of soil exhibiting load and deformation characteristics which can be measured and related directly to its stress-strain properties. Displacements, strain and stress are assumed to be uniform throughout the specimen. The longer the cylinder is in proportion to its diameter, the less are the effects of end restraint of the specimen by the test apparatus on the assumed uniform stress and strain distribution within the specimen. On the other hand, the longer the specimen is, the more likely is the occurrence of buckling. A height to diameter ratio of 2.0 is usually taken as the compromise that will lead to satisfactory static or slow test results. For dynamic testing an additional consideration is that the longer the specimen is in relation to the product of its propagation velocity and test duration, the more noticeable will be the inertial or wave effects.

The cylindrical soil specimen is failed in shear by compressing it axially. The specimen shape and testing action naturally lead to a one-dimensional view of phenomena occurring during testing. Most triaxial tests are run at a constant lateral confining pressure so that the application of axial compressive loads causes one to presume the presence of a controlling uniaxial stress: the difference between the axial stress and the lateral confining pressure or principal stress difference (PSD). The relationship between PSD and axial strain is what static and slow triaxial testing measures directly. This relationship was discussed in Chapters 3 and 4 and its representation by the linear-hyperbolic function described. When triaxial testing is dynamic, that is when inertial effects and wave phenomena are evident, the specimen can no longer be considered a differential element of the soil. The FTRXD attempts to measure the initial values and boundary conditions of the specimen. Further analysis is necessary to ascertain any constitutive relationship between PSD and axial strain.

There are decades of experience in static or slow triaxial testing of soils in which this one-dimensional approach has been employed with good success. There is considerable more recent experience in which one-dimensional wave analyses of triaxial specimens have been accomplished. These employ a resonant or standing wave of stress and strain along the axis of the specimen at very low levels of stress and strain. They are carried out with either compressive or torsional loading and measure either rod or shear wave velocities, depending on the loading. They also

determine the sensitivity of the wave velocity to the confining
pressure and to rate effects. Rate effects can be observed by
changing the frequency or wave length of the specimen standing
wave. The wave length of the specimen standing wave may be
changed by using excitation frequencies at several successive
modes or by preparing specimens with identical properties but
different lengths. Reference 5 describes resonant column triaxial
testing.

The FTRXD is intended to obtain dynamic soil properties at a
wide range of stress and strain levels and loading rates. The
specimen shape and the compressive loading suggest that the
phenomena of interest may involve one-dimensional waves of
displacements, strain, and stress propagating back and forth
through the specimen along its axis. These waves occur as a
result of the monotonically increasing displacements imposed on
the top of the specimen by the FTRXD. Within the specimen, the
resulting displacements, strains, and stresses also increase,
though neither uniformly or simultaneously. The motion of the top
of the specimen essentially precludes a decrease in the
magnitudes of stress or strain from occurring in the specimen
during the test. Thus the relationship between stress and strain
in the specimen need only reflect loading. Indeed unloading
cannot be measured. Figure 5.1 shows the physical model of the
one-dimensional FTRXD specimen and the end conditions imposed on
it.

5.2   THE ONE-DIMENSIONAL WAVE EQUATION

Shown also on Figure 5.1 is a cylindrical slice of the FTRXD
specimen whose diameter D is the same as the specimen's but whose
height is the infinitesimal dx of the axial position coordinate
x. The top of the slice is shown displaced down from its initial
position by an amount,

$$u = u(x,t).$$

The bottom of the slice is displaced down an amount,

$$u + u_x dx.$$

The displacement u is of course a function of both the position x
of the slice in the specimen and the time t elapsed since loading
of the specimen began. The symbol, u_x is the first partial
derivative of u with respect to x; for small strain theory
(ϵ < 15%), u_x equals the axial strain. Axial stress (σ) and
strain (ϵ) are shown at the top and bottom of the slice, changed
by differential amounts. They too are functions of x and t. The
symbol σ_x is the first partial derivative of stress with respect
to x and the symbol ϵ_x is the first partial derivative of strain
with respect to x. The differential changes in u, ϵ, and σ are
negative since the specimen is being increasingly compressed.
Moving down the specimen from its top in the positive x direction

40

and recalling that the top of the specimen is displaced downward
during loading while the bottom remains fixed, displacements
within the specimen decrease and stress and strain become
increasingly compressive or negative.

Applying Newton's Second Law to the slice,

$$(\sigma + \sigma_x dx)(\pi D^2/4) - \sigma(\pi D^2/4) = (gAdx)u_{tt} \qquad \text{or}$$

$$\sigma_x = gu_{tt}. \qquad (5.1)$$

The symbol u_{tt} is the second partial derivative of u with respect
to the time t; it is the acceleration of the slice. The symbol g
is the mass density of the slice and the specimen; it is taken as
constant.

The constitutive relationship is the functional relationship
between stress and strain,

$$\sigma = f(\epsilon) \qquad \text{so that} \qquad (5.2)$$

$$\sigma_x = (df/d\epsilon)(\epsilon_x) = (f_\epsilon)(u_x)_x \qquad \text{or}$$

$$\sigma_x = E u_{xx} \qquad \text{where} \qquad (5.3)$$

E (=df/dϵ =dσ/dϵ) is the first derivative of f(ϵ) with respect
to ϵ; it is the slope of the stress-strain relationship, or the
tangent modulus, and is a function of ϵ. The symbol u_{xx} is the
second partial derivative of u with respect to x.

Combining equations 5.1 and 5.3,

$$(E/g) u_{xx} = u_{tt}. \qquad (5.4)$$

Examining the kinematics of the specimen and slice,

$$du = (d\epsilon)(dx) = (dv)(dt). \qquad (5.5)$$

The term du is the change in the displacement from the top to the
bottom of the slice (through dx) during the time period dt. The
symbol v is the velocity of the slice during displacement and
deformation; it is equal to the first partial derivative of u
with respect to the time t. The term dv is the change in the
velocity from the top of the slice to its bottom (through dx)
during the time dt while the term dϵ is the change in the axial
strain through dx occurring during dt. Substituting the
appropriate derivatives and differentials into equation 5.5,

$$(\epsilon_x dx)(dx) = (v_t dt)(dt) \qquad \text{or}$$

$$(\epsilon_x)(dx/dt)(dx/dt) = (v_t) \qquad \text{or}$$

$$(u_x)_x (dx/dt)^2 = (u_t)_t \qquad \text{or}$$

41

$$C^2 u_{xx} = u_{tt} \tag{5.6}$$

The symbol C (=dx/dt) is used for the first derivative of the position x of the slice (where the differential changes or disturbances occur) with respect to time. It is the propagation velocity of the disturbances in the specimen. Comparing equation 5.4 with equation 5.6,

$$C^2 = E/g. \tag{5.7}$$

Equation 5.6 is the one-dimensional wave equation where C is the rod wave velocity. When C is constant, E must be constant also and the constitutve relationship is the linear one-dimensional Hooke's Law ($\sigma = E\epsilon$). When the linear-hyperbolic constitutive relationship is in effect, E is a function of strain once the maximum linear stress σ_1 (MLS) and corresponding maximum linear strain ϵ_1 (EL) are reached. The propagation velocity in the specimen, therefore, is a function of strain (equation 5.7) also. Equation 5.6, then, becomes the one-dimensional linear-hyperbolic wave equation.

5.3 THE ONE-DIMENSIONAL LINEAR-HYPERBOLIC WAVE EQUATION

Figure 5.2 illustrates the linear-hyperbolic stress-strain function discussed in Chapter 3 and shown on Figures 3.5 and 3.6. The curve plotted on Figure 5.2 is the lowest of the four plotted on Figure 3.5. The equations defining it are,

$$\sigma = E_o\epsilon \qquad \text{when } \epsilon < \epsilon_1 \qquad \text{and} \tag{5.8a}$$

$$(\sigma - \sigma_1) = \frac{(\epsilon - \epsilon_1)}{(1/E_o) + (1/\sigma_h)(\epsilon - \epsilon_1)} \qquad \text{when } \epsilon > \epsilon_1 \tag{5.8b}$$

where,

σ = axial stress, ϵ = axial strain,

σ_1 = maximum linear stress (MLS),

σ_{max} = maximum stress (MS),

σ_h = maximum hyperbolic stress (MS-MLS),

ϵ_1 = maximum linear strain (EL), and

E_o = slope of the linear part of the function and initial slope of the hyperbolic part.

When $\epsilon < \epsilon_1$,

$$d\sigma/d\epsilon = E = E_o \qquad \text{and}$$

$$C^2 = C_o^2 = E_o/g .$$

42

Substituting into equations 5.4 or 5.6,

$$(C_o)^2 \, u_{xx} = u_{tt} \, . \tag{5.9}$$

Equation 5.9 is the linear one-dimensional wave equation.

When $\epsilon > \epsilon_1$,

$$d\sigma/d\epsilon = E = \frac{(1/E_o)}{[(1/E_o) + (1/\sigma_h)(\epsilon - \epsilon_1)]^2} \qquad \text{so that,}$$

$$E/E_o = \frac{(\sigma_h/E_o)^2}{[(\sigma_h/E_o) + (\epsilon - \epsilon_1)]^2} \, . \tag{5.10}$$

Recalling equation 5.4,

$$(E/g) \, u_{xx} = u_{tt} \qquad \text{and}$$

$$(1/E_o)(E/g) \, u_{xx} = (1/E_o) \, u_{tt} \, . \tag{5.11}$$

Substituting equation 5.10 into 5.11,

$$\frac{(\sigma_h/E_o)^2}{[(\sigma_h/E_o) + (\epsilon - \epsilon_1)]^2} \, u_{xx} = (g/E_o) \, u_{tt} \, . \tag{5.12}$$

Rearranging and recalling that

$$C_o{}^2 = E_o/g \quad \text{and that} \quad \epsilon = u_x,$$

the linear-hyperbolic one-dimensional wave equation for $\epsilon > \epsilon_1$ may be written,

$$\frac{u_{xx}}{[(\sigma_h/E_o) + (u_x - \epsilon_1)]^2} = \frac{u_{tt}}{[C_o \sigma_h/E_o]^2} \, . \tag{5.13}$$

5.4 THE FINITE DIFFERENCE GRID

Equations 5.9 and 5.13,

for $\epsilon < \epsilon_1$
$$u_{xx} = \frac{u_{tt}}{(C_o)^2} \tag{5.9}$$

for $\epsilon > \epsilon_1$
$$\frac{u_{xx}}{[(\sigma_h/E_o) + (u_x - \epsilon_1)]^2} = \frac{u_{tt}}{[C_o \sigma_h/E_o]^2} \, . \tag{5.13}$$

are a system of second order two-dimensional partial differential equations. They are linear for strains (u_x) less than ϵ_1, and

nonlinear for strains greater than ϵ_1. They can be solved numerically for displacements, $u(x,t)$, by replacing the partial derivatives of $u(x,t)$ with respect to x and t with finite difference expressions.

Central difference expressions are convenient, accurate, and well-suited to the wave equation. Three-point formulas are the simplest possible when second derivatives are present and they provide suitable accuracy as long as the finite difference grid is sufficiently fine. The grid is made up of points in the x-t space which are equally spaced in each coordinate direction. The difference between any two successive points in the x direction, x_m and x_{m+1}, is the spatial increment δx. Similarly, the difference between any two successive points in the time direction, t_n and t_{n+1}, is the time increment δt. The index m refers to position and the index n to time. Thus,

$$x_m = (m-1)\delta x, \qquad m=1,2,3,\ldots\ldots$$

$$t_n = (n-1)\delta t, \qquad n=1,2,3,\ldots\ldots$$

The central difference expressions are "centered" on the point (x_m,t_n) in x-t space, and are identified and located by the indices (m,n). Three such expressions are required,

$$u_x = \frac{u_{m+1,n} - u_{m-1,n}}{2\delta x} \qquad (5.14a)$$

$$u_{xx} = \frac{u_{m+1,n} - 2\,u_{m,n} + u_{m-1,n}}{\delta x^2} \qquad (5.14b)$$

$$u_{tt} = \frac{u_{m,n+1} - 2\,u_{m,n} + u_{m,n-1}}{\delta t^2} \qquad (5.14c)$$

The terms subscripted by the indices m and n are the values of the displacements at the corresponding five points identified in x-t space by the indices as,
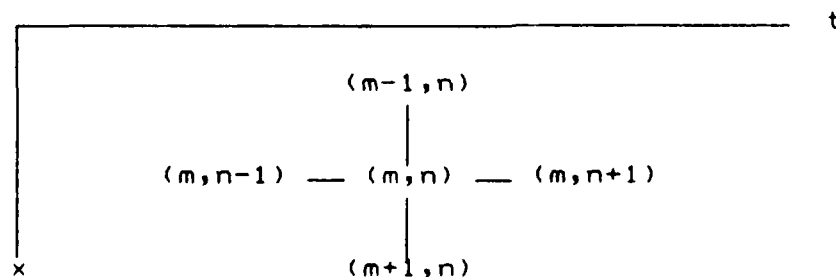
The times of the initial arrivals of the incident and
reflected waves at a point in the specimen are determined by the
initial propagation velocity C_o of the specimen and the distance
the waves have propagated through the specimen to reach the
point. These times of arrival plot as straight lines in x-t space
with slopes equal to C_o, or in dimensionless $(x/h)-(C_o t/h)$ space
with slopes equal to one. The symbol h is the height of the
specimen. Figure 5.3 illustrates the dimensionless $(x/h)-(C_o t/h)$
space in which δx has been set equal to $C_o \delta t$ and both are equal
to 0.10. The horizontal lines of points define position lines
within the specimen $(x=x_m)$ which begin at the initial times of
arrival of the incident wave. The vertical lines of points are
time lines $(t=t_n)$ which also plot only after the initial arrival
of the incident wave. The sloping lines are the plots of initial
times of arrival of the incident and reflected waves at points
throughout the specimen. Only three traverses of the initial
arrivals of waves are shown: the incident wave first propagating
down through the specimen; the first reflected wave propagating
back up through the specimen after reflecting off its bottom; and
the second reflected wave propagating back down through the
specimen after reflecting off its top. The tic marks shown locate
the points (x_m, t_n) which may be identified with their
corresponding indices (m,n). Figure 5.3 is referred to as the
finite difference grid.

5.5 THE FINITE DIFFERENCE ALGORITHM

Substituting the difference expressions (equations 5.14)
into the linear 1D wave equation (equation 5.9) results in,

$$C_o{}^2 \frac{u_{m+1,n} -2u_{m,n} +u_{m-1,n}}{\delta x^2} = \frac{u_{m,n+1} -2u_{m,n} +u_{m,n-1}}{\delta t^2} \quad \text{or}$$

$$u_{m,n+1} = (\frac{C_o \delta t}{\delta x})^2 (u_{m+1,n} -2u_{m,n} +u_{m-1,n}) + 2u_{m,n} - u_{m,n-1}$$

$$(5.15a)$$

Equation 5.15a can used to calculate the displacement at grid
point (m,n+1) provided that the displacements are known at grid
points (m,n), (m+1,n), (m-1,n), and (m,n-1). With respect to
point (m,n+1), these four points each are located at it, above
and below it by an amount δx, and earlier than it by amounts δt
or $2\delta t$ as illustrated below.

45

t_{n-1} t_n t_{n+1} t

x_{m-1} (m-1,n)

x_m (m,n-1) — (m,n) — (m,n+1)

x_{m+1} (m+1,n)

x
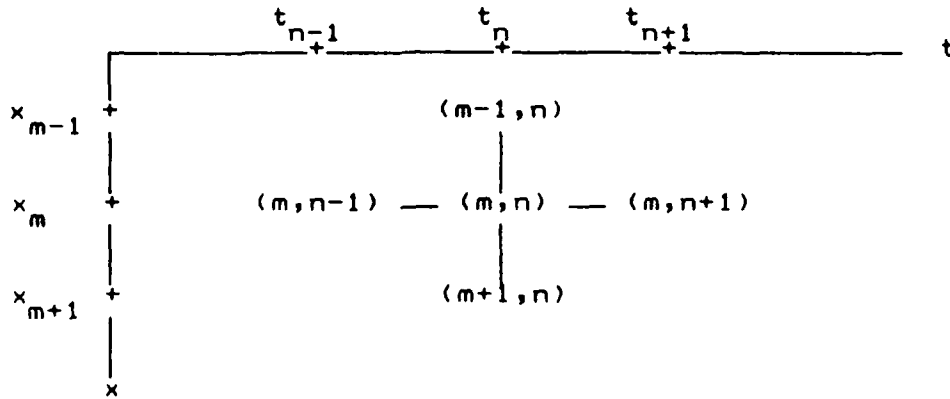
The numerical stability of the equation 5.15a is greatest when $(C_o \delta t / \delta x)$ is set equal to one (see Reference 6). In which case,

$$u_{m,n+1} = u_{m+1,n} + u_{m-1,n} - u_{m,n-1} \qquad (5.15b)$$

Similarly, substituting the difference expressions (equations 5.14) into the linear-hyperbolic 1D wave equation (equation 5.13) and setting $(C_o \delta t / \delta x)$ equal to one results in,

$$u_{m,n+1} = \frac{(\sigma_h / E_o)^2 \, (u_{m+1,n} - 2u_{m,n} + u_{m-1,n})}{(\frac{\sigma_h}{E_o} + \frac{u_{m+1,n} - u_{m-1,n}}{2\delta x} - \epsilon_1)^2} + 2u_{m,n} - u_{m,n-1} \qquad (5.15c)$$

Although equation 5.15c is more complex than equation 5.15b, both are applied to the finite difference grid in exactly the same way. When the axial strain is less than the maximum linear strain (ϵ_1), equation 5.15b applies; when the axial strain is greater than the maximum linear strain, equation 5.15c applies. Clearly the values of displacement calculated using equation 5.15c will depend on the values of the parameters $(\sigma_1, \epsilon_1, \text{and } \sigma_{max})$ which determine the linear-hyperbolic stress-strain function. Note that,

$$E_o = \sigma_1 / \epsilon_1$$

5.6 INITIAL VALUES AND BOUNDARY CONDITIONS

The application of the finite difference equations (5.15) to the finite difference grid (Figure 5.3) requires that displacements be known at the top and bottom of the grid and along its sloping left edge. These grid borders represent respectively the boundary conditions for the specimen and its initial values. The finite difference algorithm is expressed in terms of displacements, so the boundary conditions and initial values must also be known as displacements.

Since the specimen and FTRXD are at rest prior to the start
of testing, the initial values for the specimen are all zero.
That is at time t = 0, displacements are equal to zero. Moreover,
they are also equal to zero within the specimen after t = 0 and
until the initial arrival of the incident wave. Thus along the
sloping left edge of the finite difference grid the displacements
are known and are equal to zero.

For the one-dimensional problem, there are two boundaries:
the top of the specimen and its bottom. The bottom is fixed so
that the boundary condition there is simply that displacements
remain zero throughout the test. It is stated mathematically as,

$$u_{bottom} = u(h,t) = 0 \qquad\qquad (5.16a)$$

The top of the specimen moves with the upper pedestal or
piston-ram of the FTRXD as described in Chapter 4 (Section 4.3).
For tests whose durations were 30 milliseconds or more, the
two-parameter hyperbola was found to represent the velocity of
the piston-ram with reasonable accuracy and is illustrated on
Figure 4.8. Recall that,

$$v_{top} = v(0,t) = v_o t/(t_o + t),$$

and its integral is,

$$u_{top} = u(0,t) = v_o t - v_o t_o \ln(1 + t/t_o), \qquad (5.16b)$$

where $\qquad\qquad a_o$ = initial acceleration

$\qquad\qquad\qquad v_o$ = limiting velocity, and

$\qquad\qquad\qquad t_o = v_o/a_o$

Equation 5.16b is the boundary condition specified for the top of
the specimen when the test duration is 30 milliseconds or more so
that the two-parameter hyperbola is descriptive of the upper
pedestal velocity of the FTRXD.

For tests run with durations of about 2 milliseconds, the
two-parameter hyperbola does not describe the velocity of the
piston-ram. The displacement and velocity as a function of time
for these tests are illustrated on Figures 4.12 and 4.13. The
displacement turns upward more sharply during that latter part of
the test than it does for the slower tests. For the purposes of
obtaining an initial analysis of the wave and inertial effects in
the specimen for these very fast tests with these complicated but
only roughly estimated boundary conditions at the specimen top,
the motion was approximated as one of constant acceleration.
Constant acceleration produces a parabolic displacement function,
whose curvature is a better fit for these tests than the integral
of the two-parameter hyperbola. The parabolic displacement is,

$$u_{top} = u(0,t) = (a_o t^2)/2 = (v_o t^2)/(2t_o) \qquad (5.16c)$$

where $\quad a_o$ = constant acceleration,

$\quad v_o$ = velocity of the specimen top at the time the incident wave first reaches the bottom of the specimen,

$\quad t_o$ = time at which v_o is reached.

Equation 5.16c is the boundary condition specified for the top of the specimen for the very short duration tests in which equation 5.16b is not satisfactory. Note the constants v_o and t_o are useful constants which are descriptive of the upper pedestal motion, but which have different interpretations for equation 5.16c than for equation 5.16b.

The upper pedestal motion of the FTRXD (boundary condition of the top of the specimen) is an essential part of the analysis. Different results are obtained if the upper pedestal motion changes. In describing the results of analyses of the FTRXD specimens later in this chapter, the corresponding upper pedestal motions will be illustrated also.

5.7 FINITE DIFFERENCE DISPLACEMENTS

The finite difference algorithm (equations 5.15) may be viewed as a pattern in the x-t space of the finite difference grid. When the displacements at the four grid points shown below at times t_2 and t_3 are known, the displacement at the grid point at time t_4 can be calculated. The calculations would be started

```
          1           2           3           4           5         n

  1       +_____+_____ (1,3) _____+_____+_____  t
          |                     |
          |                     |
  2       +       (2,2) __ (2,3) __ (2,4)           +
          |                     |
          |                     |
  3       +              (3,3)           +           +
          |
          |
  4       +                          +           +
          |
  m       x
```
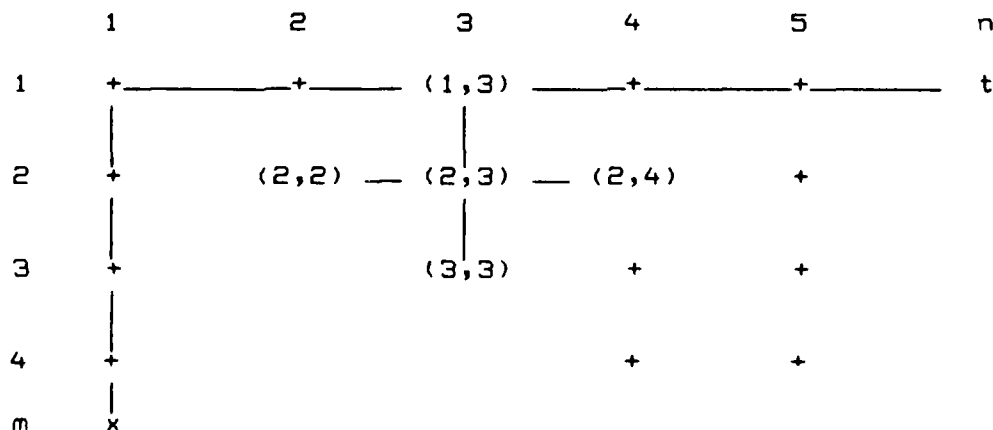
by centering the pattern on grid point (2,3), which has space time coordinates $(\delta x, 2\delta t)$. The displacement at (1,3) is known from the boundary condition at the top of the specimen; the displacements at (2,2) and (3,3) are known from the initial values in the specimen. What is missing is the value of the displacement at grid point (2,3). Indeed, all the displacements

along the sloping line parallel to the left border of the grid
and one time increment δt later are needed to use the finite
difference algorithm. The process is to move the finite
difference pattern down the sloping lines of the grid which are
parallel to the left border. The process is begun at the top left
of the grid as shown. On each successive pass of the pattern down
such lines, displacements are calculated on the sloping line one
time increment later. These newly calculated displacements are
then used in the next two passes to calculate corresponding later
displacements. In this way, a complete array of displacements,
$u_{m,n}$, is generated at the grid points in x-t space which satisfy
the wave equations (5.9 and 5.13), the initial values, and the
boundary conditions (5.16).

The constitutive relationship is initially linear so that
equation 5.15b is used until the strain exceeds the maximum
linear strain, ϵ_1. Equation 5.15b does not require the value of
the displacement, $u_{m,n}$, it is centered on. Thus displacement
values on the sloping line one time increment later than the left
border of the grid are not required for the first pass of the
finite difference pattern down that line. However, these values
are required for the second pass which is down the sloping line
two time increments from the left border. They would be required
also for other algorithms, such as beginning the calculations
with equation 5.15c for a specimen with an entirely hyperbolic
constitutive relationship. For a linear specimen in which only
equation 5.15b is employed, the pattern could be moved down
sloping lines only at odd numbers of time increments later than
the left border. Thus the requirement to first obtain the
displacement values along the sloping line one time increment
later could be avoided. It cannot be avoided in a linear-
hyperbolic specimen since equation 5.15c requires the value of
the displacement it is centered on.

The displacements on that sloping line one time increment
later than the left border of the grid, at grid points (n,n+1),
may be obtained by applying the finite difference patterns
(equations 5.15) along the left border, grid points (n,n).
Recognizing that of all of the initial values are zero,

$$u_{n,n} = 0,$$

$$v_{n,n} = 0, \qquad \frac{u_{n,n+1} - u_{n,n-1}}{2\delta t} = 0$$

$$\epsilon_{n,n} = 0, \qquad \frac{u_{n+1,n} - u_{n-1,n}}{2\delta x} = 0 \quad .$$

Substituting these relationships into equations 5.15 shows that
for either equation 5.15b ($\epsilon < \epsilon_1$) or equation 5.15c ($\epsilon > \epsilon_1$),

$$u_{n,n+1} = u_{n-1,n} \qquad\qquad (5.17)$$

Equation 5.17 is the starting equation for the finite difference algorithm. It states that the displacements along that sloping line one time increment later than the left border of the grid are each equal to the displacement of the top of the specimen one time increment after it begins to move.

5.8 FINITE DIFFERENCE STRAINS AND STRESSES

The algorithm and starting equation, equations 5.15 and 5.17, are the basic tools required to obtain the solution to the wave equation, the array of displacements, $u_{m,n}$, in the x-t space of the finite difference grid. However, the magnitude of the strain at each step in the calculations must be monitored to determine whether the linear or hyperbolic part of the specimen's stress-strain relationship is in effect. That is, strain ϵ must be calculated and compared to the maximum linear strain ϵ_1 and equation 5.15b or 5.15c invoked as appropriate.

In general, strain may be calculated with the three-point central difference expression (equation 5.14a) used to develop the finite difference algorithm (equations 5.15), or

$$\epsilon_{m,n} = \frac{u_{m+1,n} - u_{m-1,n}}{2\delta x} \quad . \tag{5.14b}$$

The displacements at $(m+1,n)$ and $(m-1,n)$ are known just prior to employing the algorithm to calculate the displacement at $(m,n+1)$. The algorithm is center-based also, centered on (m,n). Thus $\epsilon_{m,n}$ is calculated (equation 5.14b), compared to ϵ_1, and equation 5.15b or 5.15c used as appropriate.

The array of displacements, $u_{m,n}$, once generated, is needed to calculate the strain at a point in the specimen as a function of time. The stress at that point as a function of time then may be calculated using the specimen's stress-strain relationship (equations 5.8). The stresses at the top and bottom of the specimen are the ones most directly related to the force measured by the upper and lower load cells of the FTRXD. Therefore the strains at the top and bottom of the specimen must be calculated from the displacement array to obtain these stresses.

At the very top and bottom of the specimen, central difference expressions cannot be used for the strain calculation. Instead, forward difference expressions, focussed on the grid points at $x = 0$ $(m=1)$, are neccessary for the strain at the top. Backward difference expressions, focussed on the grid points at $x = h$, are necessary for the strain at the bottom. Since central difference expressions are more accurate than forward or backward difference expressions, four-point forward and backward expressions were employed in an effort to maintain the same level of accuracy that the algorithm possesses.

Referring to the finite difference grid (Figure 5.3), the strain finite difference expressions were not allowed to extend over the sloping lines which mark the initial arrivals of the incident and reflected waves. The displacements and strains immediately adjacent to either side of these lines can differ significantly, especially if the specimen has been loaded with a pulse approaching the severity of a step pulse. Thus near the grid points where the sloping lines intersect the top and bottom of the grid, the four point forward and backward difference expressions could not be used. At the first grid point on either side of the intersections, two-point formulas were used; at the second grid point on either side of the intersections, three-point formulas were used. At the other points on the top and bottom of the grid, the four-point expressions were used. The two, three, and four-point forward and backward difference expressions employed were (Reference 6),

	x_1	x_2	x_3	x_4
$\delta x\, u_x(x_1)$	-1	1	$-$	$-$
$\delta x\, u_x(x_2)$	1	-1	$-$	$-$
$\delta x\, u_x(x_1)$	$-3/2$	2	$-1/2$	$-$
$\delta x\, u_x(x_3)$	$1/2$	-2	$3/2$	$-$
$\delta x\, u_x(x_1)$	$-11/6$	3	$-3/2$	$1/3$
$\delta x\, u_x(x_4)$	$-1/3$	$3/2$	-3	$11/6$.

$$(5.18)$$

5.9 DIMENSIONLESS VARIABLES AND PARAMETERS

Given the three parameters required to define the linear-hyperbolic constitutive relationship of the specimen (E_o, σ_m, and ϵ_1), the specimen length (h) to identify the geometric size of the specimen, the mass density of the specimen (g) to quantify inertia in the specimen, and the two parameters (v_o and t_o) to define the upper pedestal motion or boundary conditions of the specimen, direct calculation of displacements using equations 5.15 will produce an entire array of displacements in x-t space for each set of values of these seven parameters. If each parameter were to assume only four values, 16384 such arrays might be calculated. For finite difference grid points separated spatially by one-tenth of a specimen length, each displacement array might contain 4000 displacement values (10x10x40). The result, of course, would be an enormous volume of displacement data. However, combining the seven parameters into dimensionless groupings and setting the finite difference grid so that δx equals $C_o \delta t$, reduces the number of parameters to three so that the number of arrays will be reduced to a small fraction of the number that would be required otherwise (64 vs 16384). That is, only three dimensionless parameters would be required to determine dimensionless displacements in dimensionless space and time.

Dimensionless space z is taken as the ratio of the spatial coordinate x to the specimen length h. Dimensionless time τ is taken as the ratio of elapsed time t to the time required for the initial wave to propagate the length of the specimen. Thus,

$$z = x/h \qquad \text{and} \qquad (5.19)$$

$$\tau = C_o t/h \qquad \text{where} \qquad (5.20)$$

$$C_o = \sqrt{(E_o/g)} \quad \text{and}$$

$$E_o = \sigma_1/\epsilon_1.$$

The upper pedestal displacement for a hyperbolic upper pedestal velocity was seen earlier to be,

$$u_{top} = v_o t - v_o t_o \ln(1 + t/t_o) \qquad (5.16b)$$

or,
$$u_{dt} = \tau - \tau_o \ln(1 + \tau/\tau_o) \qquad \text{where} \qquad (5.21a)$$

$$u_{dt} = (u_{top}/h)(C_o/v_o),$$

$$\tau_o = C_o t_o/h,$$

$$t_o = v_o/a_o,$$

$$v_o = \text{limiting upper pedestal velocity, and}$$

$$a_o = \text{initial upper pedestal acceleration.}$$

For constant upper pedestal acceleration,

$$u_{top} = (v_o t^2)/(2t_o) \qquad (5.16c)$$

or,
$$u_{dt} = \tau^2/2 \qquad \text{where again} \qquad (5.21b)$$

$$u_{dt} = (u_{top}/h)(C_o/v_o), \quad \text{but}$$

$$v_o = a_o h/C_o, \qquad \text{and}$$

$$a_o = \text{constant upper pedestal acceleration.}$$

Consistent with equations 5.21 dimensionless displacement is,

$$u_d = (u/h)(C_o/v_o). \qquad (5.22)$$

Dimensionless strain is determined as,

$$\epsilon_d = (u_{d2} - u_{d1})/(z_2 - z_1) \qquad \text{or}$$

$$= (u_2/h - u_1/h)(C_o/v_o)/(x_2/h - x_1/h)$$

$$\epsilon_d = \epsilon(C_o/v_o) \qquad (5.23)$$

Dimensionless stress is determined by using the expression for dimensionless strain (equation 5.23) on the stress-strain relationships for the specimen (equations 5.8). The result is,

for $\epsilon < \epsilon_1$, $\quad \sigma_d = \sigma/\sigma_{max} = \dfrac{\epsilon_d/\epsilon_{dh}}{\epsilon_{d1}/\epsilon_{dh} + 1}$ $\qquad$ where $\qquad$ (5.24a)

$$\epsilon_{dh} = \epsilon_h(C_o/v_o)$$

$$\epsilon_h = \text{characteristic hyperbolic strain,}$$

$$= \epsilon_o - \epsilon_1 = \sigma_{max}/E_o - \epsilon_1 .$$

For $\epsilon > \epsilon_1$, $\quad \sigma_d = \sigma/\sigma_{max} = \dfrac{(\epsilon_d - \epsilon_{d1})/(\epsilon_{dh} + \epsilon_d - \epsilon_{d1}) + \epsilon_{d1}/\epsilon_{dh}}{\epsilon_{d1}/\epsilon_{dh} + 1}$ (5.24b)

$$\epsilon_{d1} = \epsilon_1(C_o/v_o) .$$

The finite difference algorithm, equations 5.15, may be expressed in terms of dimensionless displacements by using the expression for dimensionless displacement (equation 5.22) on equations 5.15. The result is,

for $\epsilon < \epsilon_1$, $\quad u_{dm,n+1} = u_{dm+1,n} + u_{dm-1,n} - u_{dm,n-1} .$ $\qquad$ (5.25a)

For $\epsilon > \epsilon_1$,

$$u_{dm,n+1} = \frac{(u_{dm+1,n} - 2u_{dm,n} + u_{dm-1,n})}{\left(1 + \dfrac{u_{dm+1,n} - u_{dm-1,n}}{2\epsilon_{dh}\delta z} - \epsilon_{d1}/\epsilon_{dh}\right)^2} + 2u_{dm,n} - u_{dm,n-1}$$

(5.25b)

where $\qquad u_{dm,n+1} = u_{m,n+1}(C_o/v_o),$

$$\epsilon_{d1} = \epsilon_1(C_o/v_o),$$

$$\epsilon_{dh} = \epsilon_h(C_o/v_o), \quad \text{and}$$

$$\delta z = \delta(x/h) = \delta\tau = \delta(C_o t/h) .$$

Finally, the starting equation (equation 5.17) may also be expressed in dimensionless terms as,

$$u_{dn,n+1} = u_{dn-1,n}$$

(5.26)

5.10 UPPER PEDESTAL VELOCITY LIMIT

Equation 5.7 showed that the propagation velocity of displacement, strain, and stress disturbances in the specimen was,

53

$$C = \sqrt{(E/g)} ,$$

where E and thus C are functions of strain (ϵ) and therefore are functions of (x,t) or (z,τ). Clearly as time elapses after the onset of loading, the propagation velocity decreases since the tangent modulus E of the specimen's stress-strain relationship decreases. Indeed, for large strain, the propagation velocity approaches zero. On the other hand, the velocity of the upper pedestal, in general, increases as time and strain increase. The one-dimensional wave equation (equation 5.6) is valid only as long as particle or slice velocities in the specimen are controlled by Newton's Second Law and the stress-strain relationship specified. Thus the velocity of the upper pedestal must not exceed the propagation velocity in the specimen.

From equation 5.10,

$$E/E_o = \frac{(\sigma_h/E_o)^2}{[(\sigma_h/E_o)+(\epsilon-\epsilon_1)]^2} \quad \text{or} \tag{5.10}$$

$$C/C_o = \frac{\sigma_h/E_o}{\sigma_h/E_o + \epsilon - \epsilon_1} \quad \text{and}$$

$$C = \frac{C_o \epsilon_h}{\epsilon + \epsilon_h - \epsilon_1} ; \qquad \epsilon_h = \sigma_h/E_o \tag{5.27}$$

For hyperbolic upper pedestal motion,

$$v_{top} = \frac{v_o t}{t + t_o} = \frac{v_o \tau}{\tau + \tau_o} \tag{5.28}$$

Comparing equation 5.27 to 5.28 reveals that the wave equation calculations are valid for hyperbolic upper pedestal velocity as long as,

$$\epsilon_{do} = \epsilon_o C_o / v_o > (\epsilon + \epsilon_h - \epsilon_1) \frac{\tau}{\tau + \tau_o} + \epsilon_{d1} . \tag{5.29}$$

At present it is difficult to achieve experimental values for ϵ_{do} smaller than about 30 (ϵ_{d1}<15) when the upper pedestal velocity is hyperbolic. The largest that ϵ will ever be is 15% or 0.15, ϵ_o will be from 0.05 to 0.10, and ϵ_1 from 0.01 to 0.05. Thus the limit indicated in equation 5.29 will never be reached. Even when using a theoretical value of ϵ_{do} as small as 5 (ϵ_{d1}<3), the limit is not reached.

For constant upper pedestal acceleration,

$$v_{top} = a_o t = v_o \tau . \tag{5.30}$$

Comparing equation 5.27 to 5.30 reveals that the wave equation calculations are valid for constant upper pedestal acceleration as long as,

$$\epsilon_{do} = \epsilon_o C_o / v_o > (\epsilon + \epsilon_h - \epsilon_1) \tau + \epsilon_{d1}. \tag{5.31}$$

To date, experimental values of ϵ_{do} of about 20 have been achieved with a constant upper pedestal acceleration. Smaller values might also be possible. A theoretical value as small as 5 (with a constant acceleration of about 1000g and $\epsilon_{d1} = 2.5$) is useful to illustrate the limitation imposed by equation 5.31. Taking the largest reasonable ϵ (=0.15), ϵ_o (=0.10), and the corresponding ϵ_1 (=0.05), the wave equation calculations would be valid until at least a dimensionless time τ of about 12. However for these test conditions, that 15% failure strain will be reached in a dimensionless time of about $\tau=8$ so that again the limit expressed in equation 5.31 will not be reached.

5.11 PROGRAM FTSP

The one-dimensional linear-hyperbolic wave equation was solved in dimensionless terms employing equations 5.21, 5.25, and 5.26. Dimensionless strain and stress at the top and bottom of the specimen were calculated from the resulting dimensionless displacements using equations 5.23 and 5.24.

To compare the calculated top and bottom stress, which accounts for one-dimensional inertial effects in the specimen, with the stress usually derived from triaxial testing, a third stress, termed gross stress was also calculated. Gross stress is the stress obtained when the displacement of the top of the specimen divided by the length of the specimen is entered as strain into the specimen's constitutuve relationship. The strain so used is termed gross strain. Gross stress and strain were obtained in dimensionless form using equations 5.21, 5.22, 5.23, and 5.24.

The equations were coded for solution on a computer in FORTRAN (F77) as Program FTSP. A complete listing of Program FTSP is contained in Appendix A. The code runs interactively with a minimum amount of input required from the keyboard. The boundary conditions are established by providing a value for τ_o, one of the three dimensionless parameters.

$\tau_o = C_o t_o / h = 0$, for a step velocity and linearly increasing displacement of the the upper pedestal,

$\tau_o > 0$, for hyperbolic upper pedestal velocity, and

$\tau_o = 1000$ for a constant upper pedestal acceleration.

55

The finite difference grid is defined by specifying the number of increments which the specimen length is divided into and the duration over which the calculations will be made. Specifying the number of increments allows the calculation of δz and $\delta \tau$. The duration is set by stating the maximum even integer value of τ. For slow tests (duration = 28 milliseconds) in which τ ($= C_o t/h$) was about 125 at $\epsilon = 15\%$, good numerical accuracy was achieved with $\delta z = 0.10$. Rapid tests (duration = 2 milliseconds), in which τ was about 9 at $\epsilon = 15\%$, required $\delta z = 0.05$ to achieve satisfactory numerical results.

Finally, values for the remaining two dimensionless parameters, ϵ_{do} ($= \epsilon_o C_o / v_o$) and σ_1 / σ_{max} ($=$ MLDS), are entered. The program then generates an array of dimensionless displacements in dimensionless space and time, and calculates the dimensionless top, bottom, and gross stress and strain.

Program FTSP was compiled with the Microsoft FORTRAN Compiler (version 3.3) both with and without a math coprocessor. With the coprocessor, the compilied code requires 295 kilobytes of random access memory and takes 1-3 minutes for one data run on an IBM PC/XT. Without the coprocessor, 302 kilobytes of random access memory are required and a data run takes 7-15 minutes. The bulk of the random access memory requirement occurs because FTSP is written to accomodate up to 50 increments in a specimen length ($\delta z = 0.02$) and up to 1000 dimensionless time steps ($\max \tau = 1000 \delta z$).

A sample run from Program FTSP is contained in Appendix B. In this run,

$$\tau_o = C_o t_o / h = 5.0,$$

$$\epsilon_{do} = \epsilon_o C_o / v_o = 10.0,$$

$$\sigma_1 / \sigma_{max} = \text{MLDS} = 0.25,$$

$$\delta z = \delta \tau = 0.05, \qquad \text{and}$$

$$\max \tau = 40.0 \ .$$

5.12 SPECIMEN TOP, BOTTOM, AND GROSS STRESS

Figures 5.4 through 5.20 are plots of the top, bottom, and gross stress data generated by Program FTSP and illustrations of the details of the upper pedestal motion used. The plots attempt to portay a spectrum of specimen behavior as the values of the dimensionless parameters change. Five values of τ_o were used to vary the upper pedestal boundary conditions. These were,

$$
\begin{aligned}
\tau_o &= 0.0 && \text{step velocity pulse,} \\
&= 5.0 && \text{extremely rapid hyperbolic velocity,} \\
&= 10.0 && \text{very rapid hyperbolic velocity,} \\
&= 20.0 && \text{rapid hyperbolic velocity, and} \\
&= 1000 && \text{extremely rapid constant acceleration.}
\end{aligned}
$$

Six values of ϵ_{do} were used to reflect a range of constitutive behavior of the specimen from soft to stiff relative to the rapidity with which the specimen is loaded. These were,

$$\epsilon_{do} = 5.0$$
$$= 10.0$$
$$= 20.0$$
$$= 30.0$$
$$= 40.0$$
$$= 50.0$$

In general for a given test rate (v_o), the stiffer specimens have higher values of ϵ_{do} ($=\epsilon_o C_o/v_o$) than the softer specimens do.

Only one value of σ_1/σ_{max} (= MLDS = 0.25) was used. This parameter essentially reflects the overall shape of the specimen stress-strain curve which translates directly into the overall shape of stress-time or stress-gross strain plots.

Figures 5.4 to 5.7 show the stress-time and stress-gross strain behavior of a FTRXD specimen subjected to a step velocity pulse of upper pedestal motion. The motion is simple; the top of the specimen displaces linearly with time so that plots of stress versus time are identical with plots of stress versus gross strain. The step velocity pulse, however, is a very severe loading of the specimen in the initial phases of the test. It requires an enormous acceleration for a very short time at the beginning of the test. Consequently, significant inertial effects occur at the arrival of the incident wave and each reflected wave at each point in the specimen. Though the step velocity pulse cannot be achieved presently in the FTRXD, it is included here because it illustrates clearly the differences in the top, bottom, and gross stress due to inertial effects.

On Figures 5.5, 5.6, and 5.7 the gross stress plots as a smooth linear-hyperbolic stress-strain curve. The stress at the top of the specimen jumps instantaneously to a value comensurate with the step loading and a wave propagates into the specimen. The disturbance propagated is a change in strain proportional to the step velocity imposed on the specimen top. The change in strain may be interpreted as a change in stress using the specimen's constitutive relationship.

The stress at the bottom must await the arrival of the incident wave (at $\tau=1.0$). Because it is reflected off the rigid stationary lower pedestal, the stress at the bottom of the specimen jumps instantaneously at $\tau=1.0$ to a value equal to twice the value of the stress change in the incident wave. A similar event occurs at the top of the specimen when this first reflected wave arrives there (at $\tau=2.0$) and is reflected off the rigid downward moving upper pedestal. The stress at the top then increases instantaneously by an amount equal to twice the value of the stress change in the incident wave so that stress

at the top now becomes equal to three times the value of the
stress change in the wave. The process repeats at each subsequent
initial arrival of the wave at the top and bottom of the
specimen, increasing the   stress there each time by an amount
equal to twice the value of the stress disturbance in the wave.

In the early part of the test when stress varies linearly
with strain, the process is clear and simple and is illustrated
on Figures 5.5, 5.6, and 5.7. When stress and strain begin their
nonlinear relationship, the stress change in the wave as a
consequence of the strain change is progressively smaller, in
conformity with the nonlinear stress-strain relationship. The
smaller stress change means that less resistance can be offerred
to the inertial forces so that the severe step pulse on its
arrival causes an overshoot and minor oscillation as it reflects.
These phenomena are evident in the figures. The smaller stress
change also means that the stresses at the top and bottom
increase by progressively smaller amounts on each reflection.
This latter result causes the stress-time and stress-gross strain
to display a nonlinear shape characteristic of the specimen's
stress-strain relationship.

Clearly in a test with a large enough step velocity pulse
imposed to cause failure ($\epsilon=15\%$) to occur within just a few wave
traverses of the specimen (say $\tau=10$), the top, bottom, and gross
stress would differ greatly. However if the top and bottom
stresses were carefully plotted, a curve drawn through the their
intersections would trace the specimen's actual stress-strain
relationship quite reliably. Such plots could be made by plotting
upper and lower load cell readings divided by an appropriate area
against the gross strain (upper pedestal displacement divided by
the specimen length).

If the specimen were more slowly loaded so that failure did
not occur until after many traverses of the wave, the differences
among top, bottom, and gross stress would be insignificant, and
perhaps not discernible. Then either the upper or lower load cell
readings divided by the specimen area and plotted against the
gross strain could be used directly as the specimen's stress-
strain relationship.

The overshoot and minor oscillation observed with the step
velocity pulse on each reflection after the stress and strain
levels in the specimen became high enough to exhibit a nonlinear
relationship, technically invalidate the data displayed. The
finite difference algorithm and Program FTSP have no provision
for stress-strain unloading. This is because except for the step
pulse, unloading was not anticipated and never observed.
Moreover, this unloading (the oscillations) with the step pulse
is thought to have little effect on the important aspects of the
analysis. An unloading routine could be incorporated into Program
FTSP, but it would enlarge the memory requirements for the code

58

and increase its computation time. It does not appear to be
justified at this time.

Figures 5.8 through 5.15 show the top, bottom, and gross
stress in specimens subjected to hyperbolic upper pedestal
velocities. The Figures 5.8 to 5.11 are for τ_o=5.0, the fastest
hyperbolic loading of a specimen shown. A hyperbolic upper
pedestal velocity with a characteristic time t_o=0.9 millisecond
imposed on a 1.5-inch-long specimen whose rod wave velocity is
700 ft/sec would have τ_o=5.0. At t=0.9 milliseconds half its
limiting velocity would be reached; three-quarters of its
limiting velocity would be reached by t=2.7 milliseconds. Even
so, the top, bottom, and gross stress-time plots shown are much
less severe than they were for the step pulse. There is no
overshoot and the differences among the top, bottom, and gross
stress are much less.

Figure 5.10 shows the first quarter of Figure 5.9 expanded
for closer observation of the early part of the loading.
Differences among top, bottom, and gross stress are evident and
perhaps would need to be accounted for. To observe stress-gross
strain behavior, Figure 5.11 graphs the second highest curve of
Figure 5.10 (ϵ_{do}=10.0) as stress versus gross strain. Gross
stress plots as a linear-hyperbolic function as expected while
top and bottom stress oscillate in a minor way above and below
it. Because the velocity of the upper pedestal and thus the
strain and stress changes in the propagating wave are nonlinear,
the top and bottom stress oscillations about the gross stress
line are not symmetric as they were for the step velocity pulse.
Nonetheless, a trace of the intersections of the top and bottom
stress still provide a good representation of the specimen's
actual stress.

Figures 5.12 and 5.13 are for τ_o=10. The curve for ϵ_{do}=30 on
Figure 5.13 corresponds to the 28-millisecond duration tests run
on the FTRXD and shown on Figures 4.1 to 4.4, 4.9 to 4.11, and
4.14. Clearly within the one-dimensional model of the specimen,
there is little difference in the values of top, bottom, or gross
stress. The differences evident on Figures 4.1 to 4.4 and 4.14 in
upper and lower load cell readings are probably not attributable
to inertial or wave effects within the specimen. Instead, they
are more likely the result of the dynamic behavior of the FTRXD
as an assemblage of deformable components possessing mass and the
instrumentation employed during testing.

Figures 5.14 and 5.15 portray the behavior of a specimen
whose upper pedestal velocity has τ_o=20.0. From the point of view
of wave propagtion, these results are essentially static.

The truly dynamic tests were those run rapidly enough to
show significant inertial and wave effects. The fastest tests run
to date were those whose durations were about 2 milliseconds. The
results of these tests are shown on Figures 4.5 to 4.7, 4.12,

4.13, and 4.15. The upper pedestal motion of these tests was complex and could be only roughly estimated (Chapter 4, Figures 4.12 and 4.13). Consequently, constant acceleration of the upper pedestal, a simple approximation of this motion, was used for the analytical study of the inertial effects in the sample under very rapid loading. Figures 5.16 through 5.20 show the results of this study. Since only one parameter is needed to define the upper pedestal boundary condition instead of two, only two dimensionless parameters are required for the stress-time data instead of three. These are σ_1/σ_{max} (= MLDS = 0.25) and ϵ_{do} (= $\epsilon_o C_o / v_o$ = 5, 10, 20, 30, 40, & 50). Note that for constant upper pedestal acceleration, v_o is the velocity of the upper pedestal at the instant that the initial wave reaches the bottom of the specimen; it is not a limiting velocity as in the case of hyperbolic upper pedestal velocity.

The curves for ϵ_{do}=20 are the closest approximation for the 2-millisecond duration tests run on 1.5-inch-long specimens of the CARES-Dry soil. These are replotted on Figures 5.18 and 5.19 to τ=10, the dimensionless time at which ϵ is approximately 15% for constant upper pedestal accelerations of 300 to 400g (see Figure 5.16). Examination of Figure 4.13 suggests that the 2-millisecond duration tests might be approximated using constant upper pedestal accelerations of from 300 to 400g.

Gross stress plots as a smooth curve between top and bottom stress as expected, and as the linear-hyperbolic function on the stress-gross strain plots of Figure 5.19. There are clear differences among the three stresses. Top stress plots entirely above gross stress and bottom stress entirely below it. The only exceptions appear to be at τ=2 and τ=4 where all three stresses come together.

Figure 5.20 shows the curves for ϵ_{do}=5 plotted to τ=8. A 1.5-inch-long specimen whose rod wave velocity is 700 ft/sec and which is subjected to a 1200g constant acceleration of its top, might possess ϵ_{do}=5. In addition, ϵ=15% would be reached in about 1 millisecond or τ=8 and v_o=83 in/sec. The differences among top, bottom, and gross stress are clearly much greater for this much more rapidly loaded specimen. Nonetheless, gross stress plots against gross strain as a linear-hyperbolic function, the correct constitutive relationship for the specimen. It is bounded by top stress above it and bottom stress below it as it was in Figure 5.19. Though neither top or bottom stress by themselves represent the specimen's constitutive relationship well, some functional combination of the two could be found which would. No attempt was made to find such a functional relationship since it is not clear yet whether constant acceleration for the upper pedestal is the most reasonable representation of the upper pedestal boundary conditions for the very rapid tests.

The clear differences between the upper and lower load cell readings and the significant oscillations in the upper load cell

readings as shown on Figure 4.7 for the 2-millisecond duration test, RDCFS74, cannot be explained from the specimen's dynamic behavior alone. They presumably reflect the dynamic response of the FTRXD itself and perhaps the instrumentation employed.

FIG 5.1, FTRXD SPECIMEN PHYSICAL MODEL
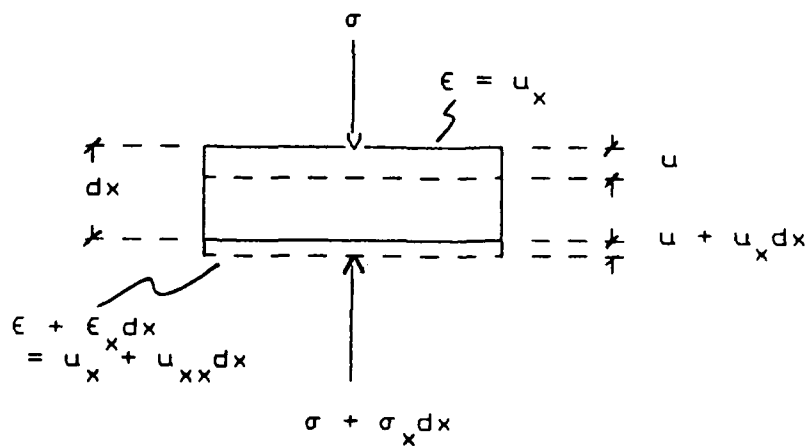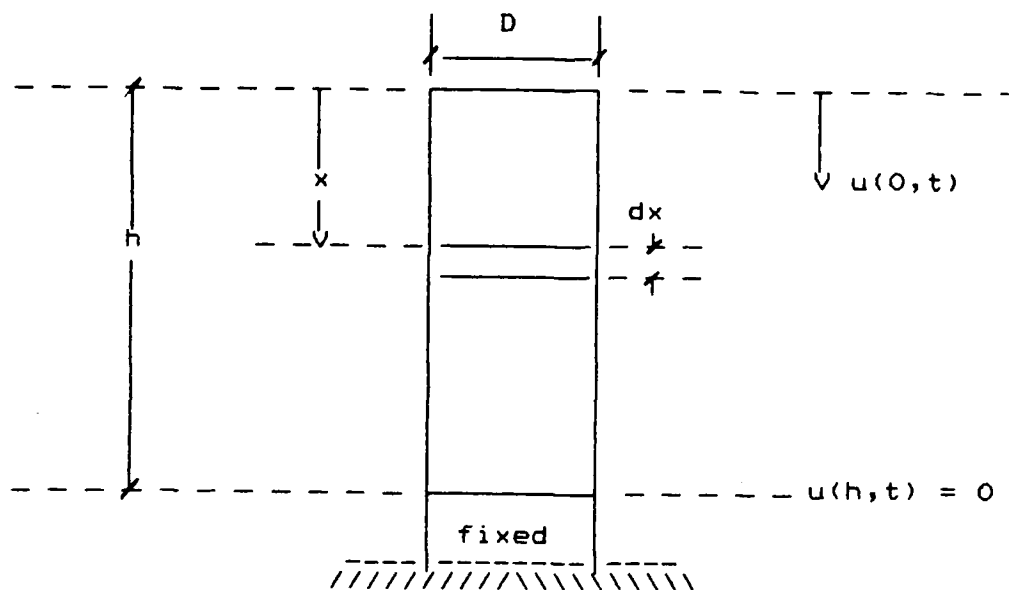
Fig 5.2, LINEAR-HYPERBOLIC FUNCTION
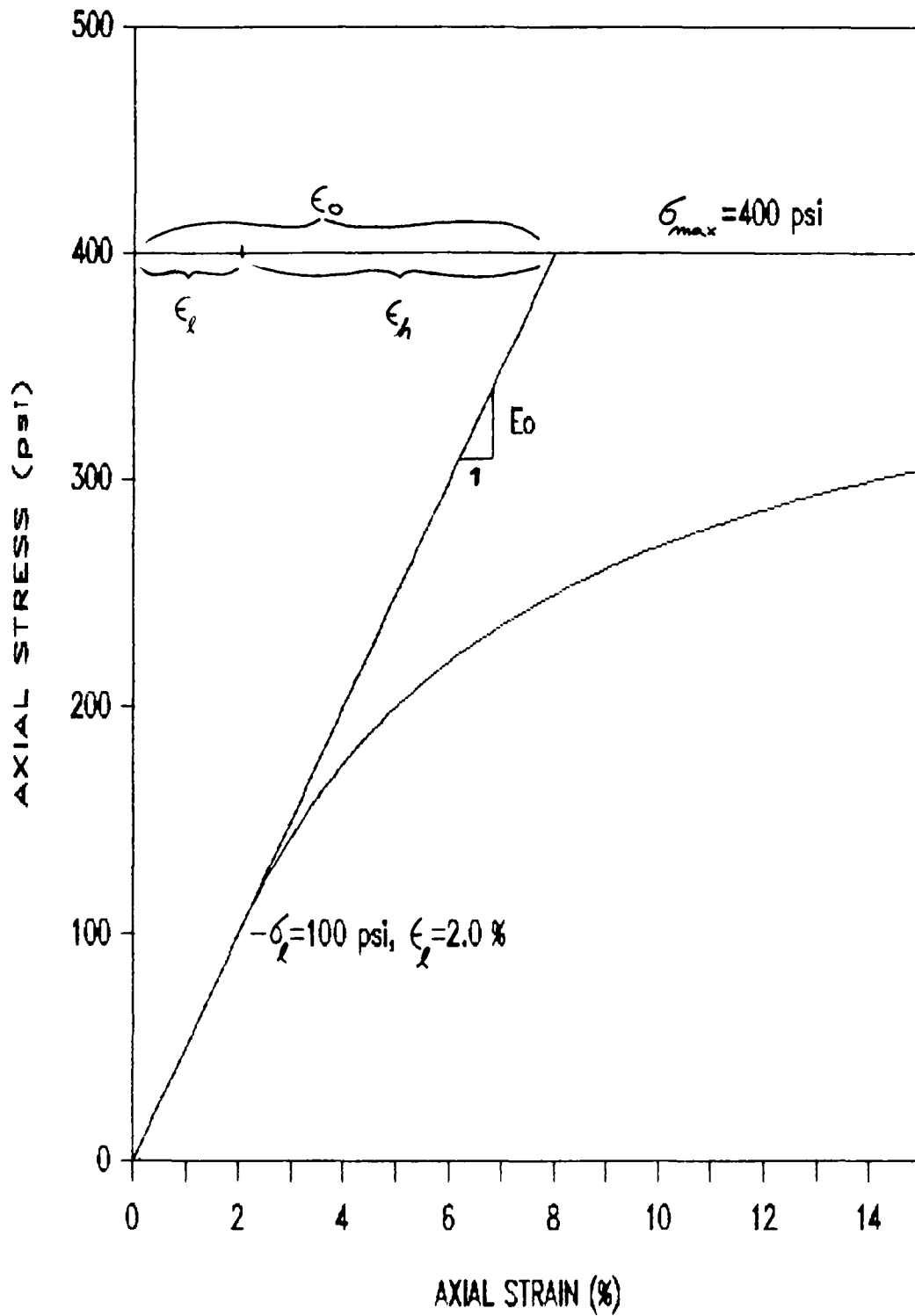
STRESS-STRAIN RELATIONSHIPS

ϵ_o

$\sigma_{max} = 400$ psi

ϵ_ℓ

ϵ_h

E_o

1

$-\sigma_\ell = 100$ psi, $\epsilon_\ell = 2.0$ %

AXIAL STRESS (psi)

AXIAL STRAIN (%)

Fig 5.3, FINITE DIFFERENCE GRID

(Co)(dt) = (dx) = 0.10

DIMENSIONLESS TIME (Cot/h)

DIMENSIONLESS POSITION (1-x/h)

Fig 5.4, UPPER PEDESTAL MOTION
HYPERBOLIC DIMENSIONLESS PLOTS

Coto/h = 0.0

€=15%, Vo=35 ips--
€=15%, Vo=42 ips--
€=15%, Vo=50 ips--
€=15%, Vo=63 ips--

DISPLACEMENT

VELOCITYx10

VEL (v/Vo) & DISPL (u/h)(Co/Vo)

TIME (Cot/h) or GROSS STRAIN (€Co/Vo)

Fig 5.5, TOP, BOTTOM, & GROSS STRESS
Coto/h = 0.0   MLDS = 0.25

€oCo/Vo=5
10
20
30
40
50

DIMENSIONLESS STRESS (S/MAX S)

TIME (Cot/h) or GROSS STRAIN (€Co/Vo)
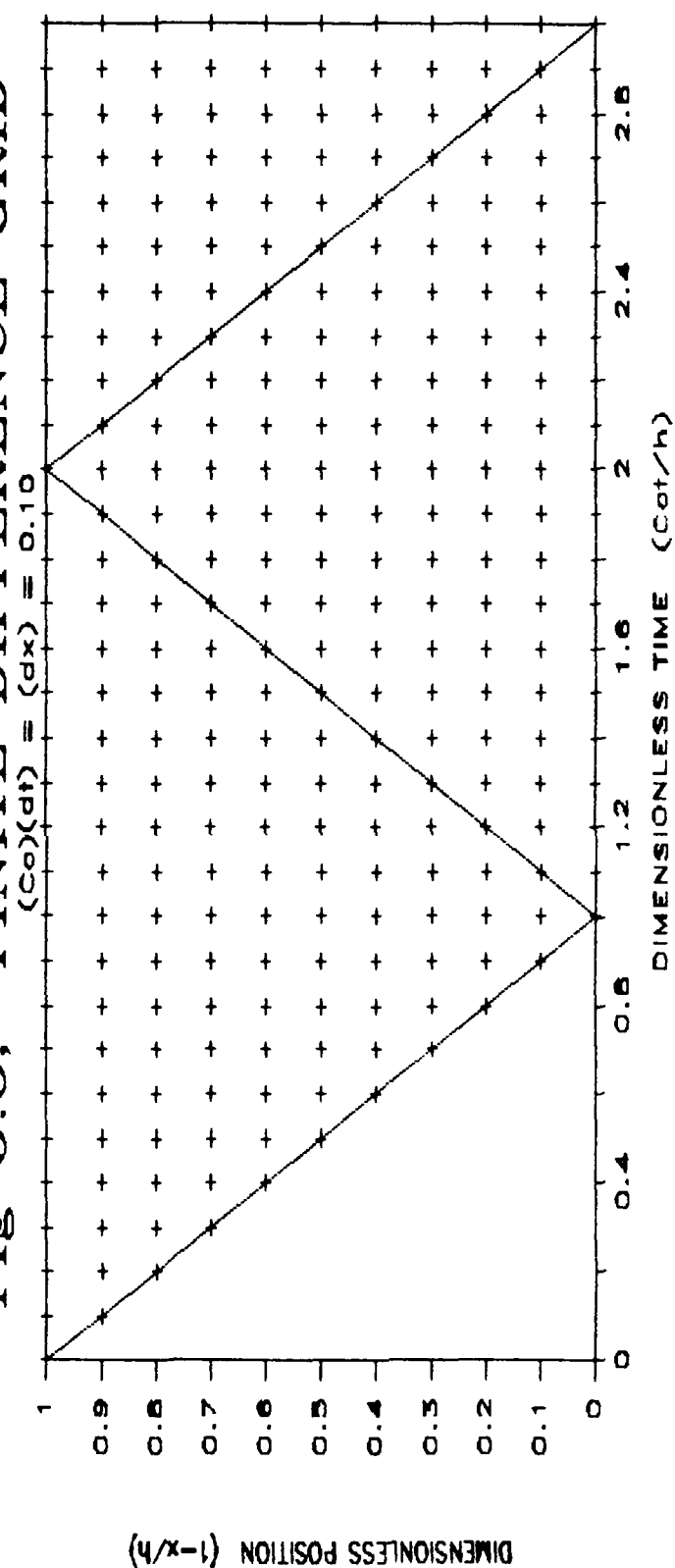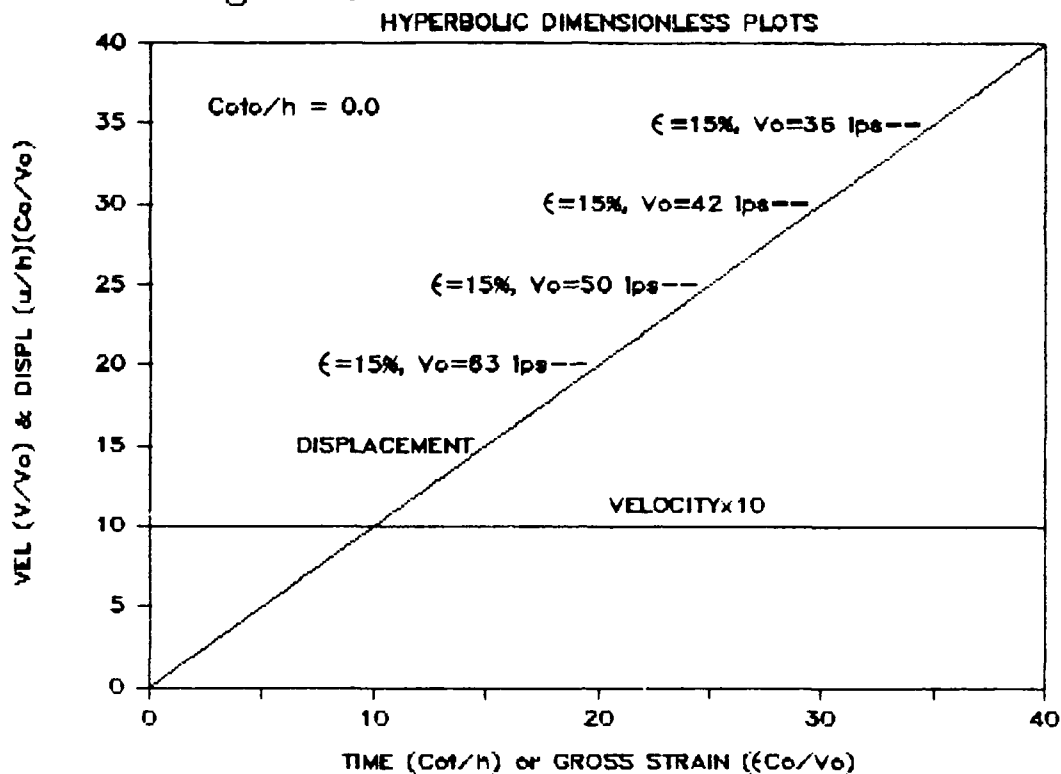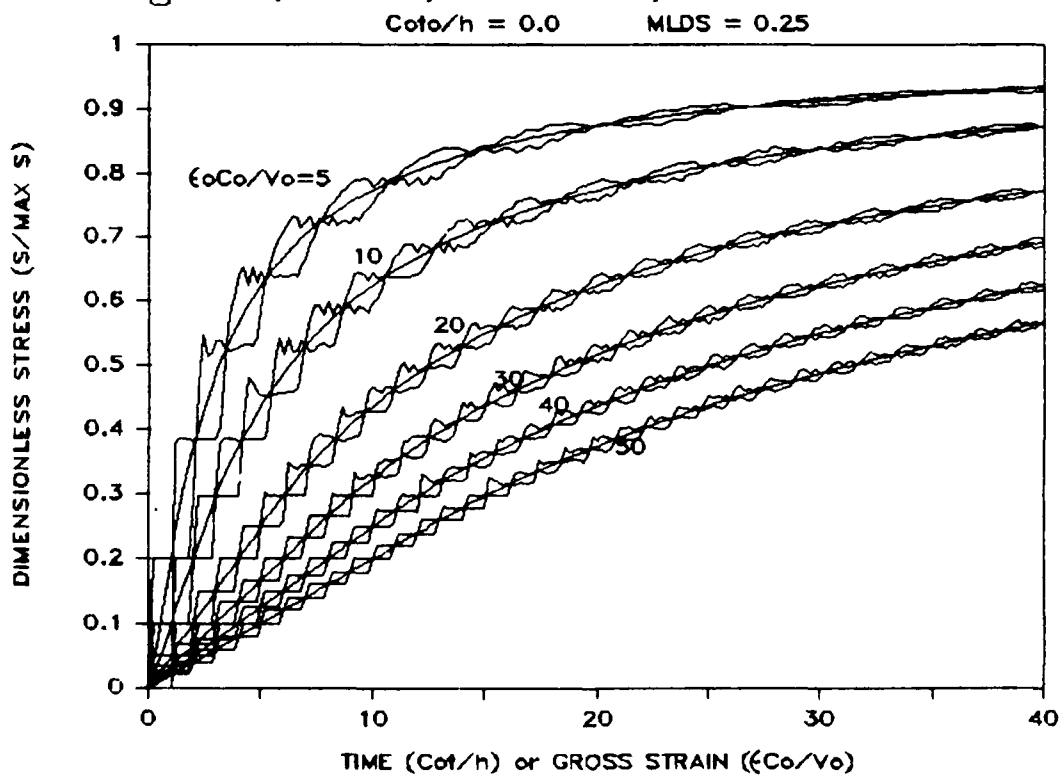
Fig 5.6,   TOP STRESS & GROSS STRESS

Coto/h = 0.0   MLDS = 0.25

DIMENSIONLESS STRESS (S/MAX S)

$\epsilon oCo/Vo=5$

10

20

30

40

50

TIME (Cot/h) or GROSS STRAIN ($\epsilon Co/Vo$)

Fig 5.7,   BOTTOM STRESS & GROSS STRESS

Coto/h = 0.0   MLDS = 0.25

DIMENSIONLESS STRESS (S/MAX S)

$\epsilon oCo/Vo=5$

10

20

30

40

50

TIME (Cot/h) or GROSS STRAIN ($\epsilon Co/Vo$)

66
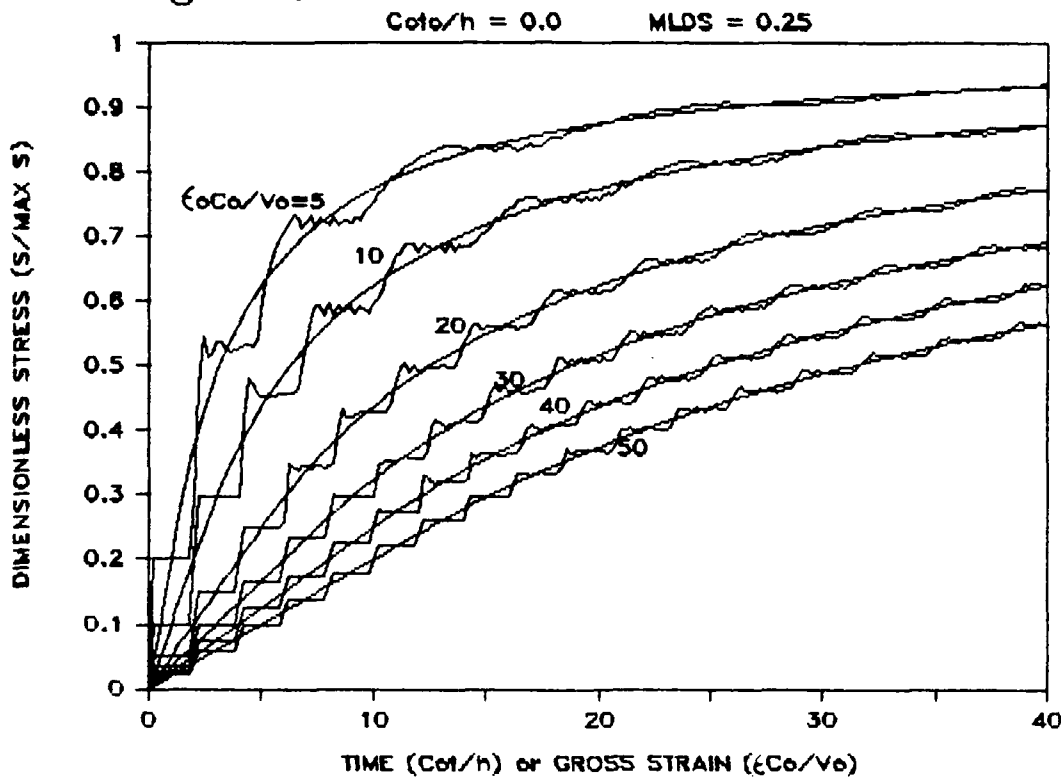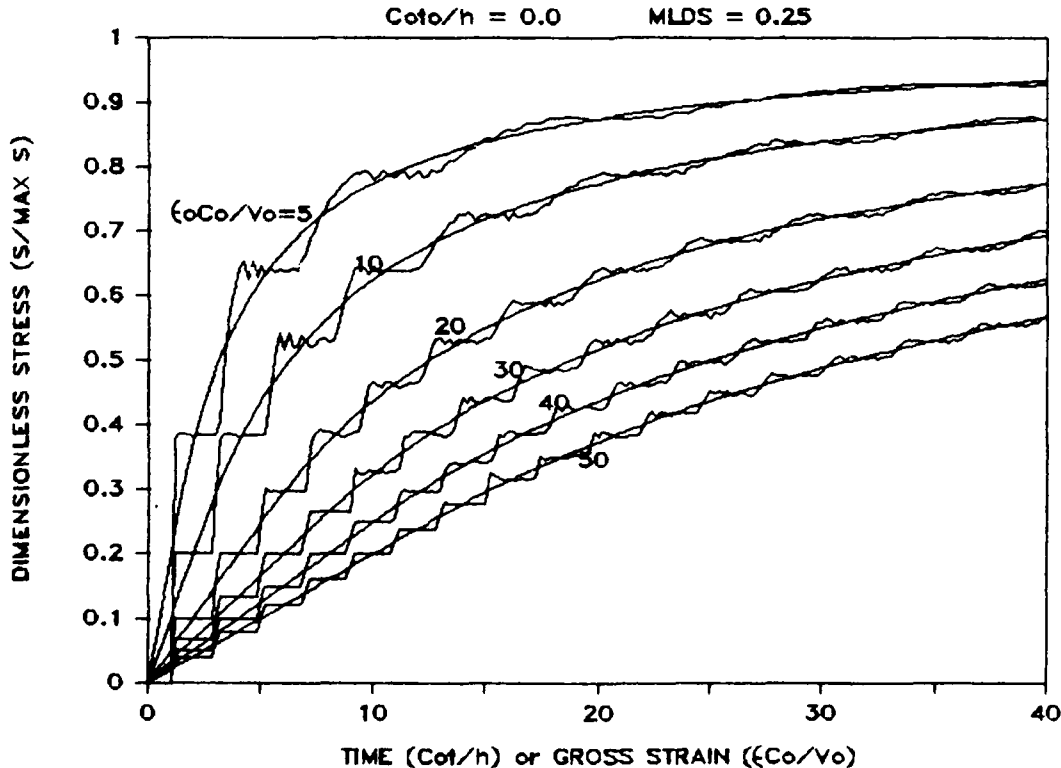
Fig 5.8, UPPER PEDESTAL MOTION

HYPERBOLIC DIMENSIONLESS PLOTS
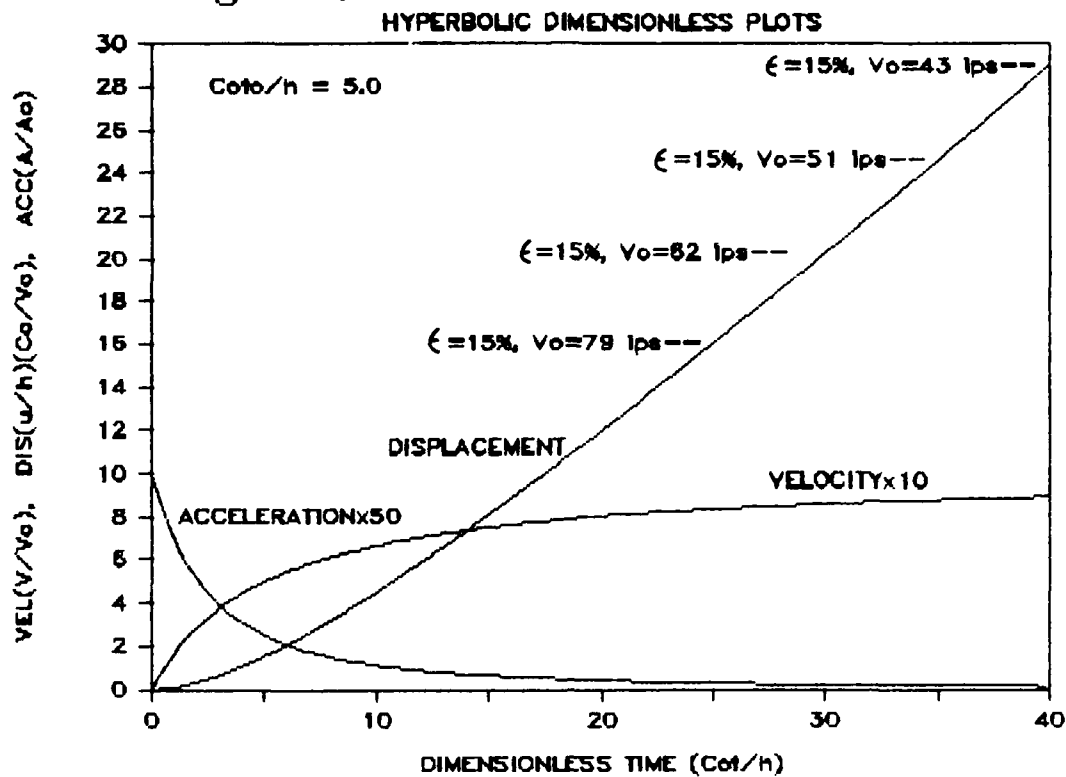
Fig 5.9, TOP, BOTTOM, & GROSS STRESS
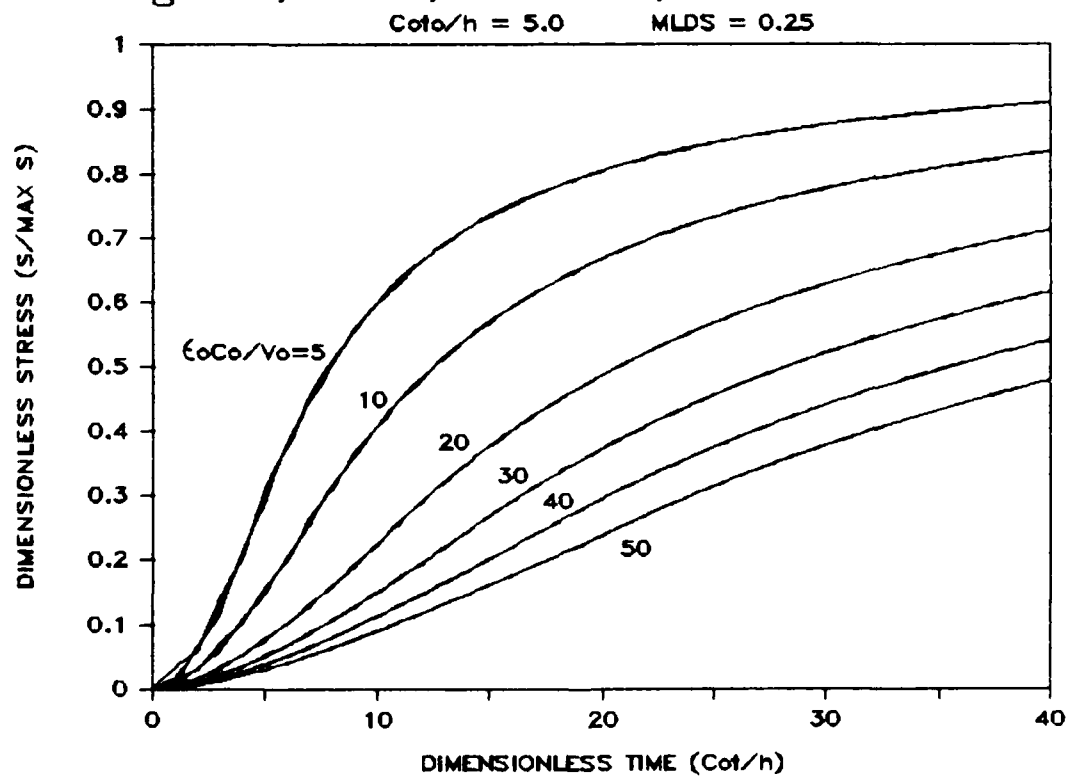
Fig 5.10, TOP, BOTTOM, & GROSS STRESS

Coto/h = 5.0   MLDS = 0.25
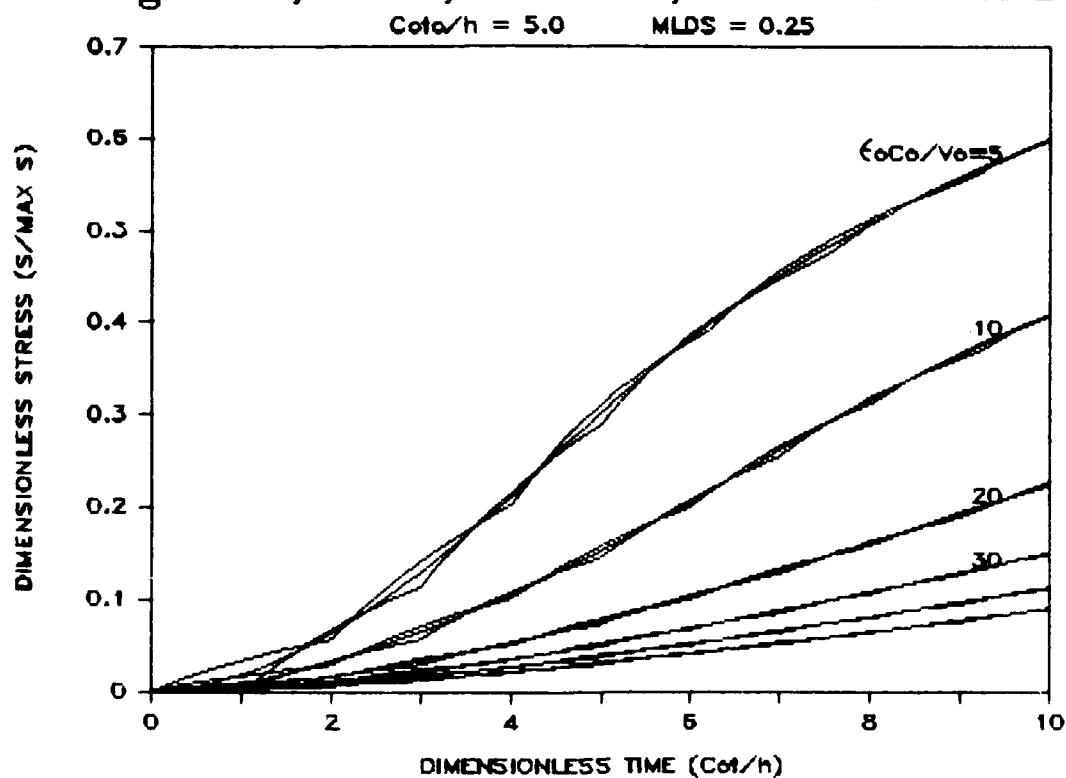
Fig 5.11, TOP, BOTTOM, & GROSS STRESS

Coto/h = 5.0   MLDS = 0.25

68
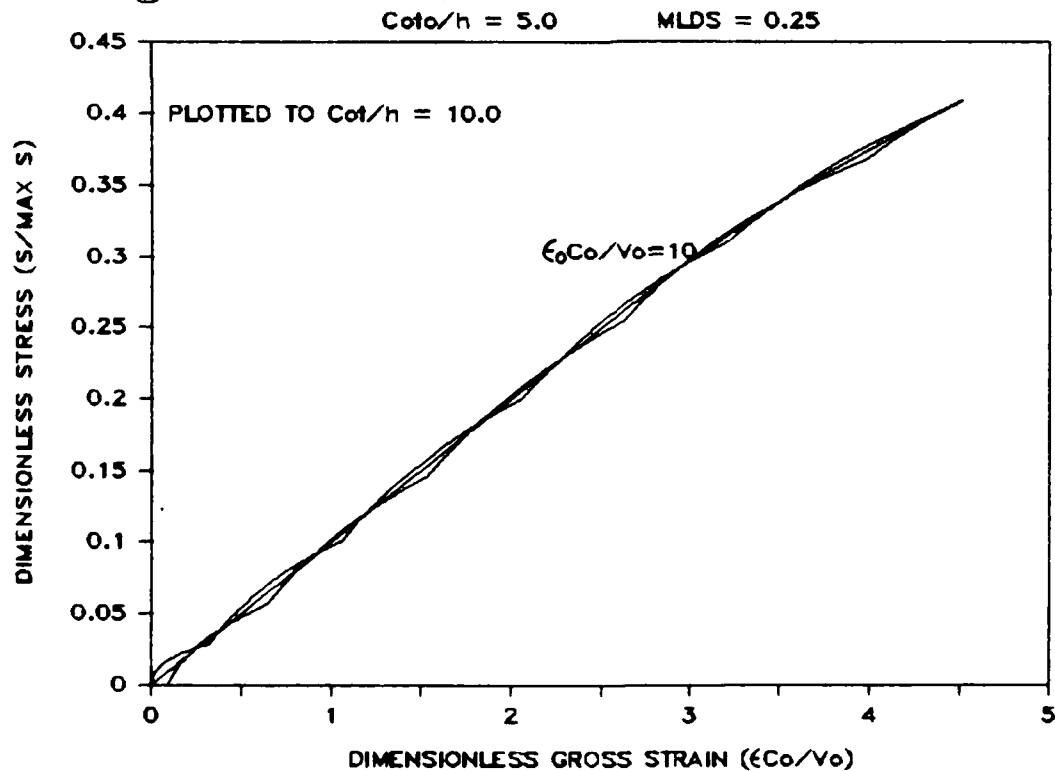
Fig 5.12, UPPER PEDESTAL MOTION

HYPERBOLIC DIMENSIONLESS PLOTS

Coto/h = 10.0

$\xi=15\%$, Vo=53 Ips—

$\xi=15\%$, Vo=63 Ips—

$\xi=15\%$, Vo=78 Ips—

$\xi=15\%$, Vo=101 Ips—

DISPLACEMENT

VELOCITYx10

ACCELERATIONx100

VEL(v/vo), DIS(u/h)(Co/Vo), ACC(A/Ao)

DIMENSIONLESS TIME (Cot/h)
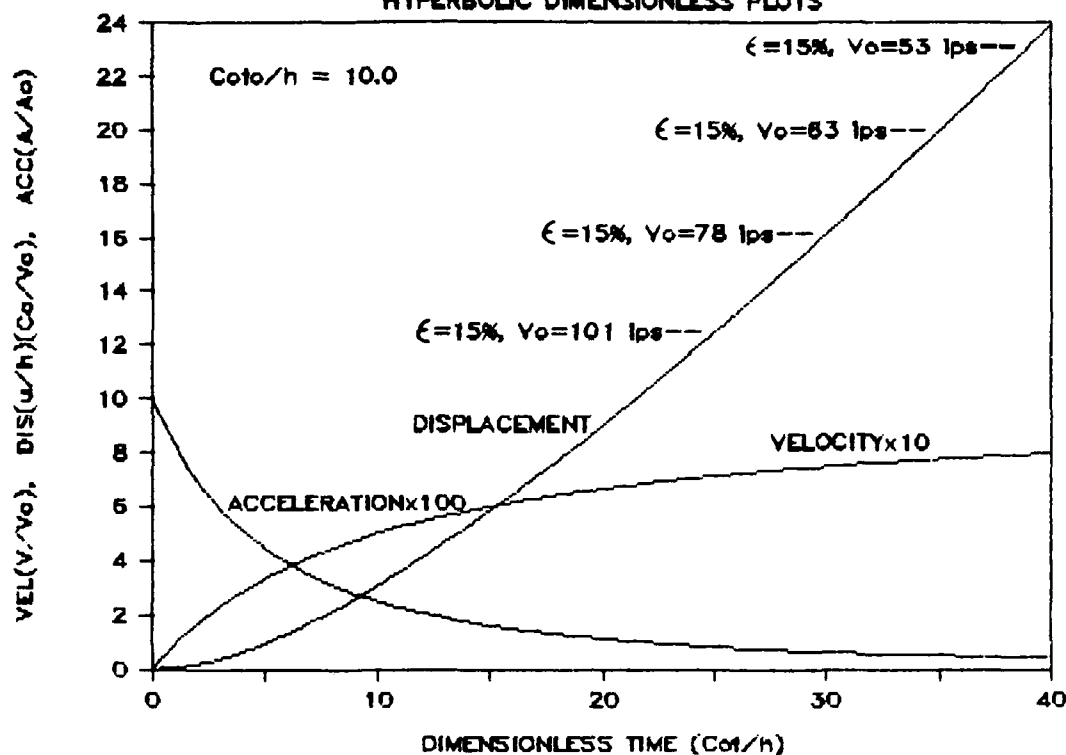
Fig 5.13, TOP, BOTTOM, & GROSS STRESS
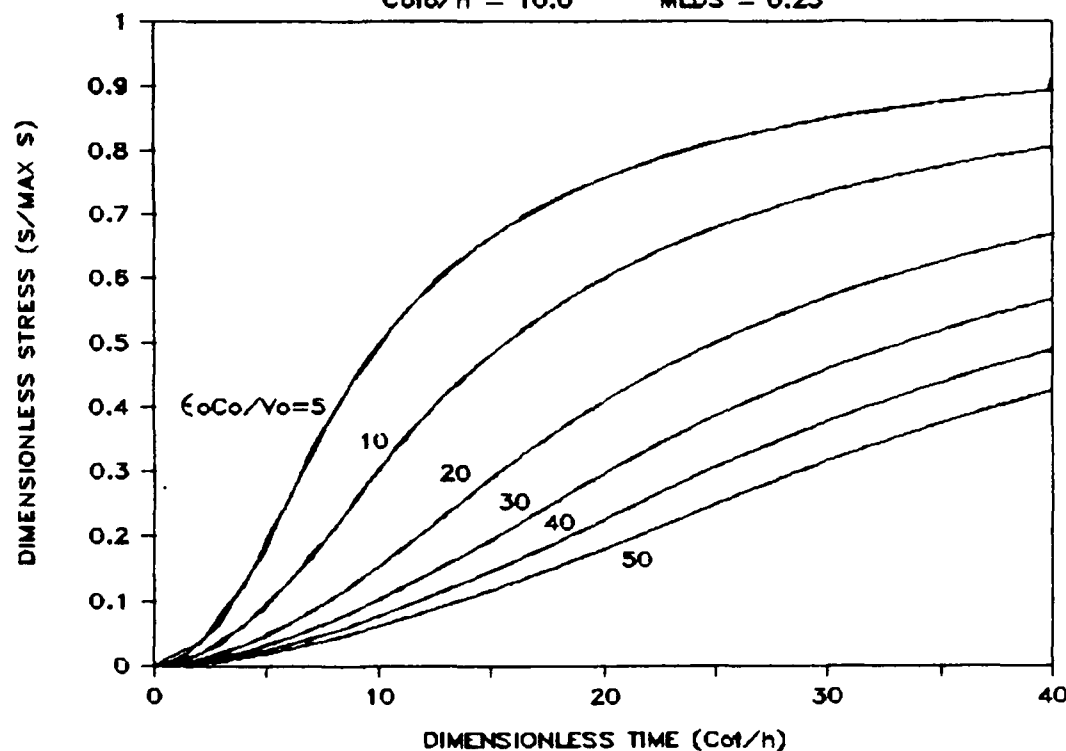
Coto/h = 10.0   MLDS = 0.25

$\xi oCo/Vo=5$

10

20

30

40

50

DIMENSIONLESS STRESS (S/MAX S)

DIMENSIONLESS TIME (Cot/h)

69

Fig 5.14, UPPER PEDESTAL MOTION

HYPERBOLIC DIMENSIONLESS PLOTS

Coto/h = 20.0

ϵ =15%, Vo=8 Ips——

ϵ =15%, Vo=9 Ips——

ϵ =15%, Vo=11 Ips——

ϵ =15%, Vo=13 Ips——

ϵ =15%, Vo=15 Ips——

DISPLACEMENT

VELOCITY×50

ACCELERATION×500

VEL(V/Vo), DIS(u/h)(Co/Vo), ACC(A/Ao)

DIMENSIONLESS TIME (Cot/h)

Fig 5.15, TOP, BOTTOM, & GROSS STRESS

Coto/h = 20.0   MLDS = 0.25

ϵoCo/Vo=5

10

20

30

40

50

DIMENSIONLESS STRESS (S/MAX S)

DIMENSIONLESS TIME (Cot/h)
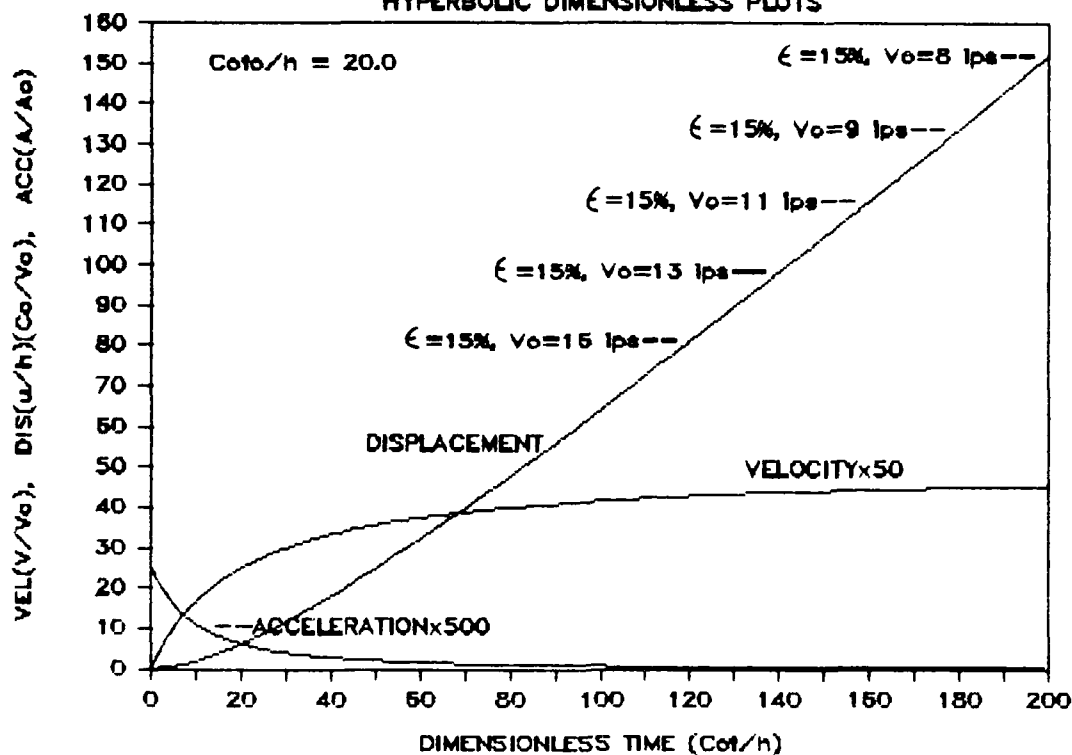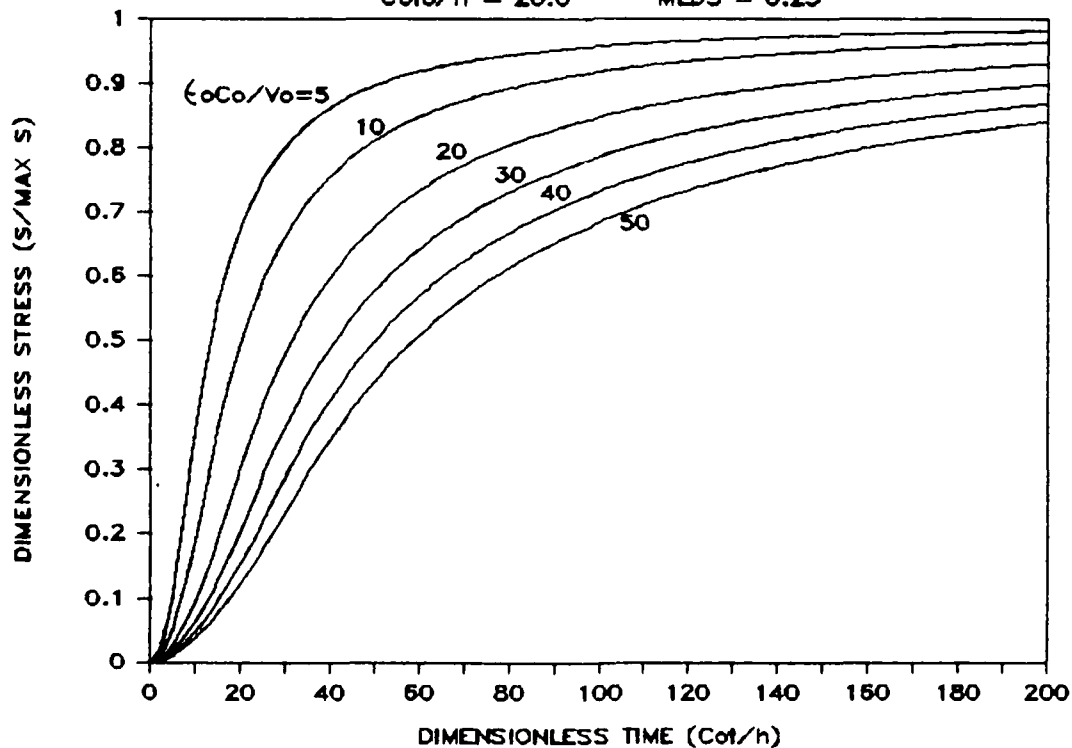
Fig 5.16, UPPER PEDESTAL MOTION

PARABOLIC DIMENSIONLESS PLOTS

NOTE: Vo is not a limiting velocity

$Vo = (Ao)*(h/Co)$

$Ao = Constant$

VELOCITY

ACCELERATIONx10

$\epsilon=15\%, Ao=91g$--

$\epsilon=15\%, Ao=113g$--

$\epsilon=15\%, Ao=143g$--

$\epsilon=15\%, Ao=187g$--

$\epsilon=15\%, Ao=254g$--

$\epsilon=15\%, Ao=400g$-- --DISPLACEMENT/20

VEL(V/Vo), DIS(u/h)(Co/Vo), ACC(A/Ao)

DIMENSIONLESS TIME (Cot/h)
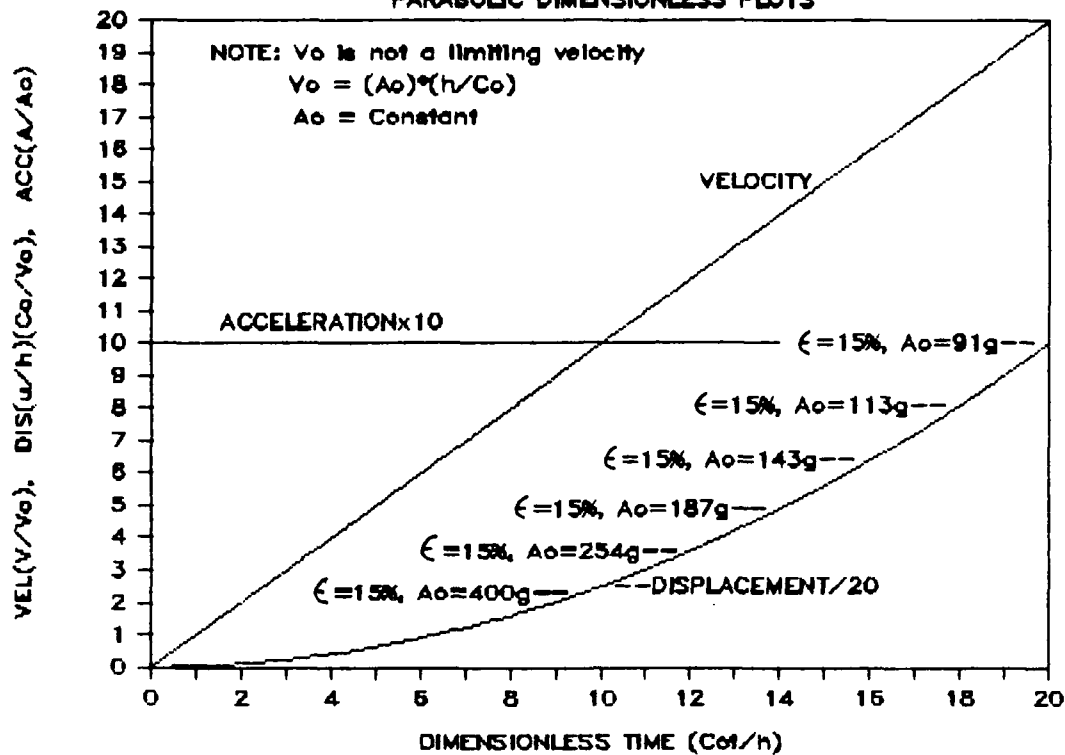
Fig 5.17, TOP, BOTTOM, & GROSS STRESS

U.P. ACCEL = Ao   MLDS = 0.25

$\epsilon oCo/Vo=5$

10

20

30

40

50

DIMENSIONLESS STRESS (S/MAX S)

DIMENSIONLESS TIME (Cot/h)

71
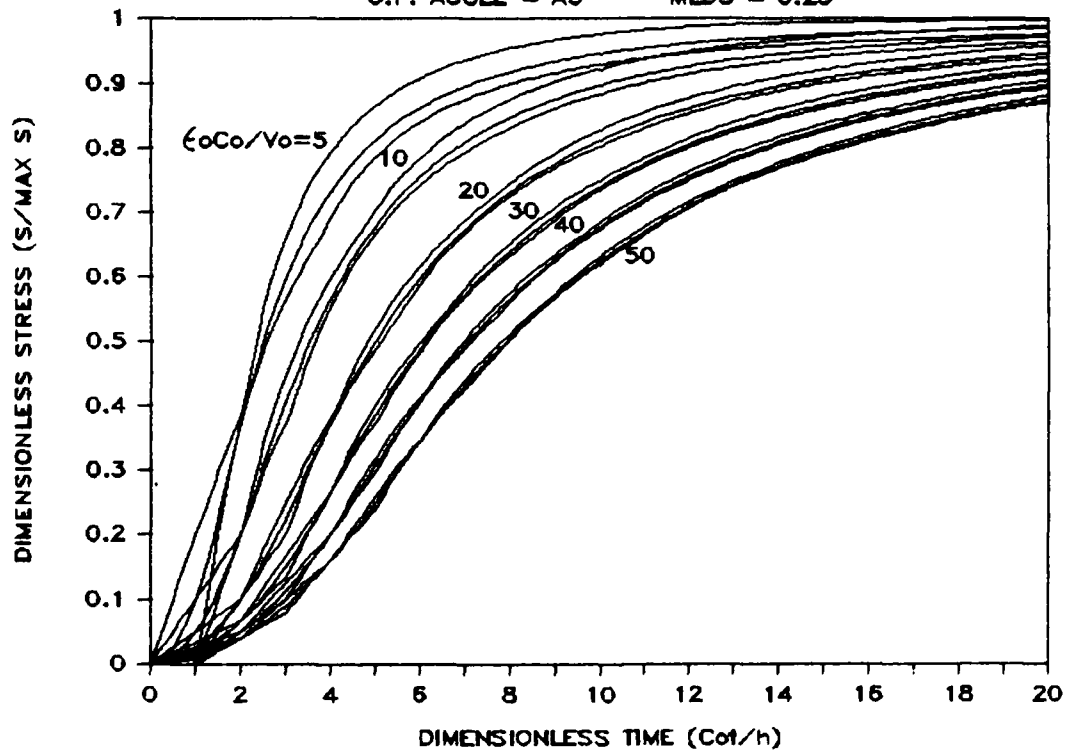
Fig 5.18, TOP, BOTTOM, & GROSS STRESS
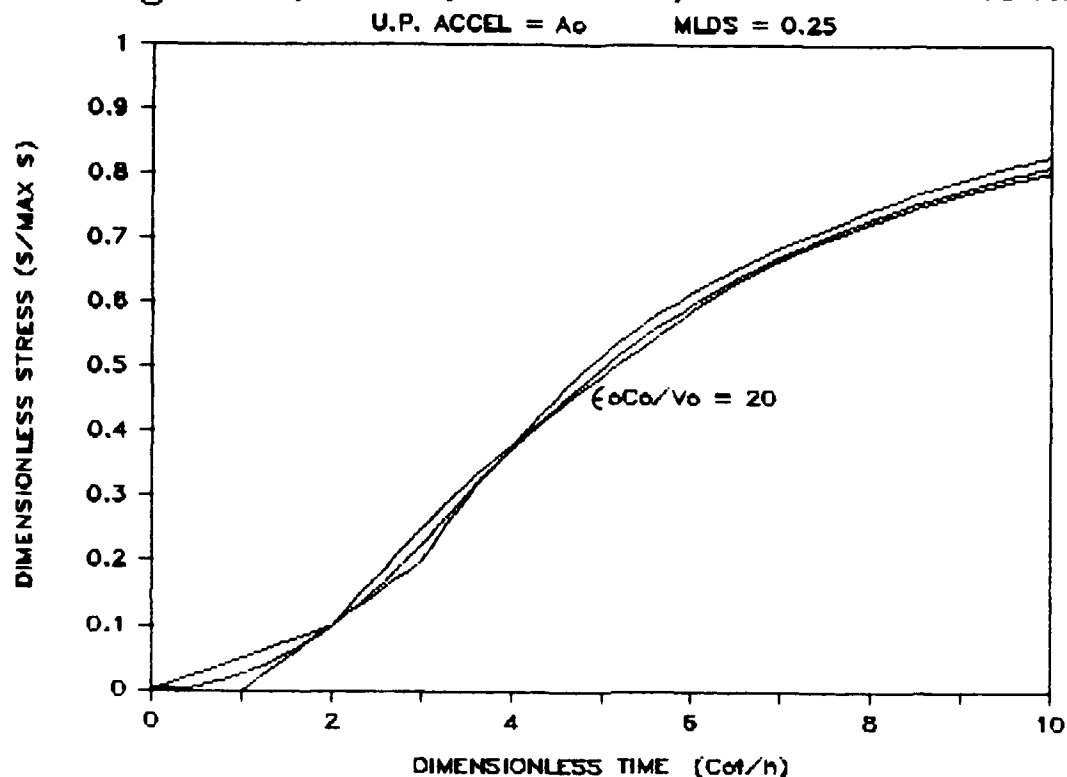
U.P. ACCEL = Ao   MLDS = 0.25

$\epsilon_o C_o / V_o = 20$

DIMENSIONLESS STRESS (S/MAX S)

DIMENSIONLESS TIME (Cot/h)

Fig 5.19, TOP, BOTTOM, & GROSS STRESS

U.P. ACCEL = Ao   MLDS = 0.25

Plotted to Cot/h = 10.0

$\epsilon_o C_o / V_o = 20$

DIMENSIONLESS STRESS (S/MAX S)

DIMENSIONLESS GROSS STRAIN ($\epsilon C_o / V_o$)

Fig 5.20, TOP, BOTTOM, & GROSS STRESS

U.P. ACCEL = Ao   MLDS = 0.25

$EoCo/Vo = 5$

Plotted to Cot/h = 8.0

DIMENSIONLESS STRESS (S/MAX S)

DIMENSIONLESS GROSS STRAIN (ECo/Vo)

73
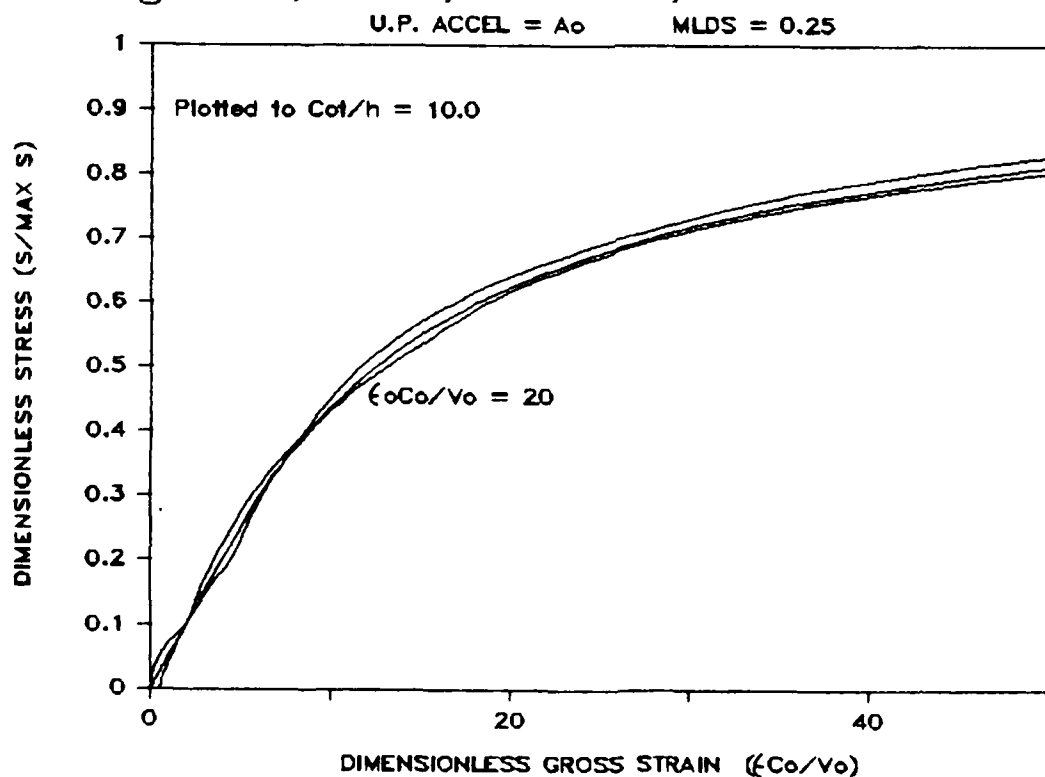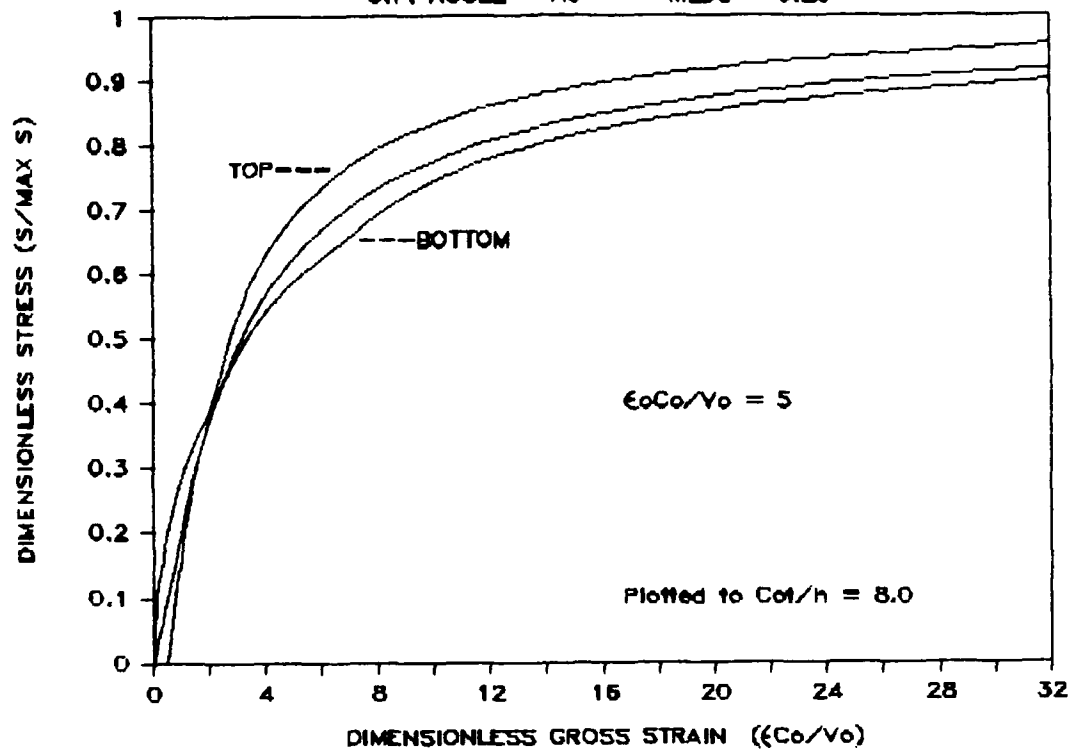
CHAPTER 6

SUMMARY, CONCLUSIONS, AND RECOMMENDATIONS

The FTRXD has demonstrated its ability to load a 1.5-inch-long specimen to failure (ϵ=15%) in 2 milliseconds. What is not yet clear, however, is the meaning of the readings from the upper and lower load cells and the Kaman displacement gage when specimens are loaded at this rate. For slower tests, those with a duration of 28 milliseconds or more, these readings can almost certainly be converted directly to the specimen's principal stress difference (PSD)-axial strain relationship for the loading conditions imposed. In these slower tests, the effects of loading rate on the specimen constitutive behavior could then be investigated by testing identical specimens at different loading rates.

The lower load cell readings were always lower than those of the upper load cell. The differences in magnitude between these readings is not totally understood. It occurred in all of the test results examined from the very slow to the very fast. The faster the test, the larger the difference — from less than 1% in the tests of 120-second duration to about 40% in the tests of 2-millisecond duration. Some of the difference in the fast tests can be accounted for by the wave and inertia effects in the specimen on the stress at the top and bottom of the specimen. These effects are apparent on Figures 5.17 to 5.20. However, a major part of the difference cannot be accounted for in this manner. It must be attributed to the dynamics of the FTRXD itself and perhaps to the instrumentation employed. Whatever the source, it must be identified and either eliminated or quantified, if the specimen's constitutive behavior is to be obtained from the load cell data. As suggested in Chapter 5, the stress-strain behavior of the specimen might be deduced from these rapid tests, but only if reliable data are available from the load cells. In the very rapid tests, data from both load cells will be needed; in the slower tests, data from one of the load cells will be necessary.

In the 2-millisecond duration tests, major oscillations occurred in the upper load cell readings while only minor oscillations were recorded by the lower load cell (see Figure 4.7). This phenomena cannot be explained from the wave and inertia effects within the specimen. Instead, the dynamics of the FTRXD must again be the source. The fact that the oscillations were essentially only recorded by the upper load cell suggests that the dynamics of the moving upper pedestal may have a major effect on the upper load cell and little or no effect on the lower load cell. Again, the stress-strain behavior of the specimen might be deduced from these very rapid tests, but only if reliable data from both the upper and lower load cells are available.

75

The 500-pound load cell, used in the tests of 28-millisecond duration or longer, had a natural period of 0.11 milliseconds. The 1000-pound load cell, used in the 2-millisecond duration tests, had a natural period of 0.07 milliseconds. Although the response times of the load cells were not an important factor in the test results examined, they must have contributed to the minor oscillations recorded in the load cell readings. The response times could be an important factor for tests in which failure occurs in less than 1 millisecond.

The 2-millisecond duration tests on specimens with low confining pressures were chaotic (see Figure 4.5 and 4.6). Perhaps the weaker specimens (lower confining pressures) were completely dominated by the dynamics of the upper pedestal.

Clearly the control and definition of the upper pedestal motion is vital to the successful operation of the FTRXD and the analysis of the test results obtained. The displacement-time plot of the upper pedestal provides the upper boundary condition for the specimen which in turn has a dominant effect on the stress-time and strain-time plots. It also forms the basis for the abscissa (strain) in stress-strain plots.

Differentiating the measured displacement-time data for the upper pedestal in the very rapid tests to obtain upper pedestal velocities, revealed oscillations in the calculated velocity data. Although the source of these oscillations is not clearly understood, measuring the acceleration of the upper pedestal in addition to its displacement should help to clarify what is happening. To measure the displacement of the upper pedestal, the Kaman gage uses a 1.625-inch-long by 0.385-inch-thick aluminum cantilever target rigidly attached to the moving pedestal. The natural period of the cantilever is 20 to 30 milliseconds. More reliable displacement data would be obtained if its natural period were 10% or less of the test duration.

The most controlled motion of the upper pedestal occurred when there was oil in the lower chamber of the load cylinder of the FTRXD. This resulted in an upper pedestal velocity that was reasonably represented as a two-parameter hyperbola. The simplicity of this motion facilitated the wave analysis of the specimen. However, the design of the load cylinder, at present, precludes bringing a specimen to failure in less than about 20 milliseconds when oil is in the lower chamber. Additional and larger orifices for the oil to leave the lower chamber during loading would increase the speed with which testing can be accomplished in this way.

With no oil in the chamber, the upper pedestal moved much faster, taking the specimen to failure in about 2 milliseconds. It can doubtless run faster yet if stronger tubular shear pins are employed in conjunction with higher pressure in the upper chamber. However, the motion will still be loosely controlled and

complex. It must be recorded definitively so that relevant boundary conditions for a wave analysis of the specimen can be employed. Clearly in faster tests, the dynamics of the FTRXD will be even more important and must be understood.

Several recommendations regarding the evaluation of the FTRXD are in order:

1. Install an accelerometer in the upper pedestal at the point of the Kaman gage cantilever target so that both the displacement and acceleration data of the upper pedestal may be obtained. The accelerometer must be able to record accelerations accurately and withstand very large acceleration "spikes."

2. Install a cantilever target for the Kaman gage with a natural period of 0.1 milliseconds or less. The shorter and the thicker it is, the better. An aluminum cantilever of the same general shape as the present one but 1.25 inches thick should possess a natural period of less than 0.1 milliseconds.

3. Modify the load cylinder so that oil in its lower chamber can be expelled faster during testing. More and symmetrically positioned orfices of larger diameter would be desirable. Recognizing the need to open the orifices simultaneously and very rapidly, more than one orifice may be impractical. As a minimum, the present orifice might be doubled in diameter. If simultaneity of openings can be achieved, additional orfices will be a great improvement.

4. Conduct a detailed examination of the load cells, their calibration, their response times, and the manner of recording data from them. The purpose of this study would be to either verify that the difference in upper and lower load cell readings is not caused by the load cells themselves, or if it is, to identify and remove the source or quantify its effects. The study could also assess the limitations of the load cells in terms of their response times.

5. Conduct a detailed dynamic analysis of the FTRXD as an assemblage of deformable components possessing mass. Such an analysis has been begun by the author. The FTRXD was modeled as a two degree of freedom system with a linear-hyperbolic massless spring representing the soil specimen, and lumped masses and linear springs representing the remainder of the system. The model shows promise, but needs refinement. Better excitation data (displacement-time or force-time) might be employed, mass might be added to the nonlinear spring, and the analysis might be extended to more than two degrees of freedom. The purpose of the analysis would be to ascertain what the upper and lower load cells should read during the very fast tests, to provide insights into when and how the dynamics of the upper pedestal can dominate the effects of the soil element, and to suggest ways to improve the FTRXD so that more usable test data may be obtained.

6. Conduct a series of rapid tests with the FTRXD on a well established soil, such as CARES-Dry soil, prepared in specimens whose lengths vary from 1.5 to 3 inches and whose diameters remain at 0.75 inches. The purpose of the testing would be to validate the modifications to the FTRXD suggested above, to validate better the one-dimensional wave analysis of the specimen described in Chapter 5, to investigate the effect of specimen strength (confining pressure) on the dynamic response of the FTRXD, and to validate and complement the dynamic analysis of the FTRXD as recommended above.

7. Conduct a two-dimensional axisymmetric wave analysis of the specimen initially as a linear elastic material. The purpose of this analysis would be to define the limits of the validity of the one-dimensional wave analysis. As required, it would be extended to a specimen possessing a postulated nonlinear constitutive relationship which reflects the yielding and shear failure anticipated in the triaxial testing of soils.

8. Conduct a series of rapid tests with the FTRXD on a variety of soils prepared in specimen sizes from 1.5 to 4 inches. The FTRXD would first be modified to accomodate specimens with diameters of 1.0 inch. The purpose of the testing would be to validate the analyses of the FTRXD and to assess its utility in testing a variety of soils for their engineering properties at very rapid loading rates.

REFERENCES

1. Carroll, William F., 1963, "Vertical Displacements of Spread Footings on Clay: Static and Impulsive Loadings," _Dynamic Bearing Capacity of Soils, Report 5_, Technical Report 3-599, US Army Engineer Waterways Experiment Station, Vicksburg, MS.

2. Cummins, Tony K., 1982, "Description of a Fast Triaxial Shear Device," Draft Report to the Defense Nuclear Agency, US Army Engineer Waterways Experiment Station, Vicksburg, MS.

3. Cargile, James D., 1984, "Geotechnical Investigation for the CARES-Dry Site: Laboratory Test Results," Report to the Air Force Ballistic Missile Office/ENSN, US Army Engineer Waterways Experiment Station, Vicksburg, MS.

4. Farr, John Vail, 1986, "Loading Rate Effects on the One-Dimensional Compressibility of Four Partially Saturated Soils, "Dissertation submitted in partial fulfillment of the requirements for the degree of Doctor of Philosophy (Civil Engineering), University of Michigan, Ann Arbor, MI.

5. Richart, F.E. jr., Hall, J.R. jr., and Woods, R.D., _Vibrations of Soils and Foundations_, Prentice Hall, Inc., (Englewood Cliffs, NJ: 1970).

6. Davis, Julian, _Finite-Difference Methods in Dynamics of Continuous Media_, Macmillan Publishing Co.. Inc., (New York: 1986).

APPENDIX A

PROGRAM FTSP (FORTRAN 77)

```
C PROGRAM FTSP BY WF CARROLL, PROFESSOR, DEPT CEES, UCF
C
C THIS CODE SOLVES A 1D NON-LINEAR WAVE EQUATION FOR NORMAL STRAIN
C AND STRESS AT THE TOP AND BOTTOM OF A TRIAXIAL SPECIMEN WHEN ITS
C UPPER PEDESTAL TRAVELS WITH A CONSTANT OR HYPERBOLIC VELOCITY OR
C WITH CONSTANT ACCELERATION AND ITS STRESS-STRAIN RELATIONSHIP IS
C INITIALLY LINEAR AND THEN HYPERBOLIC.
C THE SOLUTION IS A FINITE DIFFERENCE ONE.
C
C THE VARIABLES ARE DIMENSIONLESS:
C
C    CTH - DIMENSIONLESS TIME (TIME TIMES INITIAL PROPAGATION
C            VELOCITY (C) DIVIDED BY SPECIMEN LENGTH (H))
C   CTOH - DIMENSIONLESS CHARACTERISTIC UPPER PEDESTAL TIME;
C            CTOH=C*TO/H WHERE TO=VO/AO:
C                 TO - CHARACTERISTIC U.P. TIME
C                 VO - LIMITING U.P. VELOCITY
C                 AO - INITIAL U.P. ACCELERATION
C            CTOH = 0    YIELDS A CONSTANT U.P. VELOCITY
C                 = 1000 YIELDS A CONSTANT U.P. ACCELERATION
C            1000>CTOH>0 YIELDS HYPERBOLIC U.P. VELOCITIES
C    CVO - C DIVIDED BY VO.
C  UHCVO - DISPLACEMENT DIVIDED BY H AND MULTIPLIED BY CVO.
C   ECVO - STRAIN MULTIPLIED BY CVO; IT ALSO INCLUDES STRESS
C            DIVIDED BY THE MAX STRESS (MAX LINEAR STRESS PLUS
C            MAX HYPERBOLIC STRESS).
C    NSS - NUMBER OF INCREMENTS IN THE SPECIMEN LENGTH (H).
C   NCTH - MAX NUMBER OF TIMES THE WAVE TRAVERSES H.
C     AB - RATIO OF MAX HYPERBOLIC STRESS (1/B) TO INIT SLOPE (1/A)
C            FOR A HYPERBOLIC STRESS-STRAIN RELATIONSHIP, AB IS A
C            CHARACTERISTIC STRAIN FOR A PURELY HYPERBOLIC MEDIUM.
C      D - AB MULTIPLIED BY CVO.
C     SL - MAX LINEAR DIMENSIONLESS STRESS.
C     EL - MAX LINEAR STRAIN.
C     EO - SUM OF EL AND AB, A CHARACTERISTIC STRAIN FOR A
C            LINEAR-HYPERBOLIC MEDIUM.
C     DE - EO TIMES CVO.

      COMMON /CINIT/ NSS,NCTH,NTS1,DCTH,CTOH,DE,D,SL,EL,CF
      COMMON /CU/ UHCVO(52,1052),ECVO(7,1052)
      OPEN(9,FILE='FTSP.PRN',STATUS='NEW')
      CALL INIT
      CALL FDALG
      CALL STRAIN
      CALL WRTOP
      CLOSE(9,STATUS='KEEP')
      END
```

```fortran
      SUBROUTINE INIT
      COMMON /CINIT/ NSS,NCTH,NTS1,DCTH,CTOH,DE,D,SL,EL,CF
      COMMON /CU/ UHCVO(52,1052),ECVO(7,1052)
      WRITE(*,100)
100   FORMAT(//1X,'ENTER  THE CTO/H FOR UPPER PEDESTAL MOTION'/
     @8X,'O     FOR CONSTANT U.P. VELOCITY, OR'/
     @8X,'>O    FOR HYPERBOLIC U.P.VELOCITY, OR'/
     @8X,'1000 FOR CONSTANT U.P. ACCELERATION'//)
      READ(*,*) CTOH
      WRITE(*,110)
110   FORMAT(//1X,'ENTER: THE NR OF INCREMENTS PER SPECIMEN',
     @1X,'LENGTH (NSI)'/
     @15X,'(MAX IS 50 AND MIN IS 4)'/
     @8X,'THE MAX EVEN INTEGER VALUE OF CT/H'/
     @15X,'(MAX IS 1000/NSI)'/
     @8X,'THE SUM OF EL AND AB (=EO) MULTIPLIED BY CVO, AND'/
     @8X,'THE MAX LINEAR DIMENSIONLESS STRESS (MLDS)'//)
      READ(*,*) NSS,NCTH,DE,SL
      ANSS=NSS
      DCTH=1./ANSS
      NTS1=NSS*NCTH+1
      D=DE*(1-SL)
      EL=SL*DE
      CF=1./(1.+EL/D)
      DO 120 N=1,NTS1
      DO 120 M=1,NSS+1
      UHCVO(M,N)=0.
120   CONTINUE
      CTH=0.
      DO 140 N=2,NTS1
      CTH=CTH+DCTH
      IF(CTOH .LE. .00001) THEN
      UHCVO(1,N)=CTH
      GO TO 130
      ENDIF
      IF(CTOH .GT. 999.9 .AND. CTOH .LT. 1000.1) THEN
      UHCVO(1,N)=.5*CTH**2
      GO TO 130
      ENDIF
      UHCVO(1,N)=CTH-CTOH*ALOG(1.+CTH/CTOH)
130   ECVO(1,N)=CTH
      ECVO(4,N)=UHCVO(1,N)
      IF(ECVO(4,N) .LE. EL) ECVO(7,N)=CF*ECVO(4,N)/D
      IF(ECVO(4,N) .GT. EL) THEN
      ECVO(7,N)=CF*((EL/D)+(ECVO(4,N)-EL)/(D+ECVO(4,N)-EL))
      ENDIF
140   CONTINUE
      RETURN
      END
```

```
      SUBROUTINE FDALG
      COMMON /CINIT/ NSS,NCTH,NTS1,DCTH,CTOH,DE,D,SL,EL,CF
      COMMON /CU/ UHCVO(52,1052),ECVO(7,1052)
      DO 100 N=2,NSS
      UHCVO(N,N+1)=UHCVO(1,2)
100   CONTINUE
      DO 110 N=3,NTS1
      DO 110 M=2,NSS
      NN=M+N-2
      IF(NN .EQ. NTS1) GO TO 110
      UHCVO(M,NN+1)=UHCVO(M+1,NN)-UHCVO(M,NN-1)+UHCVO(M-1,NN)
      ET=(UHCVO(M,NN+1)-UHCVO(M+1,NN+1))/DCTH
      IF(ET .GT. EL) THEN
      UA=UHCVO(M+1,NN)-2.*UHCVO(M,NN)+UHCVO(M-1,NN)
      UB=(1.+((UHCVO(M-1,NN)-UHCVO(M+1,NN))/(2.*D*DCTH))-EL/D)**2
      UHCVO(M,NN+1)=UA/UB+2.*UHCVO(M,NN)-UHCVO(M,NN-1)
      ENDIF
110   CONTINUE
      RETURN
      END

      SUBROUTINE STRAIN
      COMMON /CINIT/ NSS,NCTH,NTS1,DCTH,CTOH,DE,D,SL,EL,CF
      COMMON /CU/ UHCVO(52,1052),ECVO(7,1052)
      DO 110 I=1,NCTH/2
      INSS=2*(I-1)*NSS
      DO 110 N=2,2*NSS+1
      NT=N+INSS
      NB=NT+NSS
      IF(NB .GT. NTS1) NB=NTS1
      IF(N .EQ. 2 .OR. N .EQ. 2*NSS) THEN
      ECVO(2,NT)=-(-UHCVO(1,NT)+UHCVO(2,NT))/DCTH
      ECVO(3,NB)=-(-UHCVO(NSS,NB))/DCTH
      GO TO 100
      ENDIF
      IF(N .EQ. 3 .OR. N .EQ. 2*NSS-1) THEN
      ECVO(2,NT)=-(-1.5*UHCVO(1,NT)+2.*UHCVO(2,NT)-.5*UHCVO(3,NT))/
     @ DCTH
      ECVO(3,NB)=-(.5*UHCVO(NSS-1,NB)-2.*UHCVO(NSS,NB))/DCTH
      GO TO 100
      ENDIF
      ECVO(2,NT)=-(-(11./6.)*UHCVO(1,NT)+3.*UHCVO(2,NT)-1.5*
     @ UHCVO(3,NT)+(1./3.)*UHCVO(4,NT))/DCTH
      ECVO(3,NB)=-(-(1./3.)*UHCVO(NSS-2,NB)+1.5*UHCVO(NSS-1,NB)
     @ -3.*UHCVO(NSS,NB))/DCTH
100   IF(ECVO(2,NT) .LE. EL) ECVO(5,NT)=CF*ECVO(2,NT)/D
      IF(ECVO(2,NT) .GT. EL) THEN
      ECVO(5,NT)=CF*((EL/D)+(ECVO(2,NT)-EL)/(D+ECVO(2,NT)-EL))
      ENDIF
      IF(ECVO(3,NB) .LE. EL) ECVO(6,NB)=CF*ECVO(3,NB)/D
      IF(ECVO(3,NB) .GT. EL) THEN
      ECVO(6,NB)=CF*((EL/D)+(ECVO(3,NB)-EL)/(D+ECVO(3,NB)-EL))
      ENDIF
110   CONTINUE
      RETURN
      END
```

```fortran
      SUBROUTINE WRTOP
      COMMON /CINIT/ NSS,NCTH,NTS1,DCTH,CTOH,DE,D,SL,EL,CF
      COMMON /CU/ UHCVO(52,1052),ECVO(7,1052)
      WRITE(*,100)
100   FORMAT(//1X,'ENTER THE DATA OUTPUT INDEX:'/
     @5X,'1 : FOR ALL OUTPUT'/
     @5X,'2 : FOR THE VALUES AT EVERY 2ND TIME INCREMENT'/
     @5X,'3 : FOR THE VALUES AT EVERY 3RD TIME INCREMENT'/
     @5X,'ETC'//)
      READ(*,*) ND
      WRITE(9,110)
110   FORMAT(//1X,'DIMENSIONLESS STRESS-STRAIN-TIME DATA FOR AN',
     @1X,'ELASTIC SPECIMEN WITH'/
     @1X,'STRESS-STRAIN BEHAVIOR THATS INITIALLY LINEAR AND',
     @1X,'THEN HYPERBOLIC')
      IF(CTOH .LE. .00001) THEN
      WRITE(9,120)
120   FORMAT(1X,'AND WITH CONSTANT UPPER PEDESTAL VELOCITY'/)
      GO TO 150
      ENDIF
      IF(CTOH .GT. 999.9 .AND. CTOH .LT. 1000.1) THEN
      WRITE(9,130)
130   FORMAT(1X,'AND WITH CONSTANT UPPER PEDESTAL ACCELERATION'/)
      GO TO 150
      ENDIF
      WRITE(9,140)
140   FORMAT(1X,'AND WITH HYPERBOLIC UPPER PEDESTAL VELOCITY'/)
150   WRITE(9,160) DCTH
160   FORMAT(1X,'FTSP FINITE DIFFERENCE SOLUTION: D(X/H) =',F6.3//)
      WRITE(9,170) CTOH,DE,SL
170   FORMAT(//2X,'CTO/H =',F8.2,9X,'EO*(C/VO) =',F6.1,10X,
     @'MLDS =',F8.4//)
      WRITE(9,180)
180   FORMAT(7X,2(7X,'TOP',4X,'BOTTOM',5X,'GROSS')/
     @3X,'TIME',3(4X,'STRAIN'),3(4X,'STRESS'))
      WRITE(9,190) ((ECVO(I,N),I=1,7),N=1,NTS1,ND)
190   FORMAT(1X,F6.2,3F10.3,3F10.4)
      RETURN
      END
```

APPENDIX B

SAMPLE DATA RUN FROM

PROGRAM FTSP (FORTRAN 77)

Hyperbolic Upper Pedestal Motion,

$$C_o t_o / h = 5.0$$

Linear-Hyperbolic Stress-Strain,

$$\sigma_1 / \sigma_{max} = MLDS = 0.25$$

$$\epsilon_o C_o / v_o = 10.0$$

DIMENSIONLESS STRESS-STRAIN-TIME DATA FOR AN ELASTIC SPECIMEN WITH
STRESS-STRAIN BEHAVIOR THATS INITIALLY LINEAR AND THEN HYPERBOLIC
AND WITH HYPERBOLIC UPPER PEDESTAL VELOCITY

FTSP FINITE DIFFERENCE SOLUTION: D(X/H) = 0.050

CTO/H =   5.00   EO*(C/VO) =   10.0   MLDS =   0.2500

TIME	TOP STRAIN	BOTTOM STRAIN	GROSS STRAIN	TOP STRESS	BOTTOM STRESS	GROSS STRESS
0.00	0.000	0.000	0.000	0.0000	0.0000	0.0000
0.20	0.038	0.000	0.004	0.0038	0.0000	0.0004
0.40	0.074	0.000	0.015	0.0074	0.0000	0.0015
0.60	0.107	0.000	0.033	0.0107	0.0000	0.0033
0.80	0.138	0.000	0.058	0.0138	0.0000	0.0058
1.00	0.167	0.000	0.088	0.0167	0.0000	0.0088
1.20	0.194	0.077	0.124	0.0194	0.0077	0.0124
1.40	0.219	0.148	0.166	0.0219	0.0148	0.0166
1.60	0.242	0.214	0.212	0.0242	0.0214	0.0212
1.80	0.265	0.276	0.263	0.0265	0.0276	0.0263
2.00	0.286	0.333	0.318	0.0286	0.0333	0.0318
2.20	0.382	0.387	0.377	0.0382	0.0387	0.0377
2.40	0.472	0.437	0.440	0.0472	0.0437	0.0440
2.60	0.556	0.485	0.506	0.0556	0.0485	0.0506
2.80	0.635	0.529	0.577	0.0635	0.0529	0.0577
3.00	0.708	0.571	0.650	0.0708	0.0571	0.0650
3.20	0.777	0.688	0.727	0.0777	0.0688	0.0727
3.40	0.842	0.797	0.806	0.0842	0.0797	0.0806
3.60	0.903	0.898	0.888	0.0903	0.0898	0.0888
3.80	0.961	0.994	0.973	0.0961	0.0994	0.0973
4.00	1.016	1.083	1.061	0.1016	0.1083	0.1061
4.20	1.145	1.168	1.151	0.1145	0.1168	0.1151
4.40	1.265	1.247	1.244	0.1265	0.1247	0.1244
4.60	1.378	1.322	1.338	0.1378	0.1322	0.1338
4.80	1.484	1.393	1.435	0.1484	0.1393	0.1435
5.00	1.583	1.460	1.534	0.1583	0.1460	0.1534
5.20	1.677	1.601	1.635	0.1677	0.1601	0.1635
5.40	1.766	1.733	1.738	0.1766	0.1733	0.1738
5.60	1.850	1.857	1.843	0.1850	0.1857	0.1843
5.80	1.930	1.973	1.949	0.1930	0.1973	0.1949
6.00	2.006	2.083	2.058	0.2006	0.2083	0.2058
6.20	2.155	2.187	2.168	0.2155	0.2187	0.2168
6.40	2.294	2.285	2.279	0.2294	0.2285	0.2279
6.60	2.426	2.379	2.392	0.2426	0.2379	0.2392
6.80	2.550	2.467	2.507	0.2549	0.2467	0.2507
7.00	2.667	2.551	2.623	0.2663	0.2551	0.2621
7.20	2.778	2.708	2.740	0.2768	0.2702	0.2733
7.40	2.884	2.854	2.859	0.2866	0.2838	0.2842
7.60	2.985	2.993	2.979	0.2956	0.2963	0.2950

TIME	TOP STRAIN	BOTTOM STRAIN	GROSS STRAIN	TOP STRESS	BOTTOM STRESS	GROSS STRESS
7.80	3.082	3.125	3.100	0.3040	0.3077	0.3056
8.00	3.175	3.250	3.222	0.3119	0.3182	0.3159
8.20	3.321	3.371	3.346	0.3240	0.3280	0.3260
8.40	3.474	3.486	3.471	0.3362	0.3371	0.3360
8.60	3.621	3.596	3.597	0.3475	0.3456	0.3457
8.80	3.762	3.702	3.724	0.3580	0.3536	0.3552
9.00	3.898	3.805	3.852	0.3678	0.3612	0.3645
9.20	4.028	3.909	3.981	0.3770	0.3686	0.3737
9.40	4.153	4.074	4.111	0.3855	0.3801	0.3826
9.60	4.274	4.230	4.242	0.3935	0.3906	0.3914
9.80	4.391	4.382	4.374	0.4010	0.4004	0.3999
10.00	4.504	4.528	4.507	0.4082	0.4096	0.4083
10.20	4.614	4.669	4.641	0.4149	0.4183	0.4165
10.40	4.723	4.806	4.775	0.4215	0.4264	0.4246
10.60	4.871	4.939	4.911	0.4301	0.4340	0.4324
10.80	5.042	5.067	5.047	0.4398	0.4413	0.4401
11.00	5.203	5.192	5.184	0.4487	0.4481	0.4477
11.20	5.354	5.313	5.322	0.4567	0.4546	0.4551
11.40	5.503	5.431	5.461	0.4644	0.4607	0.4623
11.60	5.650	5.546	5.600	0.4718	0.4666	0.4693
11.80	5.792	5.665	5.740	0.4788	0.4726	0.4763
12.00	5.929	5.822	5.881	0.4853	0.4802	0.4831
12.20	6.062	6.002	6.023	0.4915	0.4887	0.4897
12.40	6.193	6.158	6.165	0.4974	0.4959	0.4962
12.60	6.321	6.321	6.308	0.5031	0.5032	0.5026
12.80	6.446	6.476	6.451	0.5085	0.5099	0.5088
13.00	6.568	6.625	6.595	0.5137	0.5161	0.5149
13.20	6.689	6.776	6.740	0.5188	0.5223	0.5209
13.40	6.826	6.919	6.885	0.5244	0.5281	0.5267
13.60	7.002	7.059	7.031	0.5313	0.5335	0.5325
13.80	7.182	7.199	7.178	0.5382	0.5389	0.5381
14.00	7.340	7.334	7.325	0.5441	0.5439	0.5436
14.20	7.509	7.465	7.473	0.5503	0.5487	0.5490
14.40	7.662	7.596	7.621	0.5558	0.5534	0.5543
14.60	7.823	7.724	7.770	0.5613	0.5579	0.5595
14.80	7.972	7.850	7.919	0.5664	0.5623	0.5646
15.00	8.125	7.987	8.069	0.5714	0.5669	0.5696
15.20	8.270	8.152	8.219	0.5761	0.5723	0.5745
15.40	8.416	8.339	8.370	0.5807	0.5783	0.5793
15.60	8.557	8.513	8.521	0.5851	0.5837	0.5840
15.80	8.695	8.674	8.672	0.5893	0.5886	0.5886
16.00	8.834	8.845	8.825	0.5934	0.5937	0.5931
16.20	8.966	9.004	8.977	0.5972	0.5983	0.5976
16.40	9.101	9.164	9.130	0.6011	0.6029	0.6019
16.60	9.232	9.322	9.284	0.6048	0.6073	0.6062
16.80	9.374	9.475	9.438	0.6087	0.6114	0.6104
17.00	9.534	9.630	9.592	0.6130	0.6155	0.6145
17.20	9.718	9.775	9.747	0.6178	0.6193	0.6186
17.40	9.908	9.927	9.902	0.6227	0.6232	0.6225
17.60	10.074	10.068	10.057	0.6268	0.6267	0.6264
17.80	10.240	10.214	10.213	0.6309	0.6303	0.6303

TIME	TOP STRAIN	BOTTOM STRAIN	GROSS STRAIN	TOP STRESS	BOTTOM STRESS	GROSS STRESS
18.00	10.413	10.352	10.370	0.6351	0.6336	0.6340
18.20	10.579	10.493	10.526	0.6389	0.6369	0.6377
18.40	10.737	10.629	10.684	0.6426	0.6401	0.6413
18.60	10.903	10.769	10.841	0.6463	0.6433	0.6449
18.80	11.060	10.912	10.999	0.6497	0.6465	0.6484
19.00	11.214	11.073	11.157	0.6531	0.6500	0.6519
19.20	11.373	11.251	11.315	0.6564	0.6539	0.6552
19.40	11.521	11.444	11.474	0.6595	0.6579	0.6586
19.60	11.674	11.627	11.633	0.6627	0.6617	0.6618
19.80	11.822	11.797	11.793	0.6656	0.6651	0.6650
20.00	11.967	11.962	11.953	0.6685	0.6684	0.6682
20.20	12.114	12.139	12.113	0.6713	0.6718	0.6713
20.40	12.256	12.310	12.273	0.6740	0.6750	0.6744
20.60	12.399	12.471	12.434	0.6767	0.6780	0.6774
20.80	12.543	12.635	12.595	0.6794	0.6810	0.6803
21.00	12.688	12.802	12.757	0.6820	0.6840	0.6832
21.20	12.849	12.961	12.918	0.6849	0.6868	0.6861
21.40	13.020	13.116	13.080	0.6878	0.6895	0.6889
21.60	13.212	13.280	13.243	0.6911	0.6923	0.6917
21.80	13.403	13.431	13.405	0.6943	0.6948	0.6944
22.00	13.589	13.585	13.568	0.6974	0.6973	0.6971
22.20	13.759	13.739	13.731	0.7002	0.6998	0.6997
22.40	13.927	13.889	13.894	0.7028	0.7022	0.7023
22.60	14.103	14.035	14.058	0.7055	0.7045	0.7048
22.80	14.280	14.187	14.222	0.7082	0.7068	0.7074
23.00	14.451	14.332	14.386	0.7108	0.7090	0.7098
23.20	14.613	14.478	14.551	0.7132	0.7112	0.7123
23.40	14.779	14.631	14.715	0.7156	0.7135	0.7147
23.60	14.951	14.784	14.880	0.7181	0.7157	0.7171
23.80	15.112	14.951	15.045	0.7203	0.7181	0.7194
24.00	15.271	15.133	15.211	0.7225	0.7206	0.7217
24.20	15.432	15.322	15.376	0.7247	0.7232	0.7239
24.40	15.594	15.518	15.542	0.7269	0.7258	0.7262
24.60	15.751	15.707	15.708	0.7289	0.7284	0.7284
24.80	15.903	15.882	15.875	0.7309	0.7306	0.7305
25.00	16.062	16.055	16.041	0.7329	0.7328	0.7327
25.20	16.217	16.227	16.208	0.7349	0.7350	0.7348
25.40	16.363	16.403	16.375	0.7367	0.7372	0.7368
25.60	16.518	16.585	16.542	0.7386	0.7394	0.7389
25.80	16.671	16.758	16.710	0.7404	0.7415	0.7409
26.00	16.820	16.922	16.877	0.7422	0.7434	0.7429
26.20	16.975	17.090	17.045	0.7440	0.7454	0.7448
26.40	17.136	17.261	17.213	0.7459	0.7473	0.7468
26.60	17.305	17.430	17.381	0.7478	0.7492	0.7487
26.80	17.482	17.597	17.550	0.7498	0.7511	0.7506
27.00	17.672	17.755	17.718	0.7519	0.7528	0.7524
27.20	17.870	17.918	17.887	0.7540	0.7546	0.7542
27.40	18.063	18.085	18.056	0.7561	0.7563	0.7560
27.60	18.250	18.245	18.226	0.7581	0.7580	0.7578
27.80	18.433	18.401	18.395	0.7600	0.7596	0.7596
28.00	18.604	18.559	18.565	0.7617	0.7612	0.7613

TIME	TOP STRAIN	BOTTOM STRAIN	GROSS STRAIN	TOP STRESS	BOTTOM STRESS	GROSS STRESS
28.20	18.775	18.718	18.734	0.7634	0.7628	0.7630
28.40	18.957	18.876	18.904	0.7652	0.7644	0.7647
28.60	19.137	19.028	19.074	0.7670	0.7659	0.7663
28.80	19.316	19.181	19.245	0.7687	0.7674	0.7680
29.00	19.492	19.340	19.415	0.7703	0.7689	0.7696
29.20	19.659	19.499	19.586	0.7719	0.7704	0.7712
29.40	19.826	19.655	19.757	0.7734	0.7719	0.7728
29.60	19.998	19.820	19.928	0.7750	0.7734	0.7743
29.80	20.174	19.999	20.099	0.7766	0.7750	0.7759
30.00	20.346	20.180	20.270	0.7781	0.7766	0.7774
30.20	20.505	20.365	20.442	0.7795	0.7782	0.7789
30.40	20.670	20.564	20.613	0.7809	0.7800	0.7804
30.60	20.839	20.763	20.785	0.7823	0.7817	0.7819
30.80	21.001	20.954	20.957	0.7837	0.7833	0.7833
31.00	21.169	21.141	21.129	0.7851	0.7848	0.7847
31.20	21.332	21.320	21.302	0.7864	0.7863	0.7861
31.40	21.485	21.496	21.474	0.7876	0.7877	0.7875
31.60	21.647	21.673	21.647	0.7889	0.7891	0.7889
31.80	21.813	21.848	21.820	0.7902	0.7905	0.7903
32.00	21.969	22.029	21.992	0.7914	0.7919	0.7916
32.20	22.125	22.217	22.165	0.7926	0.7933	0.7929
32.40	22.284	22.397	22.339	0.7938	0.7947	0.7942
32.60	22.446	22.569	22.512	0.7951	0.7960	0.7955
32.80	22.611	22.739	22.685	0.7963	0.7972	0.7968
33.00	22.775	22.909	22.859	0.7975	0.7985	0.7981
33.20	22.943	23.083	23.033	0.7987	0.7997	0.7993
33.40	23.122	23.258	23.207	0.8000	0.8009	0.8006
33.60	23.311	23.431	23.381	0.8013	0.8022	0.8018
33.80	23.502	23.605	23.555	0.8026	0.8034	0.8030
34.00	23.697	23.771	23.729	0.8040	0.8045	0.8042
34.20	23.893	23.932	23.904	0.8053	0.8056	0.8054
34.40	24.090	24.100	24.078	0.8066	0.8067	0.8066
34.60	24.286	24.274	24.253	0.8079	0.8078	0.8077
34.80	24.472	24.440	24.428	0.8091	0.8089	0.8089
35.00	24.648	24.602	24.603	0.8103	0.8100	0.8100
35.20	24.825	24.766	24.778	0.8114	0.8110	0.8111
35.40	25.005	24.928	24.953	0.8125	0.8120	0.8122
35.60	25.186	25.089	25.128	0.8137	0.8131	0.8133
35.80	25.366	25.254	25.304	0.8148	0.8141	0.8144
36.00	25.549	25.419	25.479	0.8159	0.8151	0.8154
36.20	25.735	25.581	25.655	0.8170	0.8161	0.8165
36.40	25.919	25.740	25.831	0.8181	0.8170	0.8176
36.60	26.096	25.902	26.006	0.8191	0.8180	0.8186
36.80	26.266	26.071	26.182	0.8201	0.8190	0.8196
37.00	26.435	26.248	26.359	0.8211	0.8200	0.8206
37.20	26.609	26.423	26.535	0.8220	0.8210	0.8216
37.40	26.788	26.596	26.711	0.8230	0.8220	0.8226
37.60	26.966	26.780	26.888	0.8240	0.8230	0.8236
37.80	27.141	26.978	27.064	0.8250	0.8241	0.8246
38.00	27.313	27.177	27.241	0.8259	0.8252	0.8255
38.20	27.482	27.372	27.418	0.8268	0.8262	0.8265

TIME	TOP STRAIN	BOTTOM STRAIN	GROSS STRAIN	TOP STRESS	BOTTOM STRESS	GROSS STRESS
38.40	27.650	27.568	27.595	0.8277	0.8273	0.8274
38.60	27.819	27.766	27.772	0.8286	0.8283	0.8284
38.80	27.989	27.959	27.949	0.8295	0.8293	0.8293
39.00	28.159	28.146	28.126	0.8304	0.8303	0.8302
39.20	28.329	28.333	28.303	0.8312	0.8312	0.8311
39.40	28.500	28.514	28.481	0.8321	0.8322	0.8320
39.60	28.664	28.689	28.658	0.8329	0.8330	0.8329
39.80	28.823	28.865	28.836	0.8337	0.8339	0.8338
40.00	28.986	29.049	29.014	0.8345	0.8348	0.8346

DISTRIBUTION LIST

DEPARTMENT OF DEFENSE

Director
Defense Nuclear Agency
ATTN: DFSP (Dr. G. W. Ullrich)
      SPSD (MAJ M. A. Reed)
      SPWE (Dr. C. Canada)
      SPWE (MAJ M. Pelkey)
      Technical Library
Washington, DC 20305-1000

Defense Nuclear Agency
Nevada Operations Office
ATTN: TDNV (Mr. J. W. LaComb)
P. O. Box 208
Mercury, NV 89023

Director
Defense Advanced Research Project Agency
ATTN: Technical Library
1400 Wilson Blvd.
Arlington, VA 22209

Director
Defense Intelligence Agency
ATTN: Technical Library
Washington, DC 20301-6111

Defense Technical Information Center
Cameron Station
ATTN: TC (2 cys)
Alexandria, VA 22314

DEPARTMENT OF THE ARMY

Commander
US Army Corps of Engineers
ATTN: CERD-L (Ms. Sharon Vannucci)
      CERD-M (Mr. B. O. Benn)
      CEEC-ET (Mr. R. L. Wight)
      CEIM-SL
Washington, DC 20314-1000

Division Engineer
US Army Engineer Division, Huntsville
ATTN: CEHND-SR
P. O. Box 1600, West Station
Huntsville, AL 35807-4301

District Engineer
US Army Engineer District, Omaha
ATTN: CEMRO-ED-S (Mr. Bob Kelley)
      CEMRO-ED-SH (Mr. Bill Gaube)
215 N. 17th Street
Omaha, NE 68102-4978

Director
US Army Construction Engineering
  Research Laboratory
ATTN: Technical Library
P. O. Box 4005
Champaign, IL 61820-1305

Commander/Director
US Army Cold Regions Research and
  Engineering Laboratory
ATTN: Technical Library
72 Lyme Road
Hanover, NH 03755-1290

Commandant
US Army Engineer School
ATTN: ATZA-CD (COL Fred Parker)
      Technical Library
      Ft. Belvoir, VA 22060-5281

Commander
US Army Laboratory Command
ATTN: Technical Library
2800 Powder Mill Road
Adelphi, MD 20783-1145

Director
US Army Ballistic Research Laboratory
ATTN: Technical Library
Aberdeen Proving Ground, MD 21005-5066

Commander
US Army Nuclear and Chemical Agency
ATTN: Technical Library
7500 Backlick Road, Bldg. 2073
Springfield, VA 22150

DEPARTMENT OF THE NAVY

Naval Civil Engineering Laboratory
ATTN: Technical Library
Port Hueneme, CA 93043

Naval Facilities Engineering Command
ATTN: Technical Library
200 Stovall Street
Alexandria, VA 22332

DEPARTMENT OF THE AIR FORCE

Air Force Institute of Technology
Air University
ATTN: Technical Library
Wright-Patterson Air Force Base, OH 45433

Air Force Office of Scientific Research
ATTN: Technical Library
Bolling Air Force Base, DC 20332

Air Force Weapons Laboratory (AFSC)
ATTN: NTESG (CPT C. W. Felice)
      Technical Library
Kirtland Air Force Base, NM 87117-6008

Air Force Engineering and Services
  Center (AFSC)
ATTN: Technical Library
Tyndall Air Force Base, FL 32403

Air Force Armament Laboratory (AFSC)
ATTN: Technical Library
Eglin Air Force Base, FL 32542

DEPARTMENT OF THE AIR FORCE (Continued)

Commander
Ballistic Missile Office (AFSC)
ATTN: MYEB (LTC D. H. Gage)
        Technical Library
Norton Air Force Base, CA 92409

DEPARTMENT OF ENERGY

Lawrence Livermore National Laboratory
ATTN: Technical Library
P. O. Box 808
Livermore, CA 94550

Los Alamos National Laboratory
ATTN: Technical Library
P. O. Box 1663
Los Alamos, NM 87545

Sandia National Laboratories
ATTN: Technical Library
P. O. Box 5800
Albuquerque, NM 87185

Sandia National Laboratories
ATTN: Technical Library
Livermore, CA 94550

DEPARTMENT OF DEFENSE CONTRACTORS

Mr. J. L. Bratton
Applied Research Associates, Inc.
4300 San Mateo Blvd., NE, Suite A220
Albuquerque, NM 87110

Mr. J. D. Shinn
Applied Research Associates, Inc.
South Royalton, VT 05068

Mr. J. L. Drake
Applied Research Associates, Inc.
3202 Wisconsin Avenue
Vicksburg, MS 39180-2610

Dr. J. G. Trulio
Applied Theory, Inc.
930 S. LaBrea Avenue
Los Angeles, CA 90036

Dr. Y. Marvin Ito
California Research & Technology, Inc.
20943 Devonshire Street
Chatsworth, CA 91311-2376

Dr. E. J. Rinehart
California Research & Technology, Inc.
2017 Yale Blvd., SE
Albuquerque, NM 87106

Dr. Hon-Yim Ko
Department of Civil, Environmental, and
  Architectural Engineering
University of Colorado at Boulder
Boulder, CO 80309

Dr. K. C. Valanis
Endochronics, Inc.
8605 Northwest Lakecrest Court
Vancouver, WA 98665

Technical Library
New Mexico Engineering Research Institute
University of New Mexico
Box 25, University Station
Albuquerque, NM 87131

Dr. Don Simons
R&D Associates
P. O. Box 9695
Marina del Rey, CA 90291

Mr. L. S. Melzer
Science Applications International
  Corporation
505 West Texas Street
First City Center, Tower 2, Suite 1335
Midland, TX 79701

Dr. John Schatz
Science Applications International
  Corporation
P. O. Box 2351
La Jolla, CA 92038-2351

Dr. H. E. Read
S-Cubed
P. O. Box 1620
La Jolla, CA 92038-1620

Dr. Lynn Seaman
SRI International
333 Ravenswood Avenue
Menlo Park, CA 94025

Mr. S. J. Green
Terra Tek, Inc.
420 Wakara Way
Salt Lake City, UT 84108

Dr. M. G. Katona
TRW Defense Systems Group
P. O. Box 1310
San Bernardino, CA 92402

Dr. I. S. Sandler
Weidlinger Associates
333 Seventh Avenue
New York, NY 10001

Dr. W. F. Carroll (10 cys)
Department of Civil Engineering
  and Environmental Sciences
University of Central Florida
Orlando, FL 32816

END

DATE

FILMED

5-88

DTIC